Neural Promotion of Hedgehog-Driven Skin Cancer

by

Shelby C. Peterson

A dissertation submitted in partial fulfillment
of the requirements for the degree of
Doctor of Philosophy
(Cellular and Molecular Biology)
in the University of Michigan
2017

Doctoral Committee:

Assistant Professor Sunny Y. Wong, Chair
Assistant Professor Benjamin L. Allen
Professor Andrzej A. Dlugosz
Professor Roman J. Giger

Shelby C. Peterson

scpete@umich.edu

ORCID iD: 0000-0003-2719-8187

To the many women who have inspired me:

"I could not, at any age, be content to take my place by the fireside and simply look on. Life was meant to be lived. Curiosity must be kept alive. One must never, for whatever reason, turn [her] back on life."

- Eleanor Roosevelt

ACKNOWLEDGEMENTS

This dissertation would not have been possible without the support of my mentors, colleagues, friends, and most of all my family. Without them, I would not be the scientist or person I am today. I thank them for their advice, both scientific and personal, their patience, and for empowering me to fulfill my potential.

First, I would like to thank my mentor, Dr. Sunny Wong, for providing an exemplary example of how a scientist should think, speak, and write. Sunny has supported all aspects of my scientific training, inside and outside the lab. He pushed me to improve my critical thinking skills, empowered me to speak up and ask questions, and supported my interests outside the lab. I am honored and grateful to be the first graduate student to complete my training in his lab.

Second, I would like to thank my committee members, Dr. Andrzej Dlugosz, Dr. Ben Allen, and Dr. Roman Giger for providing me with meaningful feedback throughout my graduate career. During lab meetings, Anj provided key insight into my research, offering alternative methods and asking difficult questions, which pushed me to deepen my understanding of the literature. Anj also served as a co-mentor for my NSRA, which funded the final year of my graduate studies. Since rotating in Ben's lab, he has continued to support my development as a scientist. Through meaningful conversations, he has pushed me to carefully consider my career options, and encouraged me to pursue a path that will best utilize my skills. Roman has always provided important insight into my project, and pushed me to consider alternative explanations

for my experimental results. I am grateful to my committee for their unwavering support throughout my graduate career.

I am so lucky to have been a part of the CMB graduate program. I may be biased, but I believe that CMB houses the best faculty, students, and staff of any graduate program. Despite the size of the program, CMB made me feel welcome and valued. I must thank the CMB staff past and present for their efforts to support all aspects of CMB student well-being. Cathy Mitchell, Margarita Bekiares, Jim Musgrave, and Pat Ocelnik helped me to navigate funding, appointments, and administrative tasks. Their passion for CMB students is clear and very appreciated. As director, Dr. Robert Fuller has been a tremendous leader. Bob truly cares about the CMB program and its students, and we are grateful.

Graduate school has been full of highs and lows, but I am lucky to have shared it with the other members of the Wong lab. Natalia, Markus, Arlee, and Jacob, I am so thankful to have spent the last four years working alongside you all. You inspire me. I know you all will go on to do great things.

I have had the privilege of collaborating with several talented research groups throughout my graduate career. I would like to thank Dr. Nicole Ward and Dr. Abdelmadjid Belkadi for teaching me the surgical denervation technique, which was instrumental for my project. I thank Dr. Isaac Brownell for his scientific advice and collaboration. I thank Dr. Katherine Albers for providing the construct used to generate our hyper-innervated mouse model. And finally, I would like to thank Dr. Andrzej Dlugosz and all members of the Dlugosz lab, for sharing reagents, providing feedback at lab meetings, and for being scientific role models to me throughout my training.

They say friends are the family you choose, and I think I chose well. My friends have been an instrumental part of my sanity throughout my graduate career. They have been understanding even when they didn't understand anything I was talking about. They have encouraged me through the difficult times, and I am eternally grateful.

Since I was very young, my parents have nurtured my interest in science. They provided me with countless experiences to explore my interests. They have been my number one supporters throughout my education, and without their encouragement I would not be preparing to defend my PhD thesis. Throughout my life, my parents have modeled success, and pushed me to purse excellence. I credit them for my dissatisfaction with mediocrity, and any talent I display is a credit to them.

Finally, I have to thank my soon-to-be husband. Joe, thank you for being my safe place. Thank you for supporting my ambition. Thank you for inspiring me. Thank you for believing in me, even when I don't believe in myself. I am so lucky to have you in my life.

TABLE OF CONTENTS

LIST OF FIGURES

ABSTRACT

Basal cell carcinoma (BCC) is the most common form of skin cancer. It is caused by de-regulated Hedgehog (HH) signaling, most often due to loss-of-function mutations in the HH receptor *Patched1* (*PTCH1*). *Ptch1* deletion in mice yields BCC-like tumors that mimic human disease. Using this model, I identified several epidermal populations that are susceptible to *Ptch1*-driven BCC formation. These populations include the hair follicle (HF) isthmus and bulge regions, as well as the mechanosensory touch dome (TD). In contrast, the interfollicular epidermis (IFE) is resistant to BCC initiation. One striking difference in the micro-environment of the HF/TD versus the IFE is the presence or absence of innervation. The HF/TD niches contain sensory nerves which secrete HH ligand to activate signaling, while the IFE lacks innervation. Based on this observation, I chose to investigate the contribution of nerves to BCC tumorigenesis. First, I found that surgical denervation reduces TD-derived tumor growth, which highlights a promoting role for nerves in BCC. In addition, my preliminary data suggest hyper-innervation via expression of nerve growth factor *Neurotrophin-3* (*NT-3*) may enhance BCC initiation in the HF and TD compartments. Despite the apparent promoting role for nerves in HF/TD BCC, ectopic innervation of the IFE via *NT-3* expression is not sufficient to impart BCC susceptibility. This suggests that additional mutations are required to overcome the IFE's resistance to BCC formation. Several *in vitro* and *in vivo* studies suggest that in the absence of *Ptch1*, HH signaling is mediated by its homologue *Patched 2* (*Ptch2*). However, I found that additional loss of *Ptch2* does not affect BCC tumorigenesis or the level of HH activation.

Together, this data highlight a novel role for sensory innervation in promoting BCC tumorigenesis, and uncovers a new potential therapeutic target for BCC treatment.

Chapter I - Introduction

1.1 Abstract

It has been 20 years since researchers discovered Hedgehog signaling as the driver for basal cell carcinoma (BCC). Since then, incredible advancements have increased our understanding of HH and BCC. These advances have led scientists to develop effective targeted therapies, including the FDA approved HH inhibitors vismodegib and sonidegib, which are prescribed in the clinic today. Despite these advances, HH inhibition likely has several on-target side effects, and tumors can become resistant. Thus, further characterization of BCC is necessary to develop new, more effective treatments. This chapter introduces the HH signaling pathway and its role in epidermal development, homeostasis and BCC. I summarize key milestones in BCC research, and discuss tools used to model and study BCC. I introduce the signaling events that mediate epidermal innervation and summarize the role of nerves in several cancer types and diseases. Finally, I pose the key questions I will be addressing in following chapters.

1.2 Hedgehog Signaling in the Epidermis

1.2.1 Hedgehog pathway overview

Discovered almost 40 years ago, Hedgehog (HH) was first identified in a mutational screen for genes affecting *Drosophila* segment polarity [1, 2]. In vertebrates, HH signaling initiates when ligands (Sonic, Desert, or Indian HH [3-5]) bind the receptor Patched1 (PTCH1) [6, 7]. This binding relieves PTCH1's inhibition of the downstream effector Smoothened (SMO)

[8-10]. Active SMO then facilitates GLI protein activation of target gene transcription, including the HH pathway members *Ptch1* and *Gli1* [11, 12]. In the absence of ligand, PTCH1 inhibits SMO and GLIs repress target gene transcription (FIG 1.1, reviewed in [13, 14]).

In mammals, HH signaling requires the primary cilium, a cell surface "antenna" that senses external signals [15, 16]. In the absence of HH ligand, PTCH1 localizes to the primary cilium preventing SMO from entering [17]. Upon HH ligand binding, PTCH1 exits the cilium allowing accumulation of SMO and GLI [17-19]. Mutations in ciliary components disrupts HH signaling [16, 20].

While *Drospohila* have one HH ligand [1], mammals have three different HH ligands, Sonic, Desert, and Indian HH [3-5]. Sonic Hedgehog (SHH) is the primary activator of HH in the epidermis [21, 22]. SHH is a secreted ligand that undergoes several processing steps before it is functional in HH signaling. Initially, SHH contains a signal sequence , signaling domain, and auto-processing domain. First, the signal sequence is cleaved. Next the auto-processing domain catalyzes a cholesterol transfer at the C terminus, allowing the peptide to associate with the membrane [23, 24]. Finally, SHH undergoes an N-terminal addition of a palmitoyl moiety, which is required for long range signaling [25-29]. SHH secretion is mediated by membrane bound Dispatched (DISP)[30-33] and secreted Scube (SCUBE) [34-36].

In addition to PTCH1, mammalian HH signaling is also regulated at the cell surface by co-receptors. Positive regulators include GAS1, CDON, and BOC [37]. These co-receptors bind HH ligand and form complexes with PTCH1 to promote signaling [38]. GAS1, CDON, and BOC have distinct but overlapping roles in neural and limb patterning [37]. However, deletion of all three co-receptors causes almost complete HH blockade and early embryonic lethality, reminiscent of other HH loss-of-function mutants [37].

HH is negatively regulated at the cell surface by PTCH1, its homolog Patched 2 (PTCH2, [39]), and Hedgehog interacting protein (HHIP, [40]) which exists in both a membrane bound and secreted form. All three of these receptors are also HH target genes. Upon pathway activation, PTCH1/2 and HHIP are up-regulated in a negative feedback loop to suppress signaling. As such, loss of PTCH1 [41], PTCH2 [42], or HHIP [43] causes varying degrees of HH activation. As the primary HH receptor, *Ptch1* deletion has the most severe developmental phenotype [41]. *Ptch2* mutant mice are viable, but display a mild epidermal phenotype [42]. Dual loss of the PTCH receptors results in higher HH activation than PTCH1 loss alone *in vitro* [44] and *in vivo* [45-47]. These studies indicate partial redundancy between PTCH1 and PTCH2 inhibition of SMO in the absence of ligand. *Hhip* mutant mice die postnatally, due to respiratory failure, however patterning of limbs, skin, and central nervous system is unaffected [43]. Combined loss of PTCH1, PTCH2, and HHIP in the neural tube causes more severe defects than single mutants, highlighting the overlapping roles for these receptors in suppressing HH [45, 48].

GLI proteins are the transcriptional effectors of the HH pathway. Vertebrates have three GLI family members (GLI1-3). GLI1 was first identified in glioblastoma [49]. GLI2/3 were later identified due to sequence similarity [50]. GLI proteins contain zinc-finger domains that allow them to bind DNA [51]. All three GLIs contain a C-terminal activation domain [52]. GLI2/3 (but not GLI1) also contain an N-terminal repressor domain [53, 54]. These domains allow modulation of target gene expression under different signaling conditions.

Mouse studies have highlighted distinct roles for GLI1-3. During development, GLI1 is expressed near sources of HH ligand, while GLI2/3 are expressed more broadly [55-57]. *Gli1* is a HH target gene [58], and ectopic GLI1 mimics ectopic SHH activation in the neural tube [58, 59]. Despite this promoting role, *Gli1* mutant mice develop normally [60, 61]. Unlike GLI1,

GLI2 is required for proper development [62, 63]. In the neural tube, a ventral-dorsal HH gradient specifies different neural progenitors (reviewed in [14]). Mutation of *Gli2* causes a loss of ventral floor plate cells, which require the highest level of HH [62, 63]. However, *Gli2* mutants retain motor neurons, which require lower HH activation [62, 63]. This suggests that the neural tube requires GLI2 to activate high-level HH signaling. Unlike GLI2, GLI3 inhibits HH activation, as loss of GLI3 causes ectopic HH activation [64-66]. *Gli3* mutations in humans also cause Greig cephalopolysyndactyly syndrome, a disorder that affects the limbs, head, and face [67]. These studies suggest GLI3 functions primarily as a repressor, although full-length GLI3 can activate transcription *in vitro* [53, 54, 68], and weakly *in vivo* [69, 70].

Combined mutational studies highlight overlapping and diverging roles for GLI proteins. In the neural tube and lung, dual loss of GLI1 and GLI2 causes a slightly more severe phenotype than loss of GLI2 alone [60]. This highlights a role for GLI1 (in certain tissues) in the absence of GLI2. Limbs in *Gli1/2* double mutants develop normally [63, 71], while *Gli3* mutants display polydactyly [64-66], indicating a primary role for GLI3. In addition, *Gli2/3* double mutants display more severe skeletal defects than single mutants [72]. Taken together, these studies highlight functional redundancies in the GLI family.

GLI processing is complex and not fully understood. In the absence of HH, the activation domains of GLI2/3 are cleaved [54, 73]. This process is mediated by Protein kinase A (PKA)[54, 74, 75] , Casein Kinase 1 (CK1)[76], and Glycogen Synthase Kinases (GSKs)[76-78]. These phosphorylation events lead to ubiquitination and proteasome processing and/or degradation [79]. The repressor form of GLI2 is unstable [12, 75], which could explain why GLI3 has a more dominant repressor function *in vivo* [64-66]. GLI1 lacks the repressor domain and is not processed [53, 54, 80].

GLI processing is also regulated by Suppressor of Fused (SUFU) [81]. SUFU is a negative regulator of HH signaling [81]. As such, *Sufu* mutant mice display overactive HH signaling [82]. SUFU binding to full-length GLI2/3 prevents nuclear localization and promotes processing [83, 84]. PKA inhibits dissociation of this GLI-SUFU complex [84].

Despite their conflicting transcriptional roles, GLI activators and repressors bind similar genomic sequences [85, 86]. Promoter studies suggest that multiple high- and low-affinity GLI binding sites can regulate expression of one gene [87, 88]. These sites tune the pattern of expression in specific tissues and cell types. It is a complex system, where GLI activators and repressors bind and regulate each element based on context. Careful examination of many target gene promoters will be necessary to unravel how this process is regulated.

1.2.2 Epidermal development and hair follicle morphogenesis

The epidermis derives from the surface ectoderm. At embryonic day 12 (E12), the epidermis exists as a single layer of cells undergoing symmetrical divisions. During the next few days (E13-15), basal cells, the lowest layer of the epidermis, undergo asymmetric cell divisions [89]. This creates a second suprabasal layer of the skin, directly above the basal layer [89]. This layer continues dividing for a short period before undergoing a terminal differentiation program mediated by Notch signaling [90] (reviewed in [91]). These suprabasal cells create the spinous layer of the skin, which contains bundles of Keratins 1 and 10 [92]. A few days later (E18.5), the epidermis further stratifies creating the granular layer, characterized by the presence of dense cytoplasmic keratohyalin granules, which promote dehydration and keratin crosslinking. The outermost layer, the stratum corneum, consists of cornified cells that confer barrier function (reviewed in [93]).

During stratification, dermal-epidermal cross-talk initiates hair follicle morphogenesis. Dermal condensates form along the basement membrane and signal via Fibroblast growth factors (FGFs)[94, 95] and Noggin [96] (E15). Wnt signaling from the epidermis signals the formation of the hair germ or placode [97, 98] (E16). These placodes express SHH, which induces condensation of dermal cells to form the dermal papilla (DP)[22]. The DP then signals the follicle to grow downward and envelop the DP (E18). As the follicle matures, the cells at the base proliferate, generating the layers of the mature follicle and hair shaft (reviewed in [93, 99]) (FIG 1.2).

1.2.3 The hair cycle

Mature hair follicles cycle through phases of rest (telogen), growth (anagen), and regression (catagen). Early anagen begins with proliferation in the secondary hair germ induced by Wnt, FGF, and BMP-inhibition signals from the DP [100]. During mid-anagen, the new follicle grows and envelops the DP. Matrix cells are specified adjacent to the DP, and divide to form the inner layers of the follicle and hair shaft. Once the new follicle forms, the lumens of the new and old follicles fuse through an unknown mechanism [101]. The shaft from the old follicle is lost through the process of exogen, or shedding, although the exact mechanism is unknown [102]. During catagen, proliferation ceases and the lower anagen follicle undergoes cell death and regresses. The follicle then remains in telogen awaiting cycle activation (FIG 1.2, reviewed in [103-105]).

1.2.4 HH during epidermal development and homeostasis

Hair follicles (HFs) require HH at several stages throughout epidermal development/homeostasis. HF morphogenesis begins with placode formation. This process requires Wnt signaling. Animals lacking the Wnt effector β-catenin [106], or expressing the Wnt inhibitor DKK1 [107] do not form hair placodes, and fail to develop hair follicles. Although HH is not required during HF initiation, established hair placodes express SHH ligand (SHH)[22, 108]. As such, in *Shh-/-* animals, follicles halt after initiation [21, 108]. HH-blocking antibody (moAB) treatment on pregnant dams also causes stalling after HF initiation in newborn pups [109]. Abortive follicles in *Shh-/-* skin lack a recognizable dermal papilla (DP), and dermal condensates are negative for *Ptch1* and *Gli1* [21, 108]. Without SHH the DP fails to up-regulate several genes including Noggin, which is required for follicle maturation [110].

In adult telogen skin, HH is active in three distinct cell populations. These include the secondary hair germ (SHG), the upper bulge region (UB), and the mechanosensory touch dome (TD) (FIG 1.3) [111]. Although embryonic skin expresses SHH, its expression in telogen epidermis is negligible. This indicates that HH ligand must be coming from a non-epidermal cell population. Work from Brownell et al., showed that the UB and TD receive HH from the sensory nerves which innervate them [111, 112]. Removal of these nerves causes loss of HH activity in both the UB and TD compartments, but not the SHG. This suggests that the SHG does not receive neural SHH [111, 112]. Although surgical denervation ablates HH activity in the UB, this does not affect the hair cycle [111, 113].

HH is also important for hair cycling. Hair cycle initiation is a two-step process that begins with activation of stem cells in the SHG [100]. The SHG receives signals from the adjacent DP. These signals include BMP-inhibition [100], TGF-β [114], PDGF [115], and FGF7

[100]. The proliferating SHG gives rise to the hair follicle matrix, a population of transit amplifying cells which contributes to the growing anagen follicle [100]. A sub-set of matrix cells express high levels of SHH. When SHH is absent, proliferation within the SHG is decreased and anagen cannot progress past initiation [100]. Reminiscent of HF development, SHH is required for anagen progression, but not initiation. As such, HH monoclonal antibody-treated telogen skin cannot progress through anagen [109]. In addition, human patients on vismodegib, a HH-antagonist, often develop alopecia (hair loss) [116].

1-2 days after the SHG begins to proliferate, the stem cells within the HF bulge become proliferatively active and migrate downward contributing to the growing follicle [117]. This activation requires SHH signaling from the SHG-derived matrix [118]. Matrix cells secrete SHH ligand, which in turn activates HH target genes within the HF bulge [118]. In the absence of SHH, bulge stem cells remain quiescent and fail to contribute to the growing follicle [118]. The ability of bulge stem cells to respond to matrix-derived SHH is aided by the expression of HH co-receptor GAS1 [118]. GAS1 promotes HH activation within the bulge, and as such *Gas1-/-* animals display decreased proliferation in bulge stem cells [118].

SHH from the matrix is also important for signaling between the HF and the DP. In the absence of SHH, the DP fails to upregulate the BMP-inhibitor Noggin and FGF7, which are important for hair bulb proliferation [118].

1.3 Innervation During Epidermal Development and Homeostasis

1.3.1 Nerve functions in the skin

Being able to sense the environment is essential for survival. The epidermis contains several different types of nerve endings, with a diverse set of functions. Epidermal nerves sense

temperature, acid, pain, touch, and pressure. They then relay these signals to the brain triggering a response. Epidermal innervation relies on neurotrophic factors. The skin expresses these factors during development to maintain innervation (reviewed in [119]).

In mammalian hairy skin, there are several different types of nerve endings. Most cutaneous nerves have sensory functions, while a small subset has sympathetic function. These sympathetic nerves are located exclusively in the dermis, where fibers innervate blood and lymphatic vessels, sweat glands, hair follicles, and the arrector pilli muscle (reviewed in [120, 121]). Cutaneous nerves vary in their myelination and adaptation speed to stimuli. This variation allows their diverse functions. There are two groups of nociceptive or pain-sensing nerves in the skin [122]. Myelinated Aδ fibers are responsible for the "fast" and localized first response, while unmyelinated C fibers mediate the "slow" diffuse pain response [123]. Touch sensation is mediated by low-threshold mechanoreceptors, which contain myelinated Aβ fibers (reviewed in [124]). These Aβ fibers are either slowly adapting (SA), which display sustained firing in response to stimuli, or rapidly adapting (RA), which fire at the start and end of stimulation [125]. SA and RA Aβ fibers can be divided further into type I and type II fibers. SAI and SAII can be differentiated by their firing rates, receptive fields, and tuning properties [126]. RAI and RAII also differ in their receptive fields [127-129].

This diverse group of sensory fibers are organized into nerve "end organs". These end organs are encapsulated nerve endings which sense specific stimuli such as sensation of skin stretch, pressure, vibration, and hair movement (reviewed in [130]). Lanceolate endings wrap hair follicles. They contain RA fibers to sense hair movement [131]. Free nerve endings are present throughout the epidermis. They contain Aδ and C-fibers to sense pain [132]. Touch domes (TDs) contain Merkel cell (MC)-neurite complexes. They contain SAI fibers that sense

detailed spatial features [133]. Ruffini endings are present in the dermis, and contain SAII fibers thought to sense skin stretch [134]. Pacinian corpuscles, also located in the dermis, contain RAII fibers which sense vibration [135]. Meissner corpuscles are located in glabrous (non-hairy) skin and contain RAI fibers to sense object slip and grip [136].

1.3.2 Innervation is linked to follicular development and homeostasis

During development, sensory innervation coincides with hair follicle (HF) morphogenesis. There are no nerves present in the epidermis prior to HF induction. During early induction, nerve fibers branch towards stage 1 and 2 follicles (E16) [137]. At embryonic day 18, nerve fibers approach two target positions. The first target is the HF opening, described as follicular (neural) network A (FNA). The second is the region below the sebaceous gland, follicular (neural) network B (FNB) [138]. After birth, nerves secrete sensory neuropeptides Substance P (SP) and Calcitonin gene related peptide (CGRP), which facilitate neurotransmitter release [139, 140]. During anagen, branching continues and innervation around HFs, vasculature, and the arrector pili muscle increases in density and organization. Nerve fibers in the FNB, which first appear circumferentially, branch longitudinally. At P17, follicles begin the initiation of the first hair cycle. Throughout cycling, FNA innervation decreases, while FNB innervation remains stable (FIG 1.4) [137].

After morphogenesis, follicles continue to cycle through growth, regression, and rest phases. As this cycling occurs, the follicle experiences many structural changes. Not surprisingly, as these changes occur, the innervation pattern and density of the follicle and surrounding epidermis/dermis also changes (reviewed in [141]). As the follicle enters anagen, innervation of both the FNA and FNB increases in density [138]. This is presumed to be via

increased expression of Neural Cell Adhesion Molecule (NCAM) and Growth Associated Protein 43 (GAP-43) which are involved in neurite outgrowth [138]. Innervation is also present around the newly formed anagen bulb, although in only a small percentage of follicles [138]. In addition to follicular innervation, the nerves throughout the dermis also experience remodeling throughout the hair cycle. Dermal nerve fiber density and arborization of the deep cutaneous nervous plexus also increase in early anagen [138]. In late anagen, as follicles reach their peak growth, NCAM is down-regulated and innervation reverts to telogen levels [138].

The link between innervation and hair follicle morphogenesis/cycling suggests a possible functional role for innervation. Surgical denervation is a method that allows us to investigate how innervation affects skin function. This technique involves making a dorsal-lateral incision and snipping or plucking the cutaneous nerves from where they exit the body wall and enter the skin (see chapter II for a more detailed description). Nerves are removed or cut on one side of the mouse, leaving the other side as a sham operated control. This allows comparison of denervated and intact skin from the same animal.

Maurer et al., used this technique to examine whether intact innervation is important for hair follicle cycling [113]. In this study, both spontaneous and induced (via depilation or cyclosporine treatment) anagen were compared in intact and denervated skin. Surprisingly, despite the temporal link between hair cycling and innervation changes, the group found no significant differences in anagen induction or progression. These results indicate that innervation is not essential for hair cycling.

Because innervation and HF morphogenesis begin in utero, surgical denervation is not a viable method to study the functional relationship. However, mice which lack certain nerve growth factors, neurotrophins (see section 1.3.3), display defects in epidermal innervation and

can be used to overcome this challenge. Mice which lack nerve growth factor (NGF) display initial epidermal innervation which diminishes throughout development. These mice also display a delay in hair follicle initiation and growth [142]. Similarly, mice which are heterozygous for Neurotrophin-3 (NT-3) also display a delay [143]. In contrast, animals which over-express NT-3 in the skin display accelerated HF morphogenesis [143]. Although this method does not directly test whether innervation is essential for HF morphogenesis, it does suggest a potential role for epidermal-neural signaling during HF development.

1.3.3 Neurotrophins are required for nerve maintenance and specificity of target innervation

Several growth factors are essential for epidermal innervation. As nerves branch towards their targets, neurotrophic factors bind receptors on nerve terminals. These complexes are then internalized, activating signaling pathways which promote cell survival. Neurons which don't receive signal, undergo programmed cell death (reviewed in [119]).

The epidermis expresses several neurotrophic factors including: nerve growth factor (NGF), brain-derived neurotrophic factor (BDNF), and neurotrophins 3 and 4 (NT-3, NT-4). These 4 factors display ~50% conservation in amino acid sequence [144]. Neurotrophins bind a family of receptor tyrosine kinases (RTKs) called Tropomyosin receptor kinases (Trks) [145]. Each neurotrophin binds fairly specifically with a Trk family member, where NGF binds TrkA, BDNF and NT-4 bind TrkB, and NT-3 binds TrkC, although it can also bind TrkA and B [146, 147]. All neurotrophins also bind p75, a tumor necrosis factor superfamily member, which aids in binding specificity and affinity with Trk receptors [148-151]. Once bound, neurotrophin-receptor complexes are transported to the sensory neuron cell body. Then, through a series of

signaling events, gene expression changes support neuron survival, proliferation, outgrowth, synapse formation, and migration (FIG 1.5) [147].

Different neurotrophic factors recruit nerve fiber subtypes to specific regions in the epidermis. NGF expression specifically recruits TrkA positive fibers. These neurons display enrichment for CGRP and SP. These TrkA positive nerves are either lightly myelinated or unmyelinated, and primarily sense pain as free nerve endings [152]. NT-3-TrkC promotes survival of slowly adapting type I fibers (SAI), which innervate TDs. In NT-3-/- animals, SAI fibers are absent and TDs are gradually lost, along with associated MCs [153]. Both Meissner endings (in glabrous skin) and hair follicle endings require BDNF/TrkB signaling [154]. NT-4 overexpression causes enlarged Meissner endings, but NT-4 knockout animals have no significant defects in epidermal innervation [155], perhaps due to redundancy with BDNF.

1.3.4 GFL family promotes cutaneous nerve survival

Like Neurotrophins, the Glial cell line-derived neurotrophic factor (GFL) family also promote nerve survival. GFL family members include: GDNF, Artemin, Neurturin, and Persephin. These GFL ligands signal through a receptor complex containing a specific GFL receptor (GFRα1-4), and Ret tyrosine kinase. GDNF supports nociceptive (pain sensing) neurons in the skin [156], while Artemin overexpression leads to increased hot and cold sensitivity [157]. Neurturin overexpression in the skin also causes increased sensitivity to chemical, thermal, and mechanical stimuli [158], while Persephin doesn't appear to have a role in peripheral nerves [159].

1.4 The Touch Dome: A Mechanosensory Organ

1.4.1 Merkel and his cells

In 1875, Friedrich Merkel observed a novel population of large clear oval cells associated with cutaneous nerves [160]. Based on their location, Merkel called these cells "tastzellen" or "touch cells". This population is now referred to as Merkel cells (MCs). MCs are present in glabrous and hairy skin. In glabrous skin, MCs are located near sweat gland ridges, and sporadically throughout the basal layer of the epidermis. In murine hairy skin, MCs are present within a mechanosensory organ called the touch dome (TD) and in vibrissa follicles present in the whisker pad. The TD, originally named haarscheibe or "hair disc", was characterized by Felix Pinkus in 1902. Pinkus described TDs as specialized discs of epithelial cells [161, 162]. Later, William Straile discovered the association of mouse TDs with large tylotrich follicles, the largest and first to appear during development [163]. Ainsley Iggo confirmed TD innervation and mechanosensory ability in 1969 [133]. In mouse skin, TDs have two compartments, a columnar epidermal compartment comprised of Keratin 17 (K17) positive keratinocytes, and underlying neuroendocrine-like MCs expressing simple Keratins 8, 18 and 20 (K8, K18, K20) (FIG 1.6) [164-168]. These underlying MCs are associated with slowly adapting type 1 nerve fibers (SA1) [133].

1.4.2 TD development requires a complex signaling cascade

Mouse TDs are associated with tylotrich follicles, also called "guard" hairs. As such, their development is linked. Guard hair follicle induction begins at embryonic day 14 (E14) [169]. One day later (E15), MCs are present near guard hair germs. MCs surround the guard

hair canal, or infundibulum until birth. Then, they migrate into a characteristic crescent shape, located caudal to the follicle [170, 171].

The TD requires many factors for development and maintenance. These factors include ATOH1, SHH, and others. MC specification requires the helix-loop-helix transcription factor, ATOH1 [172, 173]. Expression of ATOH1 is also sufficient to drive ectopic MC production in the epidermis [174]. MC specification also requires SHH, and SHH-/- skin does not form MCs [170]. SHH over-expression in the skin results in ectopic MC production [175]. Although all HFs express SHH, MCs are only present near guard follicles. Polycomb repressor complex 2 (PCR2) activity in non-guard follicles prevents MC formation. As such, loss of the PCR2 complex results in ectopic MC formation near non-guard follicles [175]. MC development relies on HF-derived SHH; however it's important to note that most MCs are not derived from the SHH positive HF lineage [170].

The origin of MCs has been controversial. Merkel cells express both epidermal (keratins) and neuroendocrine markers. Early reports suggested a neuroendocrine lineage [176], but more recent reports suggest MCs derive from a Keratin 14 (K14) positive progenitor [177, 178]. Other studies suggest that in hairy skin, MCs come from the K17+/GLI1+ epidermal TD [112, 179]. The controversy over MC origin stems from the apparent slow turnover of these cells, which makes tracing difficult. Lineage tracing experiments have suggested that MCs can have a lifespan of up to 7 weeks [112, 179, 180]. However, these results are contradicted by a recent study from Marshall et al., who observed rapid remodeling of MCs and TD innervation throughout the hair cycle [181]. During anagen, MCs and light touch response diminishes, but returns when follicles re-enter telogen. Remodeling during the hair cycle has been previously reported, although these studies observed the opposite phenomenon, an increase in MCs during

anagen [182, 183]. This difference in observations could be due to species specificity, as many initial MC studies were performed in rats, or due to sampling methods. Based on these conflicting results, more detailed studies are required for full understanding of Merkel's cells.

1.4.3 Innervation is required for TD maintenance

Although TD keratinocytes are derived from the K14 positive ectoderm, resident stem cells maintain the adult TD. These stem cells require innervation for maintenance. Sensory nerves that innervate the TD secrete SHH ligand to activate HH signaling. As such, surgical denervation or *Shh* deletion in nerves results in loss of TDs [112, 184].

Together, these studies suggest that resident stem cells in the TD potentially maintain TD keratinocytes and underlying MCs. However, more recent studies suggest uni-potent ATOH1+ progenitors maintain MCs [180]. Perhaps, within the TD there are two pools of progenitors: K17+/ATOH1- cells that maintain TD keratinocytes, and K17+/ATOH1+ cells that maintain the MC population [180].

1.5 Basal Cell Carcinoma: A Hedgehog-Driven Cancer

1.5.1 Introduction to BCC

Basal cell carcinoma (BCC) is the most common human cancer, with millions of new cases in the United States each year [185, 186]. BCC was first described in the late 1820's by Dr. Arthur Jacob [187], and was named after its histological resemblance to the basal cells of the epidermis [188]. BCC tumors most often occur on regions of sun-exposed skin, especially the face and scalp [189] (reviewed in [190, 191]), and BCC has several subtypes. Superficial BCCs (sBCC) are flat lesions with fine telangiectasias, small erosions, and changes in pigmentation.

Nodular BCCs (nBCC) appear as raised lesions with large tumors nests. Invasive BCCs (iBCC) appear as structure-less, flat, shiny red lesions [192]. All BCC tumors are caused by deregulated HH signaling, regardless of subtype (reviewed in [193, 194]).

1.5.2 BCC and Hedgehog

HH was discovered as the cause of BCC through sequencing patients with Gorlin syndrome, an autosomal dominant disorder also known as nevoid basal cell carcinoma syndrome (NBCCS) [195-198]. Gorlin patients develop many BCCs throughout their lifetime. They also display other abnormalities including pitted palms and soles, and predisposition for several other tumor types including medulloblastoma (MB) [199]. Gorlin syndrome maps to chromosome 9q22. This region contains the gene encoding the HH pathway receptor PTCH1 [195, 197]. Loss of function mutations in *PTCH1* cause up to 90% of BCC tumors. These mutations prevent PTCH1 from inhibiting SMO, rendering the pathway constitutively active. Gorlin patients harbor germline mutations in one copy of *PTCH1*. For these patients, BCCs occur when the remaining copy sustains a loss-of-function mutation. Although *PTCH1* mutations cause most BCCs, activating *SMO* mutations cause a subset (~10%) of BCC tumors (FIG 1.7) [200].

1.5.3 Targeting Hedgehog in BCC

The most common treatment for BCC is surgical excision. Often this is curative. Some BCCs which are invasive, or occur in areas that are difficult to resect, such as the eyelid, cannot be surgically removed. Surgical resection is also not practical for Gorlin patients who can develop hundreds of BCCs. These patients benefit from alternative treatments, such as pharmacological HH inhibition.

In the 1960s, farmers observed a strange phenomenon in their livestock. Cows and sheep fed *Veratrum californicum*, a wild corn lily, gave birth to calves with holoprosencephaly (HPE). HPE results in an absence of midline facial structures with a proboscis and a cyclopic eye [201-204]. In 1996, Chiang et al., linked this observation to HH when they observed a similar phenotype in mice lacking Sonic hedgehog (SHH) [205]. In addition, humans with *SHH* mutations also display a similar phenotype [206, 207]. The teratogenic effects of *V. californicum* come from the alkaloid cyclopamine [208-210]. Cyclopamine inhibits HH signaling via direct binding to SMO [211-214].

Cyclopamine is not effective for treating BCC due to toxicity. However, it did highlight SMO as a potential target to treat BCC [215]. Several compounds now exist that inhibit SMO. One compound, vismodegib, is currently prescribed for Gorlin patients and advanced/metastatic BCC patients [216-218](reviewed in [219]). In phase I clinical trials, approximately 50% of patients with advanced BCC responded to treatment. Some patients even showed full regression of tumors [116]. In trials on Gorlin patients, vismodegib regressed most existing tumors, and prevented new lesion formation [220]. Despite the potency of vismodegib, often this treatment is only effective when patients remain on the drug. Tumor nodules disappear upon drug treatment, but regrow when treatment stops [221-223]. This indicates that treatment is ineffective in completely ablating tumor initiating cells. Additionally, there are significant side effects of constant HH blockade. These include muscle cramps, alopecia, ageusia (loss of taste), and others. These side effects can diminish quality of life for patients on vismodegib [220].

Besides the side effects, tumors can also be or become resistant to vismodegib. In phase I and phase II clinical trials on advanced and metastatic BCC, 30-50% of patients showed a response to treatment [116, 217, 218], suggesting that 50-70% of these patients displayed

resistant disease. Resistant tumors either have primary mutations in SMO, or they acquire additional mutations during treatment. These acquired mutations are most often in SMO, but in rare cases other downstream HH factors [221, 224-226]. Several SMO mutations within and outside the vismodegib binding pocket can confer drug resistance. Mutations outside the binding pocket can also increase the baseline activity of SMO. These mutations could be oncogenic drivers of BCC. Mutations in HH factor Suppressor of Fused (SUFU) and amplification of GLI2 also can confer resistance to vismodegib, but are not usually primary drivers [225, 227].

In addition to vismodegib, there are several other inhibitors that bind SMO [228-232]. Many of these inhibitors are structurally similar to vismodegib. Sonidegib, is a structurally similar SMO inhibitor that recently gained FDA approval for treatment of BCC [233]. Itraconazole is an FDA-approved antifungal that can inhibit SMO at a site distinct from vismodegib [234]. Although SMO inhibition can be effective to treat BCC, SMO mutations are a leading cause of drug resistance. Exome sequencing of resistant BCCs uncovered SMO mutations in 42% of tumor samples [225]. Therefore, targeting the HH pathway downstream of SMO is an attractive alternative. PSI, an atypical protein kinase C ι/λ (aPKC ι/λ) inhibitor, inhibits HH by blocking GLI activation. It also can inhibit BCC growth [235]. Arsenic trioxide also inhibits HH activity, by promoting GLI degradation [234]. However, clinical trials combining itraconazole and arsenic trioxide were unsuccessful [236].

1.6 Mouse Models of BCC

1.6.1 Introduction

To study BCC, we use a variety of mouse models. These models serve as tools to aid in the understanding of BCC, and to develop/test new treatments. The following represents a brief introduction to the contributions these models have made to our understanding of BCC.

1.6.2 Sonic hedgehog overexpression (embryonic)

To model BCC in mice, Anthony Oro et al., generated a transgene containing *Shh* downstream of the *Keratin 14* (*K14*) promoter (*K14-Shh*) [237]. This promoter is active at embryonic day 9.5 in the ectoderm, and later in the developing epidermis [238, 239]. *K14-Shh* mice display skin and skeletal abnormalities resulting in perinatal lethality. Importantly, these mice display increased expression of HH target genes (*Ptch1*) and BCC-like proliferations throughout the epidermis. Skin transplants from *K14-Shh* mice onto *scid/scid* mice form microscopic BCC lesions [237]. These animals represent the first mouse model for human BCC, and highlight *Shh* as a potential oncogene in human cancers. However, a major limitation of this study is that *Shh* is not a primary driver of human BCC.

1.6.3 Mutant Smoothened expression (embryonic)

In addition to loss of *Ptch1*, mutations in *Smo* can also drive BCC [200]. One of the first mutations identified in patients contained a G1604T mutation. The resulting protein variant was named SMO-M2 [200]. To test the oncogenic potential of SMO-M2 *in-vivo,* Xie et al., cloned the mutated sequence downstream of the *Keratin 5* (*K5*) promoter (*K5-Smo-M2*) [200]. *K5* drives expression throughout the epidermis [240]. Unlike the *K14-Shh* mice, *K5-Smo-M2* skin

macroscopically appears normal. These mice also lack the severe skeletal abnormalities seen in *K14-Shh* animals. However, upon microscopic examination, *K5-Smo-M2* skin displays characteristics reminiscent of human BCC. These mice display widespread epidermal hyperplasia, with lesions branching into the dermis, and increased expression of *Ptch1*. This is much like the phenotype seen in *K14-Shh* mice [200, 237]. Overall, this model identified activated SMO as a driver for human BCC. Unlike the *K14-Shh* model, *K5-Smo-M2* mice provided a direct model designed from patient mutations.

To overcome the embryonic lethality of SMO-M2 expression, Grachtchouk et al., generated transgenic mice expressing SMO-M2 under the control of the ΔK5 promoter. This truncated 1.3kb version of the K5 promoter drives expression in a subset of cells that express K5 [241-243]. The epidermis of *ΔK5-Smo-M2* is HH-active and hyperproliferative. However, these lesions do not resemble BCC [244]. They instead more closely resemble basaloid follicular hamartomas (BFH), benign slow growing skin tumors that resemble primitive hair follicles [244]. When compared to lesions from *K5-Smo-M2* mice and *K5-Gli2* mice (see section 1.6.5), BFH lesions display decreased HH target gene expression and lack expression of G_1 cyclins, D1 and D2 [244, 245].

1.6.4 Patched1 +/- plus radiation (UV/IR)

Ptch1 mutations cause BCCs in Gorlin patients, as well as in sporadic BCC patients. Unfortunately, *Ptch1-/-* mice do not survive, making them unsuitable for adult BCC studies [41]. *Ptch1+/-* mice display many characteristics of Gorlin syndrome including polydactyly and predisposition for medulloblastoma. However, they do not develop BCCs [41, 246]. Mutagenic chemicals, ultraviolet (UV) or ionizing (IR) radiation also do not cause BCCs

in wild type mice [247]. However, when *Ptch1*+/- mice receive UV or IR, micro- and macroscopic BCCs and trichoblastomas form after 6-12 months [248, 249]. Sequencing of these lesions revealed loss of heterozygosity of *Ptch1*. In addition, a subset of tumors had mutations in the tumor suppressor *p53*. This is consistent with human BCC sequencing data [248, 250, 251].

1.6.5 Overexpression of GLI transcription factors (embryonic)

The GLI family of proteins (GLI1-3) act as transcriptional effectors of the HH signaling pathway [49-51]. Grachtchouk et al., tested the ability of GLI2 to drive BCC formation by cloning GLI2 downstream of the bovine K5 promoter [244]. This promoter drives expression in the basal layer of the skin and hair follicles [243]. These mice form macroscopic tumors by 3 months of age, many of which resemble human BCC. These BCC-like lesions display increased expression of HH target genes, and BCC markers including Keratin 17 (K17), Bcl-2, and K5 [245]. These mice represent one of the first models for BCC in adult animals. They also highlight GLI2 as an important effector of HH signaling in BCC.

To test whether GLI1 is a downstream HH effector in BCC, Nilsson et al., cloned GLI1 downstream of the bovine K5 promoter [252]. These mice develop tumors within 1-13wks of birth, and die prematurely between 1-6 months. Tumors include nodular and superficial BCCs, trichoepitheliomas, and trichoblastomas. Sequencing of these tumors revealed no mutations in known oncogenes P53 and RAS, indicating that GLI1 is sufficient to drive cutaneous tumor formation.

1.6.6 Mutant Smoothened expression (adult)

Activating mutations in *SMO* account for approximately 10% of human BCC tumors [200]. Embryonic expression of oncogenic SMO-M2 results in a BCC phenotype. However, these mice are not viable and therefore an indirect model to study adult BCC [200]. Animals that express *Smo-M2* under the *ΔK5* promoter are viable, but do not develop BCC [244]. Because most BCCs arise in adult patients [116, 253], a conditional model of *Smo-M2* expression provides a more direct model for human BCC. Mao et al., developed an inducible system, where a conditional *Smo-M2* allele is cloned downstream of the ubiquitous *Rosa26* promoter (*Rosa26-Smo-M2*) [254, 255]. When combined with different tamoxifen inducible Cre recombinase drivers, this allele allows for spatial and temporal control of SMO-M2 expression. Combination of conditional *Smo-M2* with a ubiquitous *Cre-ER* allele (*CAAGS-Cre-ER*) yields several tumor types including rhabdomyosarcomas, medulloblastoma, and BCCs [255].

To study the effect of SMO-M2 expression in adult skin, Youssef et al., combined the *Rosa26-Smo-M2* allele with K14-CreER[256]. This drives SMO-M2 expression in the basal cells of the epidermis [257]. These mice develop microscopic BCCs 8 weeks after induction [256]. In contrast, SMO-M2 expression in hair matrix cells does not yield BCC tumors [256]. Likewise, expression in bulge cells using various drivers does not induce BCC tumors [256]. Low dose induction of *K14-CreER; Rosa26-SMO-M2* mice results in tumors derived from the interfollicular epidermis. These mice also had rare tumors derived from the infundibulum, or hair follicle opening [256]. Overall, this study suggests an interfollicular cell of origin for SMO-M2-driven BCC.

Follicular stem cells are unable to form tumors upon SMO-M2 expression. However, upon wounding these cells migrate to the wound site, where they acquire the ability to initiate BCC

tumors [258]. Taken together, these results suggest that the microenvironment can influence SMO-driven BCC formation.

1.6.7 Conditional Patched1 deletion (adult)

Conventional *Ptch1* knockout mice are not viable, and the *Ptch1 +/-* plus radiation model is indirect, due to the unknown tumor genotype. Therefore, conditional alleles of *Ptch1* present a more experimentally tractable model for human BCC tumors. Combining conditional alleles with Cre recombination drivers allows temporal and spatial control of *Ptch1* deletion. There are several conditional *Ptch1* alleles used to study BCC tumorigenesis.

Ptch1neo/neo mice allow conditional deletion of exon 3 of PTCH1. Exon3 deletion via a ubiquitous Cre-driver is lethal at E9.5-10, consistent with conventional knockouts [259]. However, deletion using *K6-Cre* (coupled with Retinoic Acid (RA) treatment to increase recombination) causes BCC in 100% of animals after 16 weeks [260-262]. Exon 3 deletion using *K14-Cre* yields tumors by 3-4 weeks [263]. Similarly, *Ptch1* deletion using *MX1-Cre* (a widespread driver) causes BCC at 8-10 weeks [263].

Ptch1$^{c/c}$ mice allow conditional deletion of exon 2 [264], and *Ptc*$^{F1\text{-}2m}$ mice allow conditional deletion of exons 1B, 1, 1A, and 2 [265]. Alternative splicing events make these models "leaky" in their ability to delete *Ptch1*, and less ideal for BCC studies [266]. *Ptch1neo(fl)Ex2(fl)* mice allow conditional deletion of exon 2[267]. When combined with *K5-Cre*PR1[268]*, which upon RU486 administration drives recombination in epidermal basal cells, BCC tumors form throughout the skin [267]. Like the SMO-M2 model, wounding enhanced the formation of BCC-like lesions [258, 267].

Ptch1^{lox} mice allow conditional deletion of exon 3 [259]. Combination of *Ptch1*^{lox} alleles with *K14-Cre*, which drives recombination primarily in follicular basal cells of the epidermis [269], strikingly has little effect on epidermal development [46]. However, between 24-28 days post birth *K14-Cre;Ptch1*^{lox} mice develop BCC-like lesions [270]. In contrast, deletion of *Ptch1* with *K5-Cre*, which drives broad recombination through the epidermis and follicles, is perinatal lethal [46]. These mice display disturbed hair follicle morphogenesis and mild epidermal hyperplasia, which does not resemble BCC. When Ptch1^{lox} alleles are deleted in adult epidermis using tamoxifen inducible *K14-CreER*^{T2} [271], mice display only a mild hyperplastic phenotype after 4 weeks [46].

Ptch^{flox} mice allow conditional deletion of exons 8 and 9 [272]. These mice do not display any "leaky" expression or disturbed splicing, and as such are ideal for tumor studies [272]. Exon 8+9 deletion via *Rosa26-CreERT2* causes microscopic BCC-like tumors 45 days after induction with tamoxifen (TAM). These tumors form preferentially in ear and tail skin [273, 274]. Deletion with *K5-Cre-ER*^{T} [275], causes BCC-like tumors in ear, tail, and hairy skin post TAM [274]. However, BCC tumors also arose in control animals (*K5-Cre-ER*^{T}*;Ptch*$^{flox/flox}$, no tamoxifen administration). This highlights leaky recombination activity of *K5-Cre-ER*^{T} in this model [274].

Since *Ptch1* mutations drive most human BCC tumors, conditional *Ptch1* alleles present the most representative model for BCC. However, differences in tumorigenic response to these conditional alleles highlight the requirement for careful characterization of these models. Based on the above results, in some contexts epidermal populations resist *Ptch1*-driven BCC formation [249, 267], while follicular deletion of *Ptch1* reliably induces BCC-like tumors [46, 262, 263, 267, 270, 273, 274]. To fully understand the cell of origin for *Ptch1*-driven BCC tumors, alleles

that display minimal "leaky" expression and disturbed splicing, such as the *Ptch1*^{lox} and *Ptch1*^{flox} alleles should be combined with reliable, tissue-specific inducible Cre recombinase drivers. By carefully examining the response of epidermal compartments to *Ptch1* deletion, we will better understand the human disease.

1.6.8 Overexpression of GLI transcription factors (adult)

Full-length GLI2 serves as a weak transcriptional activator, and is able to induce BCC formation after 4 months of expression [244]. However, removal of the N-terminal repressor domain allows GLI2 to act as a more potent activator of HH signaling [276, 277]. To investigate the tumorigenic response to GLI2ΔN expression, Grachtchouk et al., utilized a multi-allele tetracycline-controlled expression system. In this model, *Gli2ΔN* is cloned downstream of a tetracycline responsive element (*tetO-Gli2ΔN) [278]*. This element requires doxycycline (doxy) administration in the animal's food or water, and tetracycline (rtTA), which in this system is expressed conditionally under the control of the ubiquitous *Rosa26* promoter (*Rosa26-LSL-rtTA*). Conditional expression of rtTA requires deletion of a floxed stop cassette by Cre recombinase. When combined with a tissue specific Cre driver, this system allows *Gli2ΔN* to be turned on (+doxy) and off (-doxy). In this study, Grachtchouk et al., used *K15-CrePR1* which drives recombination in the lower hair follicle upon RU481 administration [279]. In the presence of doxy, microscopic BCCs arise in *K15-CrePR1;Rosa26-LSL-rtTA* mice after 3 weeks [278]. These tumors are nodular and derive from the secondary hair germ or lower bulge. *Gli2ΔN* expression driven by *Lgr5-CreER,* which requires tamoxifen and is active in a more restricted population of the lower bulge and SHG, also causes nodular BCCs [278]. Broad targeting of the epidermis via *K14-rtTA* or *K5-CreER;Rosa26-LSL-rtTA* causes widespread

tumorigenesis. These tumors derive from the interfollicular epidermis, sebaceous glands, and secondary hair germ. This study highlights the variation in tumor initiating ability amongst the basal cells of the epidermis. However, GLI2 mutations do not drive human BCC, and therefore this model does not directly mimic human BCC mutation status. As such, this remains a powerful model for epidermal transformation, but perhaps not ideal for BCC cell of origin studies.

1.6.9 Summary and future directions

Over the last 20 years, mouse models have given us insight into the genetic basis, cell of origin, and tumor dynamics of BCC. These models have highlighted several potential oncogenes capable of driving transformation in the skin and other organs. These include SHH, GLI1/2, SMO, and the tumor suppressor PTCH1. Variation in tumor initiating ability has uncovered different cells of origin for BCC. Different cell populations rely on specific mutations and levels of oncogenic signal to form tumors. For example, it appears that *Smo-M2* expression via an unnatural promoter in adult mice promotes tumor formation primarily in the interfollicular epidermis (IFE) [256]. In contrast, *Ptch1* deletion in adult mice drives follicular derived tumors [249, 267]. Expression of *Gli2ΔN* causes tumors derived from several epidermal compartments [278]. As research continues, careful dissection of how each epidermal population responds to HH activation is necessary. Studies should employ models that directly mimic human disease, through inducible deletion of *Ptch1* and expression of *Smo*-variants within specific sub-compartments of the epidermis. This will result in more effective targeted therapies and a better prognosis for BCC patients.

1.7 Neural Influence in Cancer

1.7.1 Targeting nerves in cancer

In the past, cancer studies have focused on the acquired mutations which cause tumors and confer drug resistance. However, more recent studies have begun to look at cancer from the perspective of the tumor microenvironment. These studies have given new insight into tumor growth mechanisms, uncovering new therapeutic targets. The tumor micro-environment consists of immune cells, blood vessels, nerves, fibroblasts, and the extra-cellular matrix (ECM). Numerous studies have investigated the roles for each of these cell populations in promoting tumor growth and metastasis (reviewed in [280, 281]).

Peripheral nerves innervate all tumor-prone organs, such as the skin, stomach, pancreas, and prostate. As such, the microenvironment of tumors within these tissues includes nerves. However, a promoting role for nerves in cancer has only gained traction in the last several years. One early indication of a role for nerves in promoting cancer was the correlation between peri-neural invasion and poor prognosis (reviewed in [282]). In addition, *in vitro* co-culture of cancer cells with nerve cells promotes proliferation, and *in vivo* neural stimulation can promote metastasis in several cancer types [283-287].

Direct evidence that neurogenesis promotes cancer progression and metastasis came from Magnon et al., in 2013 [288]. In this study, Magnon et al., used both chemical and surgical denervation to assess the role of nerves in prostate cancer. Their results suggest two distinct roles for innervation in promoting prostate adenocarcinoma. Adrenergic fibers support tumor initiation by promoting cell survival via β2 and β3-adrenergic receptors [288]. In contrast, cholinergic fibers promote metastasis through Cholinergic Receptor Muscarinic 1 (CHRM1)

signaling [288]. They also found an association between increased nerve density and poor prognosis in human samples [288].

Chemical and surgical denervation can slow disease progression in several animal models of cancer. Sympathectomy improves survival of rats injected with BP6-TU2 fibrosarcoma cells, presumably by disrupting norepinephrine mediated proliferation of tumor cells [289]. Surgical and chemical denervation also suppresses tumorigenesis in mouse gastric cancer models potentially through disrupting Wnt signaling [290]. Chemical denervation using capsaicin also delays tumor formation in pancreatic ductal adenocarcinoma models by inhibiting inflammation associated with oncogenic Kras expression [291].

1.7.2 A potential role for nerves in BCC

The epidermis displays dense and diverse innervation (see chapter 1.3). Since nerves promote other epithelial cancer types, one can imagine a promoting role in BCC tumorigenesis. In addition, cutaneous nerves promote psoriasis through Calcitonin gene related peptide (CGRP) signaling [292], and sympathetic innervation promotes growth of melanoma tumor cells through an unknown mechanism [293]. Epidermal sensory nerves also secrete HH ligand to activate signaling (see chapter 1.2) [111]. The ability of these nerve to activate HH make them an intriguing target for a HH-driven cancer like BCC.

1.8 Summary and Remaining Questions

Recent progress has increased our understanding of BCC. Yet, to further advance we must address new questions. One area of controversy that remains is the cell of origin for BCC. Heterologous mouse models have highlighted variation in the skin's response to HH

deregulation. This has clouded our interpretation. Moving forward, it is important to narrow our focus to models which most closely mimic human BCC. In addition, we must design experiments that allow us to study all aspects of disease progression. This includes tumor initiation, growth rate, response to treatment, resistance, and recurrence.

The role of the tumor microenvironment for BCC is an important aspect of BCC biology that has yet to be fully characterized. Resistance presents a major barrier to effective targeted therapy. As such, the microenvironment presents a potential alternative therapeutic target. I have focused my doctoral research on the following questions. Mainly: "What is the cell of origin for BCC?" and "Can cutaneous nerves promote BCC tumorigenesis?".

In chapter II, I discuss denervation as a tool for studying neural influence in normal and pathogenic skin. In chapter III, I first address the question of BCC cell of origin. For this study, I delete *Ptch1* in distinct cell populations and assess tumor growth. Also in chapter II, I begin to look at the role of nerves in BCC. For this, I use surgical denervation and evaluate the effect on tumor growth. In chapter IV, I characterize tumor formation in a hyper-innervated mouse model. Finally, in chapter V, I discuss the role of PTCH1 homologue Patched 2 (PTCH2) in BCC cell of origin and tumor growth.

1.9 Figures

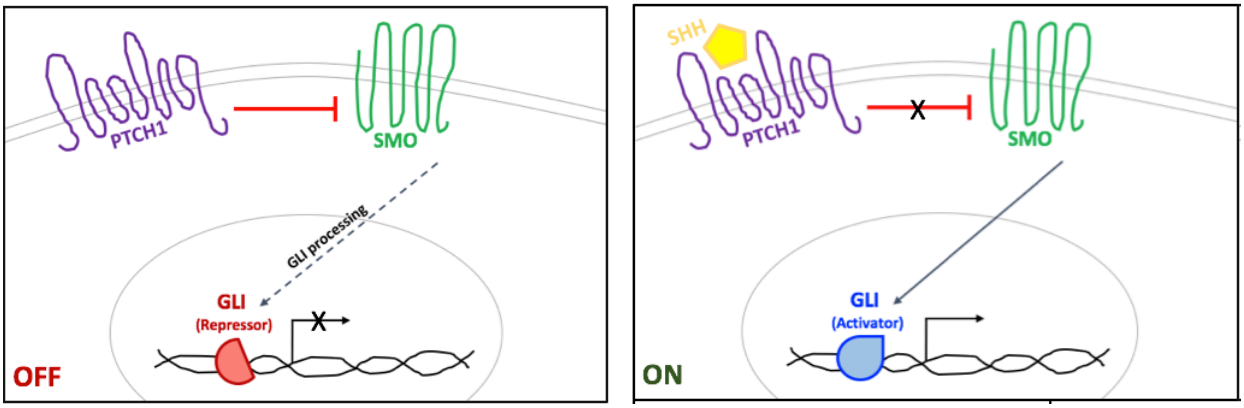

Figure 1.1: The Hedgehog (HH) signaling pathway. (Left) In the absence of signal, PTCH1 inhibits SMO and GLIs are processed allowing them to repress target gene expression. (Right) In the presence of signal, HH ligand binds the receptor PTCH1, relieving inhibition of downstream SMO. GLI transcription factors activate target gene expression.

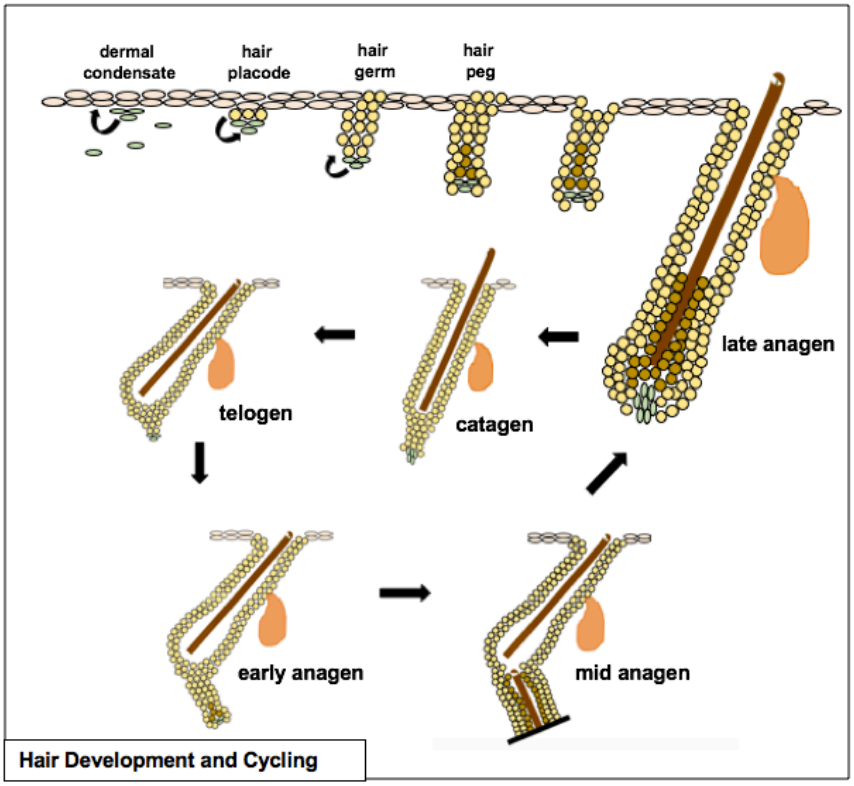

Figure 1.2: Hair follicle morphogenesis and cycling. Hair follicle morphogenesis initiates with dermal cells forming condensates along the epidermis. These condensates signal to the overlying epidermis to thicken and form the hair placode. Cross-talk between the dermal condensate (dermal papilla, DP), and the hair placode facilitates downward growth into the dermis. As the follicle grows it envelopes the DP, and cells at the base proliferate and differentiate to form the layers of the mature follicle and hair shaft. After the initial growth phase (anagen), the lower follicle undergoes cell death and regression (catagen) before entering the rest phase (telogen). The follicle remains in telogen until anagen is initiated spontaneously or through stress or wounding.

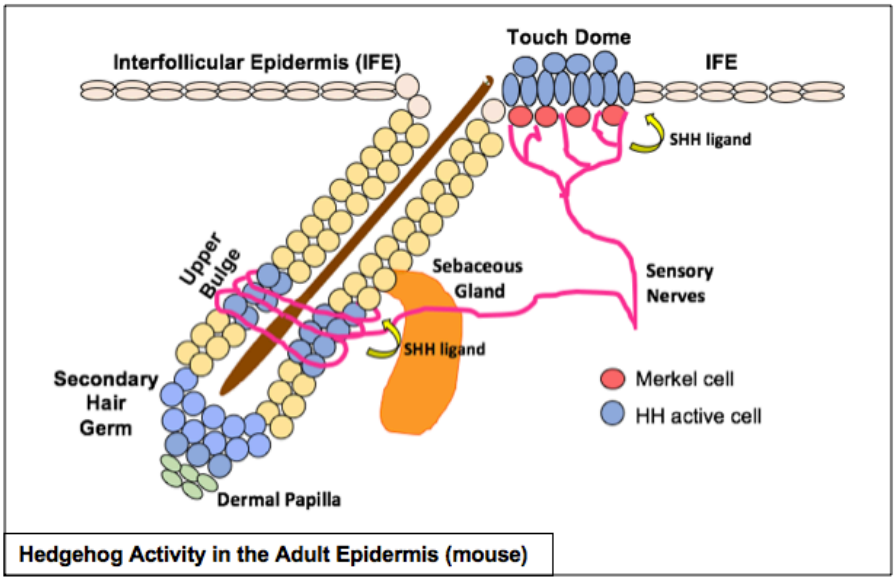

Figure 1.3: HH activity in the adult mouse epidermis. In telogen skin there are three areas of HH activity (blue). The SHG displays active HH signaling, presumably due to signaling from the DP (green). The UB and TD receive HH signal from sensory nerves (pink) which secrete SHH ligand (yellow arrows).

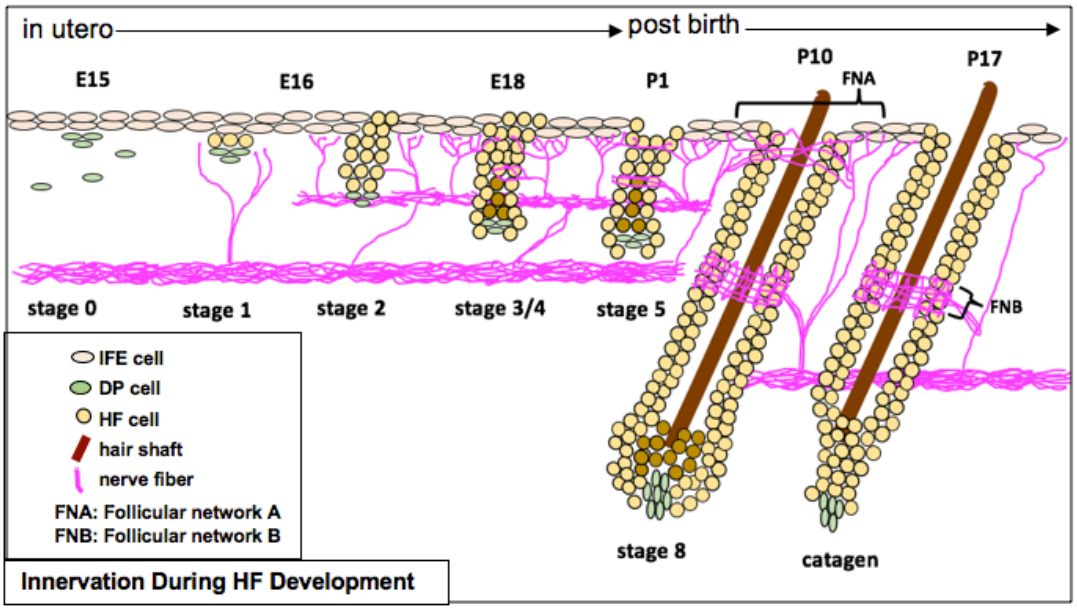

Figure 1.4: Sensory innervation during hair follicle morphogenesis. As the hair follicle initiates and grows downwards into the dermis, sensory nerves branch towards the growing follicles. As follicles mature, nerves are restricted to two zones: follicular neural network A (FNA) at the follicle opening, and follicular neural network B (FNB) in the sub-glandular region. After birth, nerve density decreases in FNA while FNB remains densely innervated. (adapted from [137])

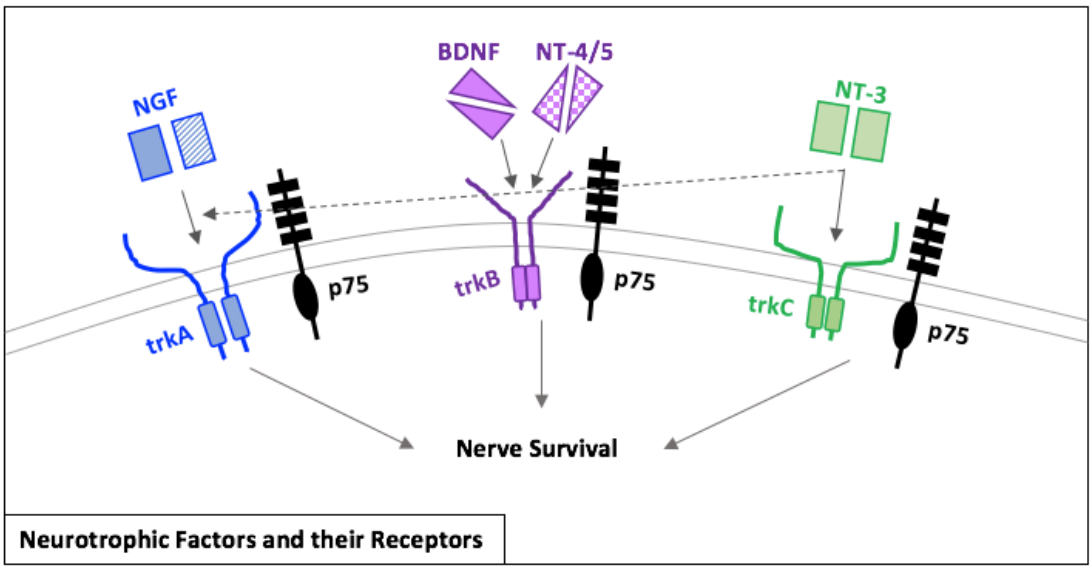

Figure 1.5: Neurotrophic factors promote nerve survival. The members of the Neurotrophin family (NGF, BDNF, NT-3, NT-4/5) are secreted by target cells and bind to specific Trk receptors (TrkA/B/C) and p75 present on nerve terminals. Once bound, the complex is internalized to activate pathways which promote nerve survival. (adapted from [294])

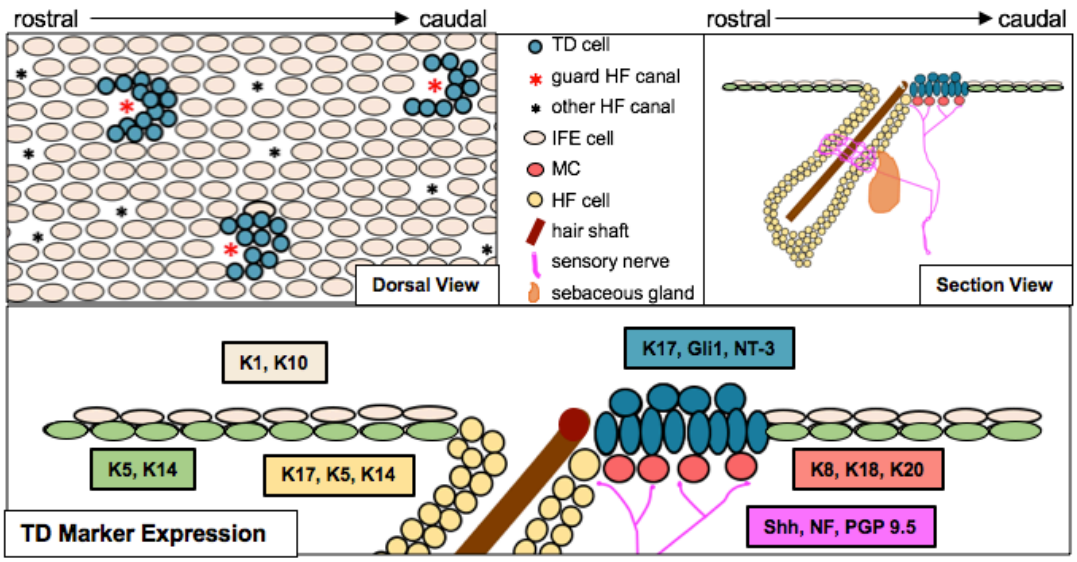

Figure 1.6: Touch dome (TD) morphology and marker expression. (Top) TDs are present in a crescent shape caudally to the opening of guard hair follicles. (Bottom) Marker expression of TDs and surrounding epidermal structures.

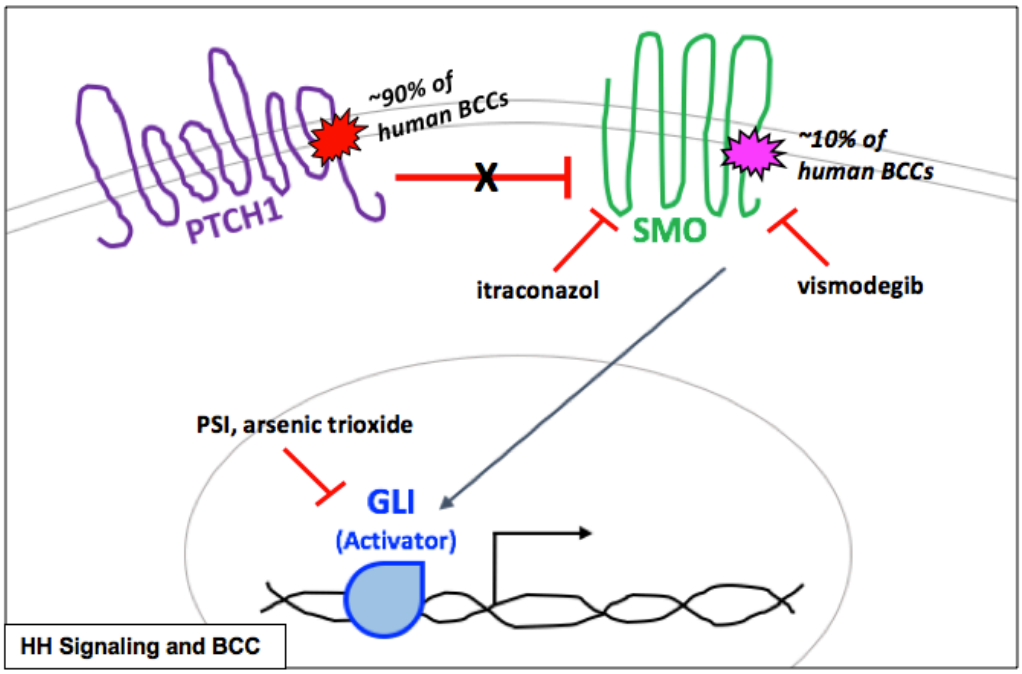

Figure 1.7: HH signaling and BCC. Up to 90% of human BCC tumors are caused by loss of function mutations in PTCH1, while the remaining 10% are caused by activating mutations in SMO. Vismodegib and itraconazol inhibit SMO by binding at distinct locations. PSI and arsenic trioxide block HH through inhibiting GLI activation and promoting degradation (respectively).

1.10 Reference List

1. Nusslein-Volhard, C. and E. Wieschaus, *Mutations affecting segment number and polarity in Drosophila.* Nature, 1980. **287**(5785): p. 795-801.
2. Lee, J.J., et al., *Secretion and localized transcription suggest a role in positional signaling for products of the segmentation gene hedgehog.* Cell, 1992. **71**(1): p. 33-50.
3. Echelard, Y., et al., *Sonic hedgehog, a member of a family of putative signaling molecules, is implicated in the regulation of CNS polarity.* Cell, 1993. **75**(7): p. 1417-30.
4. Riddle, R.D., et al., *Sonic hedgehog mediates the polarizing activity of the ZPA.* Cell, 1993. **75**(7): p. 1401-16.
5. Ingham, P.W., *Localized hedgehog activity controls spatial limits of wingless transcription in the Drosophila embryo.* Nature, 1993. **366**(6455): p. 560-2.
6. Stone, D.M., et al., *The tumour-suppressor gene patched encodes a candidate receptor for Sonic hedgehog.* Nature, 1996. **384**(6605): p. 129-34.
7. Marigo, V., et al., *Biochemical evidence that patched is the Hedgehog receptor.* Nature, 1996. **384**(6605): p. 176-9.
8. Alcedo, J., et al., *The Drosophila smoothened gene encodes a seven-pass membrane protein, a putative receptor for the hedgehog signal.* Cell, 1996. **86**(2): p. 221-32.
9. van den Heuvel, M. and P.W. Ingham, *smoothened encodes a receptor-like serpentine protein required for hedgehog signalling.* Nature, 1996. **382**(6591): p. 547-51.
10. Taipale, J., et al., *Patched acts catalytically to suppress the activity of Smoothened.* Nature, 2002. **418**(6900): p. 892-7.
11. Wang, B. and Y. Li, *Evidence for the direct involvement of {beta}TrCP in Gli3 protein processing.* Proc Natl Acad Sci U S A, 2006. **103**(1): p. 33-8.
12. Pan, Y., et al., *Sonic hedgehog signaling regulates Gli2 transcriptional activity by suppressing its processing and degradation.* Mol Cell Biol, 2006. **26**(9): p. 3365-77.
13. Jiang, J. and C.C. Hui, *Hedgehog signaling in development and cancer.* Dev Cell, 2008. **15**(6): p. 801-12.
14. Ingham, P.W. and A.P. McMahon, *Hedgehog signaling in animal development: paradigms and principles.* Genes Dev, 2001. **15**(23): p. 3059-87.
15. Singla, V. and J.F. Reiter, *The primary cilium as the cell's antenna: signaling at a sensory organelle.* Science, 2006. **313**(5787): p. 629-33.
16. Huangfu, D., et al., *Hedgehog signalling in the mouse requires intraflagellar transport proteins.* Nature, 2003. **426**(6962): p. 83-7.
17. Rohatgi, R., L. Milenkovic, and M.P. Scott, *Patched1 regulates hedgehog signaling at the primary cilium.* Science, 2007. **317**(5836): p. 372-6.
18. Corbit, K.C., et al., *Vertebrate Smoothened functions at the primary cilium.* Nature, 2005. **437**(7061): p. 1018-21.
19. Haycraft, C.J., et al., *Gli2 and Gli3 localize to cilia and require the intraflagellar transport protein polaris for processing and function.* PLoS Genet, 2005. **1**(4): p. e53.
20. Huangfu, D. and K.V. Anderson, *Cilia and Hedgehog responsiveness in the mouse.* Proc Natl Acad Sci U S A, 2005. **102**(32): p. 11325-30.
21. Chiang, C., et al., *Essential role for Sonic hedgehog during hair follicle morphogenesis.* Dev Biol, 1999. **205**(1): p. 1-9.

22. Bitgood, M.J. and A.P. McMahon, *Hedgehog and Bmp genes are coexpressed at many diverse sites of cell-cell interaction in the mouse embryo.* Dev Biol, 1995. **172**(1): p. 126-38.
23. Lee, J.J., et al., *Autoproteolysis in hedgehog protein biogenesis.* Science, 1994. **266**(5190): p. 1528-37.
24. Porter, J.A., K.E. Young, and P.A. Beachy, *Cholesterol modification of hedgehog signaling proteins in animal development.* Science, 1996. **274**(5285): p. 255-9.
25. Pepinsky, R.B., et al., *Identification of a palmitic acid-modified form of human Sonic hedgehog.* J Biol Chem, 1998. **273**(22): p. 14037-45.
26. Chen, M.H., et al., *Palmitoylation is required for the production of a soluble multimeric Hedgehog protein complex and long-range signaling in vertebrates.* Genes Dev, 2004. **18**(6): p. 641-59.
27. Chamoun, Z., et al., *Skinny hedgehog, an acyltransferase required for palmitoylation and activity of the hedgehog signal.* Science, 2001. **293**(5537): p. 2080-4.
28. Lee, J.D. and J.E. Treisman, *Sightless has homology to transmembrane acyltransferases and is required to generate active Hedgehog protein.* Curr Biol, 2001. **11**(14): p. 1147-52.
29. Buglino, J.A. and M.D. Resh, *Hhat is a palmitoylacyltransferase with specificity for N-palmitoylation of Sonic Hedgehog.* J Biol Chem, 2008. **283**(32): p. 22076-88.
30. Burke, R., et al., *Dispatched, a novel sterol-sensing domain protein dedicated to the release of cholesterol-modified hedgehog from signaling cells.* Cell, 1999. **99**(7): p. 803-15.
31. Caspary, T., et al., *Mouse Dispatched homolog1 is required for long-range, but not juxtacrine, Hh signaling.* Curr Biol, 2002. **12**(18): p. 1628-32.
32. Ma, Y., et al., *Hedgehog-mediated patterning of the mammalian embryo requires transporter-like function of dispatched.* Cell, 2002. **111**(1): p. 63-75.
33. Kawakami, T., et al., *Mouse dispatched mutants fail to distribute hedgehog proteins and are defective in hedgehog signaling.* Development, 2002. **129**(24): p. 5753-65.
34. Grimmond, S., et al., *Cloning, mapping, and expression analysis of a gene encoding a novel mammalian EGF-related protein (SCUBE1).* Genomics, 2000. **70**(1): p. 74-81.
35. Tukachinsky, H., et al., *Dispatched and scube mediate the efficient secretion of the cholesterol-modified hedgehog ligand.* Cell Rep, 2012. **2**(2): p. 308-20.
36. Johnson, J.L., et al., *Scube activity is necessary for Hedgehog signal transduction in vivo.* Dev Biol, 2012. **368**(2): p. 193-202.
37. Allen, B.L., et al., *Overlapping roles and collective requirement for the coreceptors GAS1, CDO, and BOC in SHH pathway function.* Dev Cell, 2011. **20**(6): p. 775-87.
38. Izzi, L., et al., *Boc and Gas1 each form distinct Shh receptor complexes with Ptch1 and are required for Shh-mediated cell proliferation.* Dev Cell, 2011. **20**(6): p. 788-801.
39. Motoyama, J., et al., *Ptch2, a second mouse Patched gene is co-expressed with Sonic hedgehog.* Nat Genet, 1998. **18**(2): p. 104-6.
40. Chuang, P.T. and A.P. McMahon, *Vertebrate Hedgehog signalling modulated by induction of a Hedgehog-binding protein.* Nature, 1999. **397**(6720): p. 617-21.
41. Goodrich, L.V., et al., *Altered neural cell fates and medulloblastoma in mouse patched mutants.* Science, 1997. **277**(5329): p. 1109-13.

42. Nieuwenhuis, E., et al., *Mice with a targeted mutation of patched2 are viable but develop alopecia and epidermal hyperplasia.* Mol Cell Biol, 2006. **26**(17): p. 6609-22.
43. Chuang, P.T., T. Kawcak, and A.P. McMahon, *Feedback control of mammalian Hedgehog signaling by the Hedgehog-binding protein, Hip1, modulates Fgf signaling during branching morphogenesis of the lung.* Genes Dev, 2003. **17**(3): p. 342-7.
44. Alfaro, A.C., et al., *Ptch2 mediates the Shh response in Ptch1-/- cells.* Development, 2014. **141**(17): p. 3331-9.
45. Holtz, A.M., et al., *Essential role for ligand-dependent feedback antagonism of vertebrate hedgehog signaling by PTCH1, PTCH2 and HHIP1 during neural patterning.* Development, 2013. **140**(16): p. 3423-34.
46. Adolphe, C., et al., *Patched 1 and patched 2 redundancy has a key role in regulating epidermal differentiation.* J Invest Dermatol, 2014. **134**(7): p. 1981-90.
47. Adolphe, C., et al., *Patched Receptors Sense, Interpret, and Establish an Epidermal Hedgehog Signaling Gradient.* J Invest Dermatol, 2016.
48. Jeong, J. and A.P. McMahon, *Growth and pattern of the mammalian neural tube are governed by partially overlapping feedback activities of the hedgehog antagonists patched 1 and Hhip1.* Development, 2005. **132**(1): p. 143-54.
49. Kinzler, K.W., et al., *Identification of an amplified, highly expressed gene in a human glioma.* Science, 1987. **236**(4797): p. 70-3.
50. Ruppert, J.M., et al., *The GLI-Kruppel family of human genes.* Mol Cell Biol, 1988. **8**(8): p. 3104-13.
51. Kinzler, K.W., et al., *The GLI gene is a member of the Kruppel family of zinc finger proteins.* Nature, 1988. **332**(6162): p. 371-4.
52. Dominguez, D.I., T. Hohn, and W. Schmidt-Puchta, *Cellular proteins bind to multiple sites of the leader region of cauliflower mosaic virus 35S RNA.* Virology, 1996. **226**(2): p. 374-83.
53. Sasaki, H., et al., *Regulation of Gli2 and Gli3 activities by an amino-terminal repression domain: implication of Gli2 and Gli3 as primary mediators of Shh signaling.* Development, 1999. **126**(17): p. 3915-24.
54. Dai, P., et al., *Sonic Hedgehog-induced activation of the Gli1 promoter is mediated by GLI3.* J Biol Chem, 1999. **274**(12): p. 8143-52.
55. Hui, C.C., et al., *Expression of three mouse homologs of the Drosophila segment polarity gene cubitus interruptus, Gli, Gli-2, and Gli-3, in ectoderm- and mesoderm-derived tissues suggests multiple roles during postimplantation development.* Dev Biol, 1994. **162**(2): p. 402-13.
56. Sasaki, H., et al., *A binding site for Gli proteins is essential for HNF-3beta floor plate enhancer activity in transgenics and can respond to Shh in vitro.* Development, 1997. **124**(7): p. 1313-22.
57. Platt, K.A., J. Michaud, and A.L. Joyner, *Expression of the mouse Gli and Ptc genes is adjacent to embryonic sources of hedgehog signals suggesting a conservation of pathways between flies and mice.* Mech Dev, 1997. **62**(2): p. 121-35.
58. Lee, J., et al., *Gli1 is a target of Sonic hedgehog that induces ventral neural tube development.* Development, 1997. **124**(13): p. 2537-52.
59. Hynes, M., et al., *Control of cell pattern in the neural tube by the zinc finger transcription factor and oncogene Gli-1.* Neuron, 1997. **19**(1): p. 15-26.

60. Park, H.L., et al., *Mouse Gli1 mutants are viable but have defects in SHH signaling in combination with a Gli2 mutation.* Development, 2000. **127**(8): p. 1593-605.
61. Bai, C.B., et al., *Gli2, but not Gli1, is required for initial Shh signaling and ectopic activation of the Shh pathway.* Development, 2002. **129**(20): p. 4753-61.
62. Ding, Q., et al., *Diminished Sonic hedgehog signaling and lack of floor plate differentiation in Gli2 mutant mice.* Development, 1998. **125**(14): p. 2533-43.
63. Matise, M.P., et al., *Gli2 is required for induction of floor plate and adjacent cells, but not most ventral neurons in the mouse central nervous system.* Development, 1998. **125**(15): p. 2759-70.
64. Hui, C.C. and A.L. Joyner, *A mouse model of greig cephalopolysyndactyly syndrome: the extra-toesJ mutation contains an intragenic deletion of the Gli3 gene.* Nat Genet, 1993. **3**(3): p. 241-6.
65. Masuya, H., et al., *Multigenic control of the localization of the zone of polarizing activity in limb morphogenesis in the mouse.* Dev Biol, 1997. **182**(1): p. 42-51.
66. Buscher, D., et al., *Evidence for genetic control of Sonic hedgehog by Gli3 in mouse limb development.* Mech Dev, 1997. **62**(2): p. 175-82.
67. Vortkamp, A., M. Gessler, and K.H. Grzeschik, *GLI3 zinc-finger gene interrupted by translocations in Greig syndrome families.* Nature, 1991. **352**(6335): p. 539-40.
68. Shin, S.H., et al., *GLI3 mutations in human disorders mimic Drosophila cubitus interruptus protein functions and localization.* Proc Natl Acad Sci U S A, 1999. **96**(6): p. 2880-4.
69. Bai, C.B., D. Stephen, and A.L. Joyner, *All mouse ventral spinal cord patterning by hedgehog is Gli dependent and involves an activator function of Gli3.* Dev Cell, 2004. **6**(1): p. 103-15.
70. Motoyama, J., et al., *Differential requirement for Gli2 and Gli3 in ventral neural cell fate specification.* Dev Biol, 2003. **259**(1): p. 150-61.
71. *Vismodegib granted FDA approval for treatment of basal cell carcinoma.* Oncology (Williston Park), 2012. **26**(2): p. 174, 213.
72. Mo, R., et al., *Specific and redundant functions of Gli2 and Gli3 zinc finger genes in skeletal patterning and development.* Development, 1997. **124**(1): p. 113-23.
73. Aza-Blanc, P., et al., *Proteolysis that is inhibited by hedgehog targets Cubitus interruptus protein to the nucleus and converts it to a repressor.* Cell, 1997. **89**(7): p. 1043-53.
74. Wang, B., J.F. Fallon, and P.A. Beachy, *Hedgehog-regulated processing of Gli3 produces an anterior/posterior repressor gradient in the developing vertebrate limb.* Cell, 2000. **100**(4): p. 423-34.
75. Pan, Y., C. Wang, and B. Wang, *Phosphorylation of Gli2 by protein kinase A is required for Gli2 processing and degradation and the Sonic Hedgehog-regulated mouse development.* Dev Biol, 2009. **326**(1): p. 177-89.
76. Price, M.A. and D. Kalderon, *Proteolysis of the Hedgehog signaling effector Cubitus interruptus requires phosphorylation by Glycogen Synthase Kinase 3 and Casein Kinase 1.* Cell, 2002. **108**(6): p. 823-35.
77. Chen, Y., et al., *Sonic Hedgehog dependent phosphorylation by CK1alpha and GRK2 is required for ciliary accumulation and activation of smoothened.* PLoS Biol, 2011. **9**(6): p. e1001083.

78. Kise, Y., et al., *Sufu recruits GSK3beta for efficient processing of Gli3.* Biochem Biophys Res Commun, 2009. **387**(3): p. 569-74.
79. Pan, Y. and B. Wang, *A novel protein-processing domain in Gli2 and Gli3 differentially blocks complete protein degradation by the proteasome.* J Biol Chem, 2007. **282**(15): p. 10846-52.
80. Kaesler, S., B. Luscher, and U. Ruther, *Transcriptional activity of GLI1 is negatively regulated by protein kinase A.* Biol Chem, 2000. **381**(7): p. 545-51.
81. Preat, T., *Characterization of Suppressor of fused, a complete suppressor of the fused segment polarity gene of Drosophila melanogaster.* Genetics, 1992. **132**(3): p. 725-36.
82. Svard, J., et al., *Genetic elimination of Suppressor of fused reveals an essential repressor function in the mammalian Hedgehog signaling pathway.* Dev Cell, 2006. **10**(2): p. 187-97.
83. Dunaeva, M., et al., *Characterization of the physical interaction of Gli proteins with SUFU proteins.* J Biol Chem, 2003. **278**(7): p. 5116-22.
84. Humke, E.W., et al., *The output of Hedgehog signaling is controlled by the dynamic association between Suppressor of Fused and the Gli proteins.* Genes Dev, 2010. **24**(7): p. 670-82.
85. Kinzler, K.W. and B. Vogelstein, *The GLI gene encodes a nuclear protein which binds specific sequences in the human genome.* Mol Cell Biol, 1990. **10**(2): p. 634-42.
86. Parker, D.S., et al., *The cis-regulatory logic of Hedgehog gradient responses: key roles for gli binding affinity, competition, and cooperativity.* Sci Signal, 2011. **4**(176): p. ra38.
87. Hallikas, O., et al., *Genome-wide prediction of mammalian enhancers based on analysis of transcription-factor binding affinity.* Cell, 2006. **124**(1): p. 47-59.
88. Lorberbaum, D.S., et al., *An ancient yet flexible cis-regulatory architecture allows localized Hedgehog tuning by patched/Ptch1.* Elife, 2016. **5**.
89. Lechler, T. and E. Fuchs, *Asymmetric cell divisions promote stratification and differentiation of mammalian skin.* Nature, 2005. **437**(7056): p. 275-80.
90. Blanpain, C., et al., *Canonical notch signaling functions as a commitment switch in the epidermal lineage.* Genes Dev, 2006. **20**(21): p. 3022-35.
91. Watt, F.M., S. Estrach, and C.A. Ambler, *Epidermal Notch signalling: differentiation, cancer and adhesion.* Curr Opin Cell Biol, 2008. **20**(2): p. 171-9.
92. Fuchs, E. and H. Green, *Changes in keratin gene expression during terminal differentiation of the keratinocyte.* Cell, 1980. **19**(4): p. 1033-42.
93. Fuchs, E., *Scratching the surface of skin development.* Nature, 2007. **445**(7130): p. 834-42.
94. Petiot, A., et al., *A crucial role for Fgfr2-IIIb signalling in epidermal development and hair follicle patterning.* Development, 2003. **130**(22): p. 5493-501.
95. Huh, S.H., et al., *Fgf20 governs formation of primary and secondary dermal condensations in developing hair follicles.* Genes Dev, 2013. **27**(4): p. 450-8.
96. Botchkarev, V.A., et al., *Noggin is a mesenchymally derived stimulator of hair-follicle induction.* Nat Cell Biol, 1999. **1**(3): p. 158-64.
97. Gat, U., et al., *De Novo hair follicle morphogenesis and hair tumors in mice expressing a truncated beta-catenin in skin.* Cell, 1998. **95**(5): p. 605-14.

98. DasGupta, R. and E. Fuchs, *Multiple roles for activated LEF/TCF transcription complexes during hair follicle development and differentiation.* Development, 1999. **126**(20): p. 4557-68.
99. Fuchs, E. and S. Raghavan, *Getting under the skin of epidermal morphogenesis.* Nat Rev Genet, 2002. **3**(3): p. 199-209.
100. Greco, V., et al., *A two-step mechanism for stem cell activation during hair regeneration.* Cell Stem Cell, 2009. **4**(2): p. 155-69.
101. Muller-Rover, S., et al., *A comprehensive guide for the accurate classification of murine hair follicles in distinct hair cycle stages.* J Invest Dermatol, 2001. **117**(1): p. 3-15.
102. Milner, Y., et al., *Exogen, shedding phase of the hair growth cycle: characterization of a mouse model.* J Invest Dermatol, 2002. **119**(3): p. 639-44.
103. Blanpain, C. and E. Fuchs, *Epidermal homeostasis: a balancing act of stem cells in the skin.* Nat Rev Mol Cell Biol, 2009. **10**(3): p. 207-17.
104. Cotsarelis, G., *Epithelial stem cells: a folliculocentric view.* J Invest Dermatol, 2006. **126**(7): p. 1459-68.
105. Plikus, M.V. and C.M. Chuong, *Complex hair cycle domain patterns and regenerative hair waves in living rodents.* J Invest Dermatol, 2008. **128**(5): p. 1071-80.
106. Huelsken, J., et al., *beta-Catenin controls hair follicle morphogenesis and stem cell differentiation in the skin.* Cell, 2001. **105**(4): p. 533-45.
107. Andl, T., et al., *WNT signals are required for the initiation of hair follicle development.* Dev Cell, 2002. **2**(5): p. 643-53.
108. St-Jacques, B., et al., *Sonic hedgehog signaling is essential for hair development.* Curr Biol, 1998. **8**(19): p. 1058-68.
109. Wang, L.C., et al., *Regular articles: conditional disruption of hedgehog signaling pathway defines its critical role in hair development and regeneration.* J Invest Dermatol, 2000. **114**(5): p. 901-8.
110. Woo, W.M., H.H. Zhen, and A.E. Oro, *Shh maintains dermal papilla identity and hair morphogenesis via a Noggin-Shh regulatory loop.* Genes Dev, 2012. **26**(11): p. 1235-46.
111. Brownell, I., et al., *Nerve-derived sonic hedgehog defines a niche for hair follicle stem cells capable of becoming epidermal stem cells.* Cell Stem Cell, 2011. **8**(5): p. 552-65.
112. Xiao, Y., et al., *Neural Hedgehog signaling maintains stem cell renewal in the sensory touch dome epithelium.* Proc Natl Acad Sci U S A, 2015. **112**(23): p. 7195-200.
113. Maurer, M., et al., *Intact hair follicle innervation is not essential for anagen induction and development.* Arch Dermatol Res, 1998. **290**(10): p. 574-8.
114. Oshimori, N. and E. Fuchs, *Paracrine TGF-beta signaling counterbalances BMP-mediated repression in hair follicle stem cell activation.* Cell Stem Cell, 2012. **10**(1): p. 63-75.
115. Festa, E., et al., *Adipocyte lineage cells contribute to the skin stem cell niche to drive hair cycling.* Cell, 2011. **146**(5): p. 761-71.
116. Sekulic, A., et al., *Efficacy and Safety of Vismodegib in Advanced Basal-Cell Carcinoma.* The New England Jounal of Medecine, 2012. **366**(23
): p. 2171-2179.
117. Hsu, Y.C., H.A. Pasolli, and E. Fuchs, *Dynamics between stem cells, niche, and progeny in the hair follicle.* Cell, 2011. **144**(1): p. 92-105.

118. Hsu, Y.C., L. Li, and E. Fuchs, *Transit-amplifying cells orchestrate stem cell activity and tissue regeneration.* Cell, 2014. **157**(4): p. 935-49.
119. Albers, K.M. and B.M. Davis, *The skin as a neurotrophic organ.* Neuroscientist, 2007. **13**(4): p. 371-82.
120. Roosterman, D., et al., *Neuronal control of skin function: the skin as a neuroimmunoendocrine organ.* Physiol Rev, 2006. **86**(4): p. 1309-79.
121. Vetrugno, R., et al., *Sympathetic skin response: basic mechanisms and clinical applications.* Clin Auton Res, 2003. **13**(4): p. 256-70.
122. Basbaum, A.I., et al., *Cellular and molecular mechanisms of pain.* Cell, 2009. **139**(2): p. 267-84.
123. Julius, D. and A.I. Basbaum, *Molecular mechanisms of nociception.* Nature, 2001. **413**(6852): p. 203-10.
124. Abraira, V.E. and D.D. Ginty, *The sensory neurons of touch.* Neuron, 2013. **79**(4): p. 618-39.
125. Koltzenburg, M., C.L. Stucky, and G.R. Lewin, *Receptive properties of mouse sensory neurons innervating hairy skin.* J Neurophysiol, 1997. **78**(4): p. 1841-50.
126. Wellnitz, S.A., et al., *The regularity of sustained firing reveals two populations of slowly adapting touch receptors in mouse hairy skin.* J Neurophysiol, 2010. **103**(6): p. 3378-88.
127. Knibestol, M., *Stimulus-response functions of rapidly adapting mechanoreceptors in human glabrous skin area.* J Physiol, 1973. **232**(3): p. 427-52.
128. Talbot, W.H., et al., *The sense of flutter-vibration: comparison of the human capacity with response patterns of mechanoreceptive afferents from the monkey hand.* J Neurophysiol, 1968. **31**(2): p. 301-34.
129. Vallbo, A.B. and R.S. Johansson, *Properties of cutaneous mechanoreceptors in the human hand related to touch sensation.* Hum Neurobiol, 1984. **3**(1): p. 3-14.
130. Lumpkin, E.A., K.L. Marshall, and A.M. Nelson, *The cell biology of touch.* J Cell Biol, 2010. **191**(2): p. 237-48.
131. Stucky, C.L., et al., *Neurotrophin 4 is required for the survival of a subclass of hair follicle receptors.* J Neurosci, 1998. **18**(17): p. 7040-6.
132. Seal, R.P., et al., *Injury-induced mechanical hypersensitivity requires C-low threshold mechanoreceptors.* Nature, 2009. **462**(7273): p. 651-5.
133. Iggo, A. and A.R. Muir, *The structure and function of a slowly adapting touch corpuscle in hairy skin.* J. Physiol., 1969. **200**: p. 763-796.
134. Chambers, M.R., et al., *The structure and function of the slowly adapting type II mechanoreceptor in hairy skin.* Q J Exp Physiol Cogn Med Sci, 1972. **57**(4): p. 417-45.
135. Pawson, L., et al., *GABAergic/glutamatergic-glial/neuronal interaction contributes to rapid adaptation in pacinian corpuscles.* J Neurosci, 2009. **29**(9): p. 2695-705.
136. Cauna, N. and L.L. Ross, *The fine structure of Meissner's touch corpuscles of human fingers.* J Biophys Biochem Cytol, 1960. **8**: p. 467-82.
137. Peters, E.M., et al., *Developmental timing of hair follicle and dorsal skin innervation in mice.* J Comp Neurol, 2002. **448**(1): p. 28-52.
138. Botchkarev, V.A., et al., *Hair cycle-dependent plasticity of skin and hair follicle innervation in normal murine skin.* J Comp Neurol, 1997. **386**(3): p. 379-95.
139. Assas, B.M., J.I. Pennock, and J.A. Miyan, *Calcitonin gene-related peptide is a key neurotransmitter in the neuro-immune axis.* Front Neurosci, 2014. **8**: p. 23.

140. Leeman, S.E. and R. Gamse, *Substance P in sensory neurons.* TIPS, 1981. **2**: p. 119-121.
141. Paus, R., et al., *Neural mechanisms of hair growth control.* J Investig Dermatol Symp Proc, 1997. **2**(1): p. 61-8.
142. Crowley, C., et al., *Mice lacking nerve growth factor display perinatal loss of sensory and sympathetic neurons yet develop basal forebrain cholinergic neurons.* Cell, 1994. **76**(6): p. 1001-11.
143. Botchkarev, V.A., et al., *Neurotrophin-3 involvement in the regulation of hair follicle morphogenesis.* J Invest Dermatol, 1998. **111**(2): p. 279-85.
144. Maisonpierre, P.C., et al., *NT-3, BDNF, and NGF in the developing rat nervous system: parallel as well as reciprocal patterns of expression.* Neuron, 1990. **5**(4): p. 501-9.
145. Robinson, R.C., et al., *Crystals of the neurotrophins.* Protein Science, 1996. **5**: p. 973-977.
146. Huang, E.J. and L.F. Reichardt, *Neurotrophins: roles in neuronal development and function.* Annu Rev Neurosci, 2001. **24**: p. 677-736.
147. Segal, R.A., *Selectivity in neurotrophin signaling: theme and variations.* Annu Rev Neurosci, 2003. **26**: p. 299-330.
148. Brennan, C., K. Rivas-Plata, and S.C. Landis, *The p75 neurotrophin receptor influences NT-3 responsiveness of sympathetic neurons in vivo.* Nat Neurosci, 1999. **2**(8): p. 699-705.
149. Roux, P.P. and P.A. Barker, *Neurotrophin signaling through the p75 neurotrophin receptor.* Progress in Neurobiology, 2002. **67**: p. 203-233.
150. Epa, W.R., K. Markovska, and G.L. Barrett, *The p75 neurotrophin receptor enhances TrkA signalling by binding to Shc and augmenting its phosphorylation.* J Neurochem, 2004. **89**(2): p. 344-53.
151. Zampieri, N. and M.V. Chao, *Mechanisms of neurotrophin receptor signalling.* Biochem Soc Trans, 2006. **34**(Pt 4): p. 607-11.
152. Rice, F.L., et al., *Differential dependency of unmyelinated and A delta epidermal and upper dermal innervation on neurotrophins, trk receptors, and p75LNGFR.* Dev Biol, 1998. **198**(1): p. 57-81.
153. Airaksinen, M.S., et al., *Specific Subtypes of Cutaneous Mechanoreceptors Require Neurotrophin-3 following peripheral target innervation.* Neuron, 1996. **16**: p. 287-295.
154. Gonzalez-Martinez, T., et al., *BDNF, but not NT-4, is necessary for normal development of Meissner corpuscles.* Neurosci Lett, 2005. **377**(1): p. 12-5.
155. Fan, G., et al., *Knocking the NT4 gene into the BDNF locus rescues BDNF deficient mice and reveals distinct NT4 and BDNF activities.* Nat Neurosci, 2000. **3**(4): p. 350-7.
156. Albers, K.M., et al., *Glial cell-line-derived neurotrophic factor expression in skin alters the mechanical sensitivity of cutaneous nociceptors.* J Neurosci, 2006. **26**(11): p. 2981-90.
157. Elitt, C.M., et al., *Artemin overexpression in skin enhances expression of TRPV1 and TRPA1 in cutaneous sensory neurons and leads to behavioral sensitivity to heat and cold.* J Neurosci, 2006. **26**(33): p. 8578-87.
158. Wang, T., et al., *Neurturin overexpression in skin enhances expression of TRPM8 in cutaneous sensory neurons and leads to behavioral sensitivity to cool and menthol.* J Neurosci, 2013. **33**(5): p. 2060-70.

159. Milbrandt, J., et al., *Persephin, a novel neurotrophic factor related to GDNF and neurturin.* Neuron, 1998. **20**(2): p. 245-53.
160. Merkel, F., *Tastzellen and Tastkorperchen bei den Hausthieren und bein Menschen.* Arch. Mikr. Anat. , 1875. **11**: p. 636-652.
161. Pinkus, F., *Ueber einen bisher unbekannten Nebenapparat am Haarsystem des Menschen- Haarcheiben.* Dermatol. Z., 1902. **9**: p. 465-469.
162. Halata, Z., M. Grim, and K.I. Bauman, *Friedrich Sigmund Merkel and his "Merkel cell", morphology, development, and physiology: review and new results.* Anat Rec A Discov Mol Cell Evol Biol, 2003. **271**(1): p. 225-39.
163. Straile, W.E., *Sensory hair follicles in mammalian skin: the tylotrich follicle.* American Journal of Anatomy, 1960. **106**(2): p. 133-147.
164. Moll, I. and R. Moll, *Early development of human Merkel cells.* Exp Dermatol, 1992. **1**(4): p. 180-4.
165. Moll, I., R. Paus, and R. Moll, *Merkel Cells in Mouse Skin: Intermediate Filament Pattern, Localization, and Hair Cycle-Dependent Density.* Journal of Investigative Dermatology, 1996. **106**(2): p. 281-286.
166. Moll, I., R. Moll, and W.W. Franke, *Formation of epidermal and dermal Merkel cells during human fetal skin development.* J Invest Dermatol, 1986. **87**(6): p. 779-87.
167. Vielkind, U., et al., *Dynamics of Merkel cell patterns in developing hair follicles in the dorsal skin of mice, demonstrated by a monoclonal antibody to mouse keratin 8.* Acta Anat (Basel), 1995. **152**(2): p. 93-109.
168. Morrison, K.M., et al., *Mammalian Merkel cells are descended from the epidermal lineage.* Dev Biol, 2009. **336**(1): p. 76-83.
169. Duverger, O. and M.I. Morasso, *Epidermal patterning and induction of different hair types during mouse embryonic development.* Birth Defects Res C Embryo Today, 2009. **87**(3): p. 263-72.
170. Xiao, Y., et al., *A Cascade of Wnt, Eda, and Shh Signaling Is Essential for Touch Dome Merkel Cell Development.* PLoS Genet, 2016. **12**(7): p. e1006150.
171. Chang, H., et al., *The spatio-temporal domains of Frizzled6 action in planar polarity control of hair follicle orientation.* Dev Biol, 2016. **409**(1): p. 181-93.
172. Ben-Arie, N., et al., *Functional conservation of atonal and Math1 in the CNS and PNS.* Development, 2000. **127**(5): p. 1039-48.
173. Maricich, S.M., et al., *Merkel cells are essential for light-touch responses.* Science, 2009. **324**.
174. Ostrowski, S.M., et al., *Ectopic Atoh1 expression drives Merkel cell production in embryonic, postnatal and adult mouse epidermis.* Development, 2015. **142**(14): p. 2533-44.
175. Perdigoto, C.N., et al., *Polycomb-Mediated Repression and Sonic Hedgehog Signaling Interact to Regulate Merkel Cell Specification during Skin Development.* PLoS Genet, 2016. **12**(7): p. e1006151.
176. Szeder, V., et al., *Neural crest origin of mammalian merkel cells.* Developmental Biology, 2003. **253**.
177. Van Keymeulen, A., et al., *Epidermal progenitors give rise to Merkel cells during embryonic development and adult homeostasis.* J Cell Biol, 2009. **187**(1): p. 91-100.

178. Woo, S.H., et al., *Identification of epidermal progenitors for the Merkel cell lineage.* Development, 2010. **137**(23): p. 3965-71.
179. Doucet, Y.S., et al., *The touch dome defines an epidermal niche specialized for mechanosensory signaling.* Cell Rep, 2013. **3**(6): p. 1759-65.
180. Wright, M.C., et al., *Unipotent, Atoh1+ progenitors maintain the Merkel cell population in embryonic and adult mice.* J Cell Biol, 2015. **208**(3): p. 367-79.
181. Marshall, K.L., et al., *Touch Receptors Undergo Rapid Remodeling in Healthy Skin.* Cell Rep, 2016. **17**(7): p. 1719-1727.
182. Moll, I., R. Paus, and R. Moll, *Merkel cells in mouse skin: intermediate filament pattern, localization, and hair cycle-dependent density.* J Invest Dermatol, 1996. **106**(2): p. 281-6.
183. Nakafusa, J., et al., *Changes in the number of Merkel cells with the hair cycle in hair discs on rat back skin.* Br J Dermatol, 2006. **155**(5): p. 883-9.
184. Peterson, S.C., et al., *Basal Cell Carcinoma Preferentially Arises from Stem Cells within Hair Follicle and Mechanosensory Niches.* Cell Stem Cell, 2015. **16**(4): p. 400-12.
185. Rogers, H.W., et al., *Incidence Estimate of Nonmelanoma Skin Cancer (Keratinocyte Carcinomas) in the U.S. Population, 2012.* JAMA Dermatol, 2015. **151**(10): p. 1081-6.
186. Bleyer, A., A. Viny, and R. Barr, *Cancer in 15- to 29-year-olds by primary site.* Oncologist, 2006. **11**(6): p. 590-601.
187. Jacob, A., *Observations respecting an ulcer of peculiar character, which attacks the eye-lids and other parts of the face.* Dublin Hospital Reports, 1827. **4**: p. 232-239.
188. Ten Seldam, R.E.J. and E.B. Helwig, *Histological typing of skin tumors.* Geneva, Switzerland: World Health Organization, 1974.
189. Jacob, A., *Observations respecting an ulcer of peculiar character, which attacks the eye-lids and other parts of the face.* . Dublin Hospital Reports, 1827: p. 231-239.
190. Rubin, A.I., E.H. Chen, and D. Ratner, *Basal-cell carcinoma.* N Engl J Med, 2005. **353**(21): p. 2262-9.
191. Wong, S.Y. and A.A. Dlugosz, *Basal cell carcinoma, Hedgehog signaling, and targeted therapeutics: the long and winding road.* J Invest Dermatol, 2014. **134**(e1): p. E18-22.
192. Longo, C., et al., *Classifying distinct basal cell carcinoma subtype by means of dermatoscopy and reflectance confocal microscopy.* J Am Acad Dermatol, 2014. **71**(4): p. 716-724 e1.
193. Epstein, E.H., *Basal cell carcinomas: attack of the hedgehog.* Nat Rev Cancer, 2008. **8**(10): p. 743-54.
194. Kasper, M., et al., *Basal cell carcinoma - molecular biology and potential new therapies.* J Clin Invest, 2012. **122**(2): p. 455-63.
195. Hahn, H., et al., *Mutations of the human homologue of drosophila patched in the nevoid basal cell carcinoma syndrome.* Cell, 1996. **85**: p. 841-851.
196. Bonifas, J.M., et al., *Parental origin of chromosome 9q22.3-q31 lost in basal cell carcinomas from basal cell nevus syndrome patients.* Hum Mol Genet, 1994. **3**(3): p. 447-8.
197. Johnson, R.L., et al., *Human homolog of patched, a candidate gene for the basal cell nevus syndrome.* Science, 1996. **272**(5268): p. 1668-71.
198. Gorlin, R.J. and R.W. Goltz, *Multiple nevoid basal-cell epithelioma, jaw cysts and bifid rib. A syndrome.* N Engl J Med, 1960. **262**: p. 908-12.

199. Kimonis, V.E., et al., *Clinical manifestations in 105 persons with nevoid basal cell carcinoma syndrome.* Am J Med Genet, 1997. **69**(3): p. 299-308.
200. Xie, J., et al., *Activating Smoothened mutations in sporadic basal-cell carcinoma.* Nature, 1998. **391**(6662): p. 90-2.
201. Binns, W., L.F. James, and J.L. Shupe, *Toxicosis of Veratrum Californicum in Ewes and Its Relationship to a Congenital Deformity in Lambs.* Ann N Y Acad Sci, 1964. **111**: p. 571-6.
202. Keeler, R.F. and W. Binns, *Chemical Compounds of Veratrum Californicum Related to Congenital Ovine Cyclopian Malformations: Extraction of Active Material.* Proc Soc Exp Biol Med, 1964. **116**: p. 123-7.
203. Keeler, R.F., *Cyclopamine and related steroidal alkaloid teratogens: their occurrence, structural relationship, and biologic effects.* Lipids, 1978. **13**(10): p. 708-15.
204. Binns, W., et al., *A Congenital Cyclopian-Type Malformation in Lambs Induced by Maternal Ingestion of a Range Plant, Veratrum Californicum.* Am J Vet Res, 1963. **24**: p. 1164-75.
205. Chiang, C., et al., *Cyclopia and defective axial patterning in mice lacking Sonic hedgehog gene function.* Nature, 1996. **383**(6599): p. 407-13.
206. Belloni, E., et al., *Identification of Sonic hedgehog as a candidate gene responsible for holoprosencephaly.* Nat Genet, 1996. **14**(3): p. 353-6.
207. Roessler, E., et al., *Mutations in the human Sonic Hedgehog gene cause holoprosencephaly.* Nat Genet, 1996. **14**(3): p. 357-60.
208. Keeler, R.F. and W. Binns, *Teratogenic compounds of Veratrum californicum (Durand). V. Comparison of cyclopian effects of steroidal alkaloids from the plant and structurally related compounds from other sources.* Teratology, 1968. **1**(1): p. 5-10.
209. Binns, W., et al., *Effects of teratogenic agents in range plants.* Cancer Res, 1968. **28**(11): p. 2323-6.
210. Keeler, R.F. and W. Binns, *Possible teratogenic effects of veratramine.* Proc Soc Exp Biol Med, 1966. **123**(3): p. 921-3.
211. Cooper, M.K., et al., *Teratogen-mediated inhibition of target tissue response to Shh signaling.* Science, 1998. **280**(5369): p. 1603-7.
212. Incardona, J.P., et al., *The teratogenic Veratrum alkaloid cyclopamine inhibits sonic hedgehog signal transduction.* Development, 1998. **125**(18): p. 3553-62.
213. Taipale, J., et al., *Effects of oncogenic mutations in Smoothened and Patched can be reversed by cyclopamine.* Nature, 2000. **406**(6799): p. 1005-9.
214. Chen, J.K., et al., *Small molecule modulation of Smoothened activity.* Proc Natl Acad Sci U S A, 2002. **99**(22): p. 14071-6.
215. Lipinski, R.J., et al., *Dose- and route-dependent teratogenicity, toxicity, and pharmacokinetic profiles of the hedgehog signaling antagonist cyclopamine in the mouse.* Toxicol Sci, 2008. **104**(1): p. 189-97.
216. Robarge, K.D., et al., *GDC-0449-a potent inhibitor of the hedgehog pathway.* Bioorg Med Chem Lett, 2009. **19**(19): p. 5576-81.
217. LoRusso, P.M., et al., *Phase I trial of hedgehog pathway inhibitor vismodegib (GDC-0449) in patients with refractory, locally advanced or metastatic solid tumors.* Clin Cancer Res, 2011. **17**(8): p. 2502-11.

218. Von Hoff, D.D., et al., *Inhibition of the Hedgehog Pathway in Advanced Basal-Cell Carcinoma.* The New England Jounal of Medecine, 2009. **361**: p. 1164-1172.
219. Amakye, D., Z. Jagani, and M. Dorsch, *Unraveling the therapeutic potential of the Hedgehog pathway in cancer.* Nat Med, 2013. **19**(11): p. 1410-22.
220. Tang, J.Y., et al., *Inhibiting the hedgehog pathway in patients with the basal-cell nevus syndrome.* N Engl J Med, 2012. **366**(23): p. 2180-8.
221. Brinkhuizen, T., et al., *Acquired resistance to the Hedgehog pathway inhibitor vismodegib due to smoothened mutations in treatment of locally advanced basal cell carcinoma.* J Am Acad Dermatol, 2014.
222. Metcalfe, C. and F.J. de Sauvage, *Hedgehog fights back: mechanisms of acquired resistance against Smoothened antagonists.* Cancer Res, 2011. **71**(15): p. 5057-61.
223. Wolfe, C.M., et al., *Basal cell carcinoma rebound after cessation of vismodegib in a nevoid basal cell carcinoma syndrome patient.* Dermatol Surg, 2012. **38**(11): p. 1863-6.
224. Dijkgraaf, G.J., et al., *Small molecule inhibition of GDC-0449 refractory smoothened mutants and downstream mechanisms of drug resistance.* Cancer Res, 2011. **71**(2): p. 435-44.
225. Atwood, S.X., et al., *Smoothened variants explain the majority of drug resistance in basal cell carcinoma.* Cancer Cell, 2015. **27**(3): p. 342-53.
226. Sharpe, H.J., et al., *Genomic analysis of smoothened inhibitor resistance in basal cell carcinoma.* Cancer Cell, 2015. **27**(3): p. 327-41.
227. Urman, N.M., et al., *Tumor-Derived Suppressor of Fused Mutations Reveal Hedgehog Pathway Interactions.* PLoS One, 2016. **11**(12): p. e0168031.
228. Pan, S., et al., *Discovery of NVP-LDE225, a Potent and Selective Smoothened Antagonist.* ACS Med Chem Lett, 2010. **1**(3): p. 130-4.
229. Tremblay, M.R., et al., *Discovery of a potent and orally active hedgehog pathway antagonist (IPI-926).* J Med Chem, 2009. **52**(14): p. 4400-18.
230. Frank-Kamenetsky, M., et al., *Small-molecule modulators of Hedgehog signaling: identification and characterization of Smoothened agonists and antagonists.* J Biol, 2002. **1**(2): p. 10.
231. Munchhof, M.J., et al., *Discovery of PF-04449913, a Potent and Orally Bioavailable Inhibitor of Smoothened.* ACS Med Chem Lett, 2012. **3**(2): p. 106-11.
232. Wang, C., et al., *Structure of the human smoothened receptor bound to an antitumour agent.* Nature, 2013. **497**(7449): p. 338-43.
233. Migden, M.R., et al., *Treatment with two different doses of sonidegib in patients with locally advanced or metastatic basal cell carcinoma (BOLT): a multicentre, randomised, double-blind phase 2 trial.* Lancet Oncol, 2015. **16**(6): p. 716-28.
234. Kim, J., et al., *Itraconazole and arsenic trioxide inhibit Hedgehog pathway activation and tumor growth associated with acquired resistance to smoothened antagonists.* Cancer Cell, 2013. **23**(1): p. 23-34.
235. Atwood, S.X., et al., *GLI activation by atypical protein kinase C iota/lambda regulates the growth of basal cell carcinomas.* Nature, 2013. **494**(7438): p. 484-8.
236. Ally, M.S., et al., *Effects of Combined Treatment With Arsenic Trioxide and Itraconazole in Patients With Refractory Metastatic Basal Cell Carcinoma.* JAMA Dermatol, 2016. **152**(4): p. 452-6.

237. Oro, A.E., et al., *Basal cell carcinomas in mice overexpressing sonic hedgehog.* Science, 1997. **276**(5313): p. 817-21.
238. Byrne, C., M. Tainsky, and E. Fuchs, *Programming gene expression in developing epidermis.* Development, 1994. **120**(9): p. 2369-83.
239. Saitou, M., et al., *Inhibition of skin development by targeted expression of a dominant-negative retinoic acid receptor.* Nature, 1995. **374**(6518): p. 159-62.
240. Byrne, C. and E. Fuchs, *Probing keratinocyte and differentiation specificity of the human K5 promoter in vitro and in transgenic mice.* Mol Cell Biol, 1993. **13**(6): p. 3176-90.
241. Casatorres, J., et al., *Analysis of the control of expression and tissue specificity of the keratin 5 gene, characteristic of basal keratinocytes. Fundamental role of an AP-1 element.* J Biol Chem, 1994. **269**(32): p. 20489-96.
242. Brown, K., et al., *The malignant capacity of skin tumours induced by expression of a mutant H-ras transgene depends on the cell type targeted.* Curr Biol, 1998. **8**(9): p. 516-24.
243. Ramirez, A., et al., *Sequences 5′ of the bovine keratin 5 gene direct tissue- and cell-type-specific expression of a lacZ gene in the adult and during development.* Differentiation, 1994. **58**(1): p. 53-64.
244. Grachtchouk, V., et al., *The magnitude of hedgehog signaling activity defines skin tumor phenotype.* EMBO, 2003. **22**(11): p. 2741-2751.
245. Grachtchouk, M., et al., *Basal cell carcinomas in mice overexpressing Gli2 in skin.* Nature Genetics, 2000. **24**: p. 216-217.
246. Hahn, H., et al., *Rhabdomyosarcomas and radiation hypersensitivity in a mouse model of Gorlin syndrome.* Nat Med, 1998. **4**(5): p. 619-22.
247. Bogovski, P., *Tumours of the skin.* IARC Sci Publ, 1994(111): p. 1-45.
248. Aszterbaum M., et al., *Ultraviolet and ionizing radiation enhance the growth of BCCs and trichoblastomas in patched heterozygous knockout mice.* Nature Medecine, 1999. **5**(11): p. 1285-1291.
249. Wang, G.Y., et al., *Basal cell carcinomas arise from hair follicle stem cells in Ptch1(+/-) mice.* Cancer Cell, 2011. **19**(1): p. 114-24.
250. van der Riet, P., et al., *Progression of basal cell carcinoma through loss of chromosome 9q and inactivation of a single p53 allele.* Cancer Res, 1994. **54**(1): p. 25-7.
251. Gailani, M.R., et al., *Relationship between sunlight exposure and a key genetic alteration in basal cell carcinoma.* J Natl Cancer Inst, 1996. **88**(6): p. 349-54.
252. Nilsson, M., et al., *Induction of basal cell carcinomas and trichoepitheliomas in mice overexpressing GLI-1.* Proc Natl Acad Sci U S A, 2000. **97**(7): p. 3438-43.
253. Yasar, B., et al., *Common variants modify the age of onset for basal cell carcinomas in Gorlin syndrome.* Eur J Hum Genet, 2015. **23**(5): p. 708-10.
254. Soriano, P., *Generalized lacZ expression with the ROSA26 Cre reporter strain.* Nat Genet, 1999. **21**(1): p. 70-1.
255. Mao, J., et al., *A novel somatic mouse model to survey tumorigenic potential applied to the Hedgehog pathway.* Cancer Res, 2006. **66**(20): p. 10171-8.
256. Youssef, K.K., et al., *Identification of the cell lineage at the origin of basal cell carcinoma.* Nat Cell Biol, 2010. **12**(3): p. 299-305.

257. Vasioukhin, V., et al., *The magical touch: genome targeting in epidermal stem cells induced by tamoxifen application to mouse skin.* Proc Natl Acad Sci U S A, 1999. **96**(15): p. 8551-6.
258. Wong, S.Y. and J.F. Reiter, *Wounding mobilizes hair follicle stem cells to form tumors.* Proc Natl Acad Sci U S A, 2011. **108**(10): p. 4093-8.
259. Ellis, T., et al., *Patched 1 conditional null allele in mice.* Genesis, 2003. **36**(3): p. 158-61.
260. Rothnagel, J.A., et al., *The mouse keratin 6 isoforms are differentially expressed in the hair follicle, footpad, tongue and activated epidermis.* Differentiation, 1999. **65**(2): p. 119-30.
261. Mahony, D., et al., *Analysis of mouse keratin 6a regulatory sequences in transgenic mice reveals constitutive, tissue-specific expression by a keratin 6a minigene.* J Invest Dermatol, 2000. **115**(5): p. 795-804.
262. Adolphe, C., et al., *Patched1 functions as a gatekeeper by promoting cell cycle progression.* Cancer Res, 2006. **66**(4): p. 2081-8.
263. Siggins, S.L., et al., *The Hedgehog receptor Patched1 regulates myeloid and lymphoid progenitors by distinct cell-extrinsic mechanisms.* Blood, 2009. **114**(5): p. 995-1004.
264. Mak, K.K., et al., *Wnt/beta-catenin signaling interacts differentially with Ihh signaling in controlling endochondral bone and synovial joint formation.* Development, 2006. **133**(18): p. 3695-707.
265. Taniguchi, E., et al., *Bortezomib reverses a post-translational mechanism of tumorigenesis for patched1 haploinsufficiency in medulloblastoma.* Pediatr Blood Cancer, 2009. **53**(2): p. 136-44.
266. Shimokawa, T., F. Rahnama, and P.G. Zaphiropoulos, *A novel first exon of the Patched1 gene is upregulated by Hedgehog signaling resulting in a protein with pathway inhibitory functions.* FEBS Lett, 2004. **578**(1-2): p. 157-62.
267. Kasper, M., et al., *Wounding enhances epidermal tumorigenesis by recruiting hair follicle keratinocytes.* Proc Natl Acad Sci U S A, 2011. **108**(10): p. 4099-104.
268. Zhou, Z., et al., *In utero activation of K5.CrePR1 induces gene deletion.* Genesis, 2002. **32**(2): p. 191-2.
269. Jonkers, J., et al., *Synergistic tumor suppressor activity of BRCA2 and p53 in a conditional mouse model for breast cancer.* Nat Genet, 2001. **29**(4): p. 418-25.
270. Villani, R.M., et al., *Patched1 inhibits epidermal progenitor cell expansion and basal cell carcinoma formation by limiting Igfbp2 activity.* Cancer Prev Res (Phila), 2010. **3**(10): p. 1222-34.
271. Li, M., et al., *Skin abnormalities generated by temporally controlled RXRalpha mutations in mouse epidermis.* Nature, 2000. **407**(6804): p. 633-6.
272. Uhmann, A., et al., *The Hedgehog receptor Patched controls lymphoid lineage commitment.* Blood, 2007. **110**(6): p. 1814-23.
273. Zibat, A., et al., *Time-point and dosage of gene inactivation determine the tumor spectrum in conditional Ptch knockouts.* Carcinogenesis, 2009. **30**(6): p. 918-26.
274. Nitzki, F., et al., *Patched knockout mouse models of Basal cell carcinoma.* J Skin Cancer, 2012. **2012**: p. 907543.
275. Indra, A.K., et al., *Temporally-controlled site-specific mutagenesis in the basal layer of the epidermis: comparison of the recombinase activity of the tamoxifen-inducible Cre-ER(T) and Cre-ER(T2) recombinases.* Nucleic Acids Res, 1999. **27**(22): p. 4324-7.

276. Sheng, H., et al., *Dissecting the oncogenic potential of Gli2: deletion of an NH(2)-terminal fragment alters skin tumor phenotype.* Cancer Res, 2002. **62**(18): p. 5308-16.
277. Roessler, E., et al., *A previously unidentified amino-terminal domain regulates transcriptional activity of wild-type and disease-associated human GLI2.* Hum Mol Genet, 2005. **14**(15): p. 2181-8.
278. Grachtchouk, M., et al., *Basal cell carcinomas in mice arise from hair follicle stem cells and multiple epithelial progenitor populations.* J Clin Invest, 2011. **121**(5): p. 1768-81.
279. Morris, R.J., et al., *Capturing and profiling adult hair follicle stem cells.* Nat Biotechnol, 2004. **22**(4): p. 411-7.
280. Joyce, J.A., *Therapeutic targeting of the tumor microenvironment.* Cancer Cell, 2005. **7**(6): p. 513-20.
281. Albini, A. and M.B. Sporn, *The tumour microenvironment as a target for chemoprevention.* Nat Rev Cancer, 2007. **7**(2): p. 139-47.
282. Liebig, C., et al., *Perineural invasion in cancer: a review of the literature.* Cancer, 2009. **115**(15): p. 3379-91.
283. Ayala, G.E., et al., *In vitro dorsal root ganglia and human prostate cell line interaction: redefining perineural invasion in prostate cancer.* Prostate, 2001. **49**(3): p. 213-23.
284. Simon, R.H., et al., *Electrical stimulation of the midbrain mediates metastatic tumor growth.* Science, 1980. **209**(4461): p. 1132-3.
285. Visintainer, M.A., J.R. Volpicelli, and M.E. Seligman, *Tumor rejection in rats after inescapable or escapable shock.* Science, 1982. **216**(4544): p. 437-9.
286. Thaker, P.H., et al., *Chronic stress promotes tumor growth and angiogenesis in a mouse model of ovarian carcinoma.* Nat Med, 2006. **12**(8): p. 939-44.
287. Schuller, H.M., et al., *Regulation of pancreatic cancer by neuropsychological stress responses: a novel target for intervention.* Carcinogenesis, 2012. **33**(1): p. 191-6.
288. Magnon, C., et al., *Autonomic nerve development contributes to prostate cancer progression.* Science, 2013. **341**(6142): p. 1236361.
289. Lackovicova, L., et al., *Chemical sympathectomy suppresses fibrosarcoma development and improves survival of tumor-bearing rats.* Neoplasma, 2011. **58**(5): p. 424-9.
290. Zhao, C.M., et al., *Denervation suppresses gastric tumorigenesis.* Sci Transl Med, 2014. **6**(250): p. 250ra115.
291. Saloman, J.L., et al., *Ablation of sensory neurons in a genetic model of pancreatic ductal adenocarcinoma slows initiation and progression of cancer.* Proc Natl Acad Sci U S A, 2016. **113**(11): p. 3078-83.
292. Ostrowski, S.M., et al., *Cutaneous denervation of psoriasiform mouse skin improves acanthosis and inflammation in a sensory neuropeptide-dependent manner.* J Invest Dermatol, 2011. **131**(7): p. 1530-8.
293. Horvathova, L., et al., *Sympathectomy reduces tumor weight and affects expression of tumor-related genes in melanoma tissue in the mouse.* Stress, 2016. **19**(5): p. 528-34.
294. Pezet, S. and S.B. McMahon, *Neurotrophins: mediators and modulators of pain.* Annu Rev Neurosci, 2006. **29**: p. 507-38.

Chapter II – Cutaneous surgical denervation: a method for testing the requirement for nerves in mouse models of skin disease

2.1 Abstract

Cutaneous somatosensory nerves function to detect diverse stimuli that act upon the skin. In addition to their established sensory roles, recent studies have suggested that nerves may also modulate skin disorders including atopic dermatitis, psoriasis and cancer. Here, we describe protocols for testing the requirement for nerves in maintaining a cutaneous mechanosensory organ, the touch dome (TD). Specifically, we discuss methods for genetically labeling, harvesting and visualizing TDs by whole-mount staining, and for performing unilateral surgical denervation on mouse dorsal back skin. Together, these approaches can be used to directly compare TD morphology and gene expression in denervated as well as sham-operated skin from the same animal. These methods can also be readily adapted to examine the requirement for nerves in mouse models of skin pathology. Finally, the ability to repeatedly sample the skin provides an opportunity to monitor disease progression at different stages and times after initiation.

2.2 Introduction

Over the past few years, there has been a widening appreciation for the influence of nerves on diseases not typically regarded as classical neuropathies [1-4]. In the skin, recent experimental evidence has suggested that sensory nerves can modulate diverse pathologies ranging from psoriasis to cancer [5-9]. This has been demonstrated using techniques such as

surgical denervation and pharmacological inhibition of neural function in rodents. In the case of psoriasis, these studies have provided a mechanistic framework for understanding why human psoriatic plaques regress following loss of neural function [7, 10-12]. Cutaneous nerves can also affect gene expression [13, 14] and are critical for mechanosensing in normal skin [15]. In particular, touch dome (TD) epithelia are comprised of a patch of columnar epidermal cells in juxtaposition with neuroendocrine Merkel cells innervated by slowly adapting type 1 (SA1) nerve fibers [16-18]. TDs mediate light touch sensation and have been shown to display Hedgehog pathway activity [5, 19]. TD maintenance depends on innervation [20, 21], as nerves secrete Hedgehog ligands to sustain normal TDs and their associated Merkel cells [19]. In addition, innervation promotes Hedgehog-dependent tumor formation from TD epithelia [5]. Together, these studies reinforce the notion that intricate molecular interactions occurring between nerves and the surrounding cells in their niche are crucial for normal TD physiology as well as disease.

To interrogate the nature of these interactions, we describe here a series of *in vivo* techniques for manipulating gene expression in the TD, as well as for harvesting skin biopsies for TD visualization after lineage tracing. Finally, we describe procedures for performing unilateral surgical denervation, wherein nerves are removed from one side of the mouse dorsal skin, while leaving the contralateral side intact as a sham internal control. Several weeks after surgery, denervated and sham control skin are compared to assess changes that occur when nerves are ablated. Although these techniques are described in the context of normal TDs, the denervation procedure has been used to examine the requirement for nerves in mouse models of psoriasis [6], wound healing [13] and tumorigenesis [5]. Finally, since the skin is amenable to

repeated biopsies, this provides an opportunity to monitor the long-term fates of labeled cells or to assess disease progression over multiple time points.

2.3 Protocol

All procedures described in this protocol were performed in accordance with regulations established by the University of Michigan Unit for Laboratory Animal Medicine.

2.3.1 Induce Genetic Recombination in Mice

Note: The *Gli1*$^{tm3(cre/ERT2)Alj}$*/J* mouse strain (*Gli1-Cre*^{ERT2})[22] enables targeting of tamoxifen-induced genetic recombination to TD epithelia. Cross this strain with *B6.129S4-Gt(ROSA)26Sor*^{tm1Sor}*/J* reporter mice (*LacZ*)[23] to generate *Gli1;LacZ* animals to visualize TD cells by whole-mount staining below.

1. Prepare tamoxifen solution to a concentration of 12.5 mg/ml in corn oil.
2. In a 1.5 ml tube, add up to 20 mg of crystalline tamoxifen, and then 1 ml of corn oil. Firmly tape the tube to a vortex mixer, and vortex continuously at the highest setting at RT until the tamoxifen has fully dissolved (2-4 hr), as confirmed by examining the tube under a dissecting microscope for the absence of tamoxifen particulates.
3. Transfer the solution to a 15 ml tube and dilute the tamoxifen to a final concentration of 12.5 mg/ml with additional corn oil. Mix by vortexing the

viscous solution for an additional 30 sec. Store this solution for up to 1 week at 4 °C in the dark.

4. Inject the tamoxifen solution intraperitoneally into *Gli1*;*LacZ* mice, at a volume of 200 µl per 20 g of mouse body weight, for an effective tamoxifen dose of 2.5 mg per 20 g mouse weight.

2.3.2 Harvest Skin Biopsies

Note: Depending on the experiment, harvest skin biopsies several days to weeks after tamoxifen induction. For all surgeries, follow standard protocols for rodent surgery, including using sterile gloves, wearing a surgical mask or hair net, and covering the animal with a sterile surgical drape during the procedure.

1. Prepare 10x stock anesthetic solution by mixing 90 mg/ml ketamine and 6.5 mg/ml xylazine in water. Dilute this stock solution 1:10 into sterile PBS just prior to use, and store at RT in the dark for up to 8 months.
2. Alternatively, anesthetize mice by isoflurane inhalation, beginning with a gas concentration of 4% with oxygen to fully anesthetize the animal, and then subsequently lowering this to 1-2% for the duration of the procedure.
3. Inject the anesthetic solution intraperitoneally at a dose of 200 µl per 20 g mouse body weight. Check that the animal has reached the proper plane of sedation by toe pinch assay, and confirm that heart and respiratory rates are normal (approximately 600 beats and 160 breaths per min, respectively).

4. Use an electric clipper to remove the hair from the site of biopsy on the dorsal back skin, being careful not to nick or damage the underlying skin.
5. Prepare the surgical site by wiping the shaved area in an anterior-to-posterior direction using Betadine and alcohol wipes. Ensure all hair clippings are removed from the site.
6. Outline the biopsy site using a black marker, place the animal on a warming pad in an aseptic surgical area, and cover with a sterile surgical drape (for demonstration purposes, sterile drape was omitted to increase visibility).

   Note: To obtain longitudinal sections of hair follicles, the longer edge of the biopsy (the edge to be sectioned for histology, ~1 cm) should run in an anterior-posterior direction (parallel to the direction of the hair follicles), parasagittal to the dorsal midline (FIG 2.1A).
7. Use a sterile #11 scalpel to make a full thickness excision along the marked area without damaging the underlying muscular fascia.

   Note: The excised skin tissue includes the epidermis, dermis, subcutaneous fat and panniculus carnosus. Bleeding is typically minimal.
8. Flatten the excised skin sample on a dry paper towel, dermis side down, trim away the excess paper towel, and store the sample in cold PBS for up to 1 hr if other samples need to be collected. When ready, proceed to Steps 3.1 or 3.2 to process samples for histology, or Step 4 for whole-mount β-galactosidase (LacZ) staining.
9. Suture close the biopsy site using 6-0 nylon sutures, in a simple interrupted pattern spaced roughly 3 mm apart.

10. Do not return mice that have undergone surgery into the same cage as other animals until after full recovery.
11. Monitor animals immediately after surgery until they regain consciousness, and also daily until the surgical area has healed, typically within 1 week. Use analgesics in accordance with designated institutional animal care and use guidelines if mice exhibit signs of pain or distress. Remove sutures within 7-10 days after surgery. Note: If needed, prepare analgesic solution by diluting carprofen (50 mg/ml stock solution) 1:100 in sterile water. Inject the solution subcutaneously between the shoulder blades near the scruff of the neck, at a dose of 200 µl per 20 g body weight (5 mg/kg mouse body weight).

2.3.3 Process Samples for Histology

Note: To fix and process the excised tissue, use either method below depending on application.

1. To generate paraffin-embedded histological samples, fix the skin in 3.7% formalin in PBS O/N at RT and store in 70% ethanol for up to 2 weeks. Remove the paper towel before embedding into paraffin.
2. For generating frozen histological samples, submerge the tissue in cold 4% paraformaldehyde in PBS and gently shake for 1 hr. Remove the solution and wash the sample with 3 changes of PBS, roughly 5 min each. Next, submerge the sample in 30% sucrose in PBS to cryoprotect the tissue ("sucrose sinking").

3. Incubate with gentle shaking O/N at 4 °C. The next day, remove the paper towel and trim away excess adipose tissue from the dermal side of the skin. Embed the tissue directly into OCT and store the frozen block at -80 °C.

   Note: After sectioning, either paraffin or frozen samples can be stained by immunohistochemistry to identify TDs, Merkel cells and nerves using antibodies against Keratin 17, Keratin 8 and Neurofilament, respectively, as previously described [5, 19].

2.3.4. Visualize Samples by Whole-mount X-Gal Staining

1. Prepare X-gal staining solution.
2. Combine 0.94 g sodium phosphate monobasic, and 2.6 g sodium phosphate dibasic in 250 ml of sterile water. Adjust pH to 7.3. To this, add 0.5 ml of 1 M magnesium chloride, 0.528 g of potassium ferrocyanide, and 0.412 g of potassium ferricyanide. Add 250 µl of octylphenyl-polyethylene glycol and 125 mg of deoxycholate. The base solution can be stored at 4 °C for up to 6 months in the dark.
3. Prepare 50x stock X-gal solution by adding dimethylformamide to the X-gal stock bottle to generate a 50 mg/ml solution. Store this solution at -20 °C in the dark.
4. Just prior to use, dilute stock X-gal solution 1:50 into X-gal base solution to generate staining solution. For smaller biopsies (<1 cm^2), aliquot 1-2 ml of staining solution per sample.
5. Fix the skin sample collected in Step 2.7 in a solution containing 2% paraformaldehyde/0.2% glutaraldehyde in cold PBS for 30 min, gently shaking on ice.

For smaller biopsies (<1 cm^2), use 1-2 ml of fixative solution per sample.

Note: Alternatively, fix samples in 2-4% paraformaldehyde only, or in 0.5% glutaraldehyde only. Optimal fixation conditions depend on the tissue, degree of LacZ expression and application.

6. Remove the fixative solution, and rinse samples with 3 changes of PBS, 5 min each, on a shaker at RT.
7. Remove the paper towel underneath the sample and cut away excess adipose tissue from the dermal side of the skin by gripping the fat with blunt forceps and trimming with dissecting scissors.
8. Submerge the sample in X-gal staining solution, and incubate at 37 °C O/N. LacZ expression will be visible as a blue stain under a dissecting microscope (FIG 2.1B).

   Note: If the signal intensity is weak, replace the staining solution the next day and repeat the O/N incubation. If the background staining is too intense, reduce the time of staining, or incubate the sample at RT instead of 37 °C.
9. Remove the staining solution and wash the samples in 3 changes of PBS containing 3% DMSO for approximately 5 min, gently shaking at RT.
10. Wash samples in 2-3 changes of 70% ethanol for 5 min each. Store samples in 70% ethanol.

2.3.5. Surgical Denervation

1. Anesthetize the animal as in Step 2.2 and shave the entire dorsal skin.

2. Prepare the surgical area of the back skin using Betadine and alcohol wipes, and cover the animal with a sterile surgical drape (for demonstration purposes, sterile drape was omitted to increase visibility). Keep the animal warm using a heating pad while operating in an aseptic surgical area.
3. Make an incision using a sterile #11 scalpel along the dorsal midline from the base of the neck to roughly 0.5 cm above the tail.
4. Using blunt forceps, gently reflect the skin on the left side away from the flank to visualize the underlying tissue from the scapular fat pads near the neck to just above the hind limb.

   Note: Dorsal cutaneous nerves appear as white strands that travel caudally through the translucent fascia of the trunk wall before making sharp bends and entering the loose connective tissue underneath the skin (FIG 2.2).
5. Using ultra-fine forceps under a dissecting light microscope, remove the nerves exclusively from the left side of the animal located at anatomical sites T3-12 by plucking from where the segments bend at the trunk wall to their entry sites into the skin (FIG 2.2).
6. Orient forceps vertically and remove the nerves by grasping approximately 0.5 cm below their bend sites and pulling upwards, causing the nerve to stretch and separate from the surrounding tissue (FIG 2.22C-E). Be careful to avoid rupturing adjacent blood vessels.
7. Continue until all nerves extending from the trunk wall to the skin are removed. Do not disrupt the nerves within the dense fascia of the trunk wall. Keep the tissue

moist throughout the procedure by periodically applying drops of sterile 0.9% saline solution.

8. Alternatively, remove nerves by grasping their proximal ends near the trunk wall with forceps and snipping with fine scissors. Afterwards, sever the distal ends near the skin (FIG 2.2F-H). Finally, remove the intervening nerve segments (FIG 2.2I).
9. Remove any nerves from the skin flap exposed in Step 5.4. These fibers comprise the distal branches of the dorsal cutaneous nerves and appear as white branching strands located sporadically within the connective tissue on the dermal side of the skin flap (FIG 2.2J-K).
10. To remove these fine branches, position the fine forceps roughly parallel to the dermal surface, grasp the nerves and pluck upwards to avoid disrupting blood vessels and puncturing the skin. Continue until all visible nerves have been removed.
11. Using blunt dissection, reflect the skin on the right side of the dorsal midline incision, but do not remove the nerves. This will serve as the contralateral sham-operated control.
12. Suture along the dorsal midline in a simple interrupted pattern to close the incision. Monitor the animal during recovery and post-operatively as previously demonstrated (Steps 2.8-10). Remove sutures within 7-10 days after surgery.
13. To functionally assess stable denervation up to several weeks after surgery, remove the hair from the dorsal skin using an electric clipper.

14. Gently prick the denervated skin area using a hypodermic needle, and note whether the animal responds, typically by shuddering or turning its head. If the skin area has been stably denervated, the animal will exhibit little or no response.
15. Using a black marker, outline the area of no response, as well as an area of similar size and location on the contralateral sham side.
16. Collect biopsies from these sites as in Steps 2.1-2.9 for analysis.

    Note: Alternatively, the entire dorsal back skin, including denervated and sham-operated regions, can be removed as a single sheet for whole-mount staining, similar to as described in Step 4.

2.4 Representative Results

By generating mice expressing tamoxifen-inducible *Gli1-CreERT2* and a *LacZ* reporter allele, it is possible to visualize TD epithelia and track the fates of these cells over time. The entire denervation procedure typically can be completed within 1 hr per mouse and should cause minimal distress to the animal.

Our previous studies have indicated that nerves are crucial for maintaining both normal TDs as well as their associated Keratin 8^+ Merkel cells (FIG 2.3A-C) [5, 19]. Nerves are also critical for promoting *Gli1* expression in the TD (FIG 2.3D). Given the relatively infrequent appearance of TD clusters throughout the skin (FIG 2.1B), it is imperative to sample multiple frozen sections to accurately quantitate TD frequency. Typically, we assess 15 non-consecutive sections (each 10 μm thick and ~1 cm long) from both sham and denervated skin from each animal. Following denervation, stable loss of nerves, both at the TD and throughout the skin,

can be confirmed by the absence of immunohistochemical staining for standard pan-neural markers such as Neurofilament in either frozen or paraffin sections (FIG 2.3A and 2.3C), and as previously reported [5]). Alternatively, nerves can also be identified by expression of β3-tubulin or PGP9.5 [6, 9].

By using *Gli1;LacZ* mice, it is also possible to confirm both the requirement for nerves in activating Hedgehog signaling in the TD and in maintaining TD cell fate by varying the sequence of tamoxifen-induced recombination and denervation. If denervation is performed prior to recombination, for instance, this would test the requirement for nerves in activating the Hedgehog pathway, as monitored by Cre recombinase activity and levels, which are correlated with *Gli1* expression in these animals. On the other hand, if denervation is performed after recombination, this would assess the requirement for nerves in maintaining already-labeled cells in the TD.

2.5 Discussion

Nerves serve crucial functions not only in sensation, but also in mammalian organ development, maintenance and regeneration [13, 24-27]. As nerves have recently been implicated in diverse skin disorders, the techniques described here can be used to study the requirement for innervation in a variety of animal disease models. Indeed, the unilateral denervation technique allows for the direct comparison of skin with either intact or disrupted nerves from the same mouse. This provides an ideal internal control to compensate for animal-to-animal differences, with subsequent data analyses making use of a paired t-test. While the procedures described here largely utilize the *LacZ* reporter gene, these experiments can be adapted such that the *Gli1-CreERT2* allele is combined with other fluorescent reporter or

conditional alleles to modify gene expression in the TD. For instance, *Gli1-CreERT2* mice can be crossed with animals harboring conditional alleles of *Patched1* (*B6N.129-Ptch1^{tm1Hahn}/J*)[28] to generate mice that form TD-derived tumors after tamoxifen induction [5]. It is important to note that the *Gli1-CreERT2* strain also induces recombination in a subset of *Gli1*$^{+}$hair follicle stem cells that are physically separated from those in the TD [13].

Following denervation, nerves in the skin remain stably ablated for several months (FIG 2.3C) [5, 19]. In other studies, however, some re-innervation has been reported to occur over time [6]. The perdurance of the denervated phenotype may depend on the thoroughness of nerve removal, as it is absolutely critical to excise nerve segments between their exit from the chest wall to a point close to the sites of insertion into the dermis of the skin.

Completely removing the hair from the skin prior to biopsy can enhance the ability to subsequently visualize TDs by whole-mount staining (FIG 2.1B). This is accomplished by applying depilatory cream to clipped skin for 2 min, and then wiping the hair away in an anterior-to-posterior direction using cotton balls. Please note that depilation can affect hair cycle kinetics by promoting entry into the anagen growth phase. Alternatively, hair can be completely removed using a razor blade. In addition, whole mount immunohistochemistry can be performed to visualize TDs and Merkel cells on epithelial sheets separated from the dermis, as has been previously described [29].

The possibility remains that surgical denervation may cause inflammation at the surgical site, potentially confounding any observed phenotypes. In our experience, we have not observed significant inflammation after denervation, likely because the collateral tissue damage incurred in the skin is slight if the procedure is done properly. To minimize the possibility that inflammation may affect results, additional controls can be incorporated into the experiment.

For instance, we observed that denervation specifically inhibited TD-derived tumors, but not adjacent hair follicle-associated lesions in the same skin samples, arguing that denervation–and not a general wound-induced inflammatory response–likely inhibited tumorigenesis at the TD [5].

It is important to note that surgical denervation ablates all cutaneous nerves, including sensory and sympathetic fibers [5], and thus provides a general overall assessment of the influence of these nerves on either normal or diseased skin. Other experimental approaches, for instance using pharmacologics such as Botulinum neurotoxin to block neurotransmission, may yield more detailed mechanistic insights [7], although it is unclear whether these agents inhibit retrograde secretion of cytokines such as Hedgehog ligands. Alternatively, compounds such as 6-hydroxydopamine have been used to ablate sympathetic nerves in the skin [9]. In addition, targeting the receptors for nerve-derived factors such as Calcitonin gene-related peptide and Substance P may be useful for interrogating specific interactions between nerves and the surrounding cells within their niche [6]. Ultimately, multiple strategies may be utilized in combination to identify, or at least rule out, potential signaling mechanisms.

Finally, targeted genetic deletion of nerve-derived factors in the neural lineage using either Wnt1-Cre or Advillin-Cre may represent the gold standard for elucidating the signals that are exchanged between nerves and their niche [19]. As neither of these strains are tamoxifen-inducible, however, some caution needs to be taken to ensure that disruption of these signals does not impair nerve development or proper targeting of neural afferents. Use of a tamoxifen-inducible Cre such as Advillin-CreERT2 may help circumvent these issues [30].

Overall, the techniques described here–a combination of lineage tracing, cell visualization and surgical denervation–offer powerful approaches for studying the influence of

nerves on normal and diseased skin. With experience, these procedures can be performed routinely and reliably, while causing minimal distress to the animal–or the investigator.

2.6 Acknowledgements

This chapter was published in the *Journal of Visualized Experiments* and is included in this dissertation with the permission of the journal editors.

Peterson, S. C., Brownell, I., Wong, S. Y. Cutaneous Surgical Denervation: A Method for Testing the Requirement for Nerves in Mouse Models of Skin Disease. *J. Vis. Exp.* (112), e54050, doi:10.3791/54050 (2016).

The authors would like to thank Autumn Peterson for assistance with mouse photography, Daniel Thoresen for assistance with mice, and Drs. Nicole Ward and Abdelmadjid Belkadi for assistance with surgical denervation. These studies were supported by funding from the National Institute of Arthritis and Musculoskeletal and Skin Diseases (grants R00AR059796 and R01AR065409); the University of Michigan Department of Dermatology; the Biological Sciences Scholars Program; the Center for Organogenesis; the University of Michigan Comprehensive Cancer Center; and the John S. and Suzanne C. Munn Cancer Fund. S.C.P. was supported by funding from the National Institute of General Medical Sciences (grant T32 GM007315). This work was also supported by the NIH Intramural Research Program, Center for Cancer Research, National Cancer Institute.

2.7 Author Contributions

S.C.P, S.Y.W. and I.B. conceived and performed experiments, wrote the manuscript and secured funding.

2.8 Figures

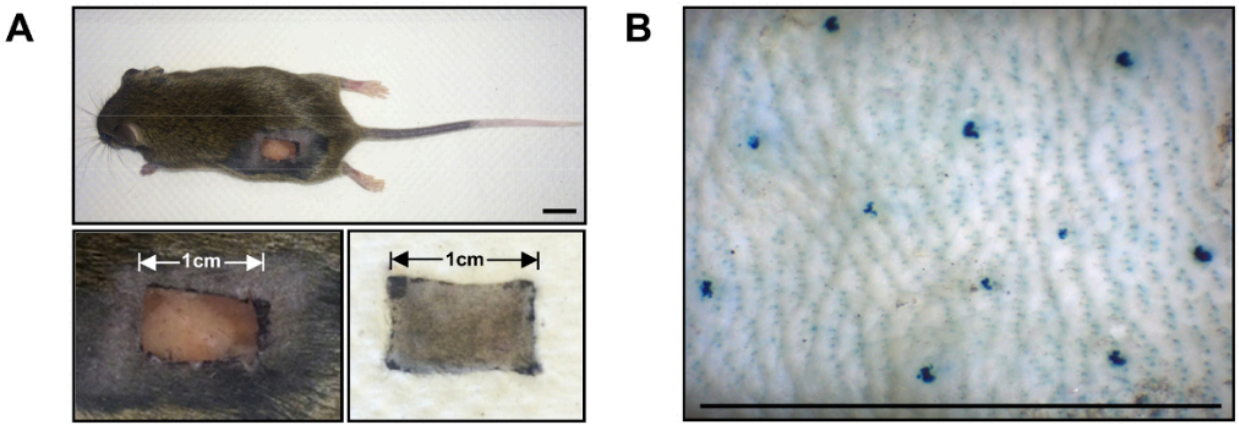

Figure 2.1 Skin biopsy and whole-mount LacZ staining of TD epithelia.
A. (Top) Photograph of mouse after biopsy and prior to suturing. (Lower left) Enlarged image of biopsy site. (Lower right) Skin sample obtained from biopsy with its dermis side spread flat on a dry paper towel. **B**. Whole-mount LacZ staining of skin from a *Gli1;LacZ* mouse, 7 days after tamoxifen induction, depilated just prior to biopsy to improve skin visualization.
$Gli1^{+}/LacZ^{+}$ TDs are labeled as intense blue clusters. Scale bar = 1 cm.

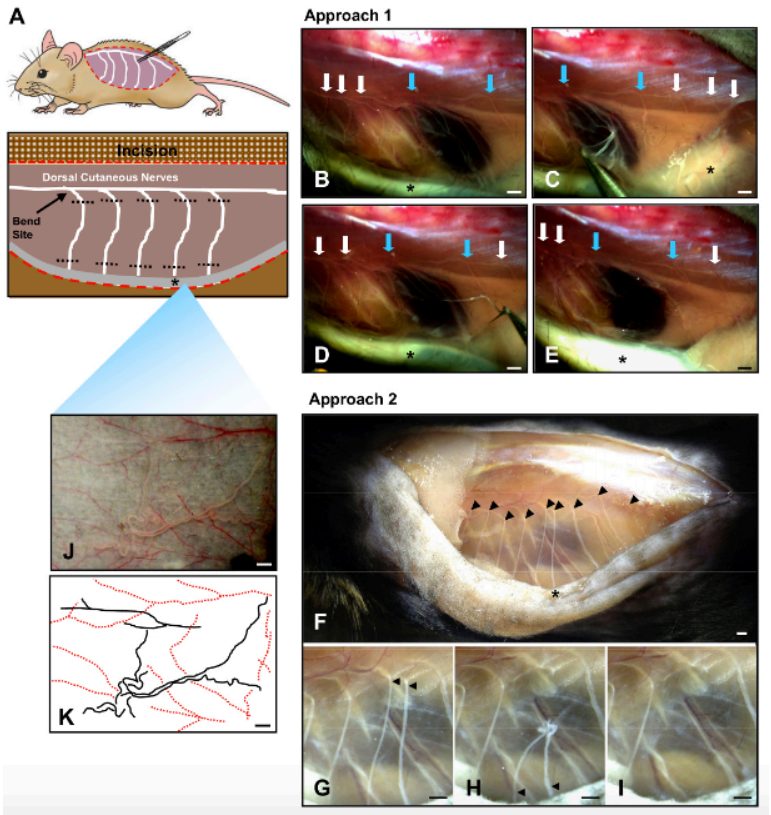

Figure 2.2 Two approaches for denervating dorsal skin.
A. Cartoon diagram of innervated mouse skin. Red dotted lines indicate a single excision made along the dorsal midline to expose the underlying musculature on the trunk wall (purple) as well as the dermis (grey, asterisk) beneath the reflected skin. Dorsal cutaneous nerves traveling caudally appear to "bend" as they leave the trunk wall (the black arrow indicates one such bend). Nerve segments to be excised are demarcated by black dotted lines.
B. Photograph of intact nerves with sites of bending indicated (arrows). Blue arrows point to 2 nerve segments that will be removed.
C-D. Photographs showing denervation technique. Using ultra-fine forceps, grip the nerves 0.5 cm below their sites of bending and pull outwards.
E. Photograph showing the body cavity after removal of 2 nerve segments (blue arrows). The remaining nerves also need to be removed.
F-G. An alternative approach for nerve removal is depicted, where nerves are snipped at their proximal ends just below where they bend (arrowheads) and also distally, close to their site of entry into the skin (arrowheads)
H. Note that the midline incision in these images is longer than typical for the purpose of better visualization.
J. Photograph of dermal side of the reflected skin flap to one side of the midline.
K. Nerves are outlined (black lines), with larger blood vessels indicated in red. The nerves located on the dermis side of the skin flap also need to be excised. Asterisk, underlying dermis from the reflected skin flap. Scale bar = 1 mm.

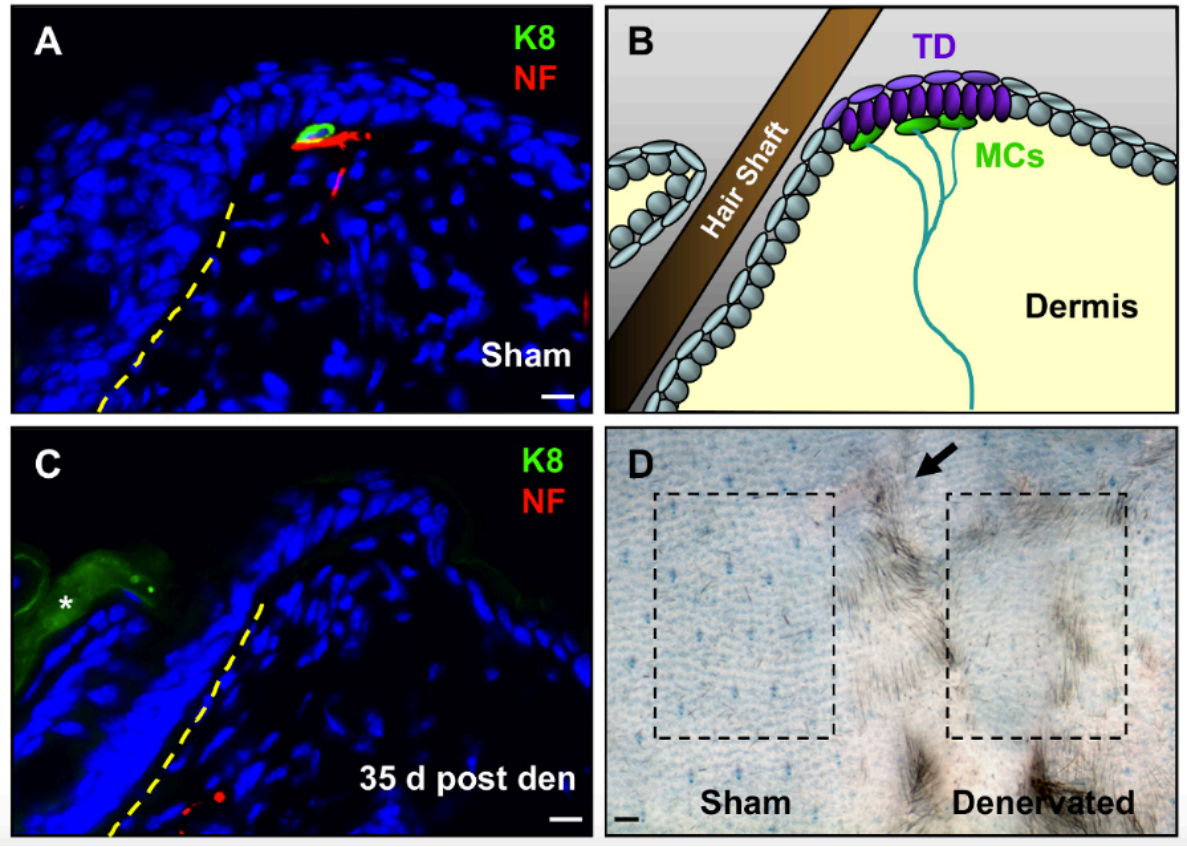

Figure 2.3 Stable loss of nerves and deterioration of TDs after denervation.
A. Immunohistochemistry showing TD epithelia with Keratin 8^{+} Merkel cells (K8, green) and Neurofilament^{+} nerves (NF, red) in sham-operated skin.
B. Cartoon depiction, with TD epithelia highlighted in purple, Merkel cells in green, and sensory nerves in blue.
C. Immunohistochemistry showing denervated skin (den) lacking Merkel cell-neurite complexes within the TD area. Dashed yellow lines, hair follicle epithelium. Asterisk, background staining.
D. Whole-mount LacZ staining of dorsal back skin from *Gli1*$^{LacZ/+}$ mouse 2 weeks after unilateral skin denervation. In the box to the left of the healed midline incision (arrow), abundant labeled TD epithelia are observed in sham-operated skin. To the right of the midline, TDs are not visible in denervated skin. Scale bar = 10 μm for (**A**), (**C**); and 1 mm for (**D**).

Table 2.1 List of Materials

Name	Company	Catalog	Comments
Alcohol prep pads	PDI	B339	
AnaSed (Xylazine)	Lloyd	NADA 139-236	
Antibody, anti-Keratin	Developmental Studies	TROMA-I	rat antibody, use at 1:500
Antibody, anti-Keratin	Cell Signaling	#4543	rabbit antibody, use at 1:1,000
Antibody, anti-	Cell Signaling	C28E10	rabbit antibody, use at 1:500
Betadine prep pads	Medline	MDS093917	
Carprofen (Rimadyl)	Zoetis		
Cordless rechargable	Wahl	trimmer model	
Corn Oil	Sigma-Aldrich	C8267	
Cryostat	Leica	CM1860	
DAPI	ThermoFisher	D1306	use at 1:1,000 concentration
Deoxycholate	Sigma-Aldrich	D6750	
Depilatory Cream	Nair	N/A	

Dimethylforamide	Sigma-Aldrich	319937	
Dimethyl Sulfoxide	Sigma-Aldrich	D8418	
Glutaraldehyde	Sigma-Aldrich	G5882	
ImmEdge Pen	Vector Laboratories	H-4000	
Ketamine HCl	Hospira	NDC 0409-	
Magnesium chloride	Sigma	M8266	
Micro cover glass	VWR	48404-454	
Micro Slides	VWR	48311-703	
10% Neutral Buffered	VWR	BDH0502-4LP	
6-0 nylon sutures	DemeTECH	NL166012F4P	
Octylphenyl-	Sigma-Aldrich	I8896	
O.C.T. Compound	Sakura Tissue-Tek	4583	
Paraformaldehyde	Sigma-Aldrich	158127	
Potassium	Sigma-Aldrich	P9387	
Potassium ferricyanide	Sigma-Aldrich	702587	

Sodium phosphate	Sigma-Aldrich	P9791	
Sodium phosphate	Sigma-Aldrich	S5136	
Sucrose	Sigma-Aldrich	84097	
Tamoxifen	Sigma-Aldrich	T5648-1G	
Ultra-fine forceps	Dumont	0103-5-PO	
Vectashield	Vector Laboratories	H1000	
X-gal	Roche	10 651 745 001	Dissolve in dimethylforamide to create 50x stock prior to use

2.9 Reference List

1. Magnon, C., et al., *Autonomic nerve development contributes to prostate cancer progression.* Science, 2013. **341**(6142): p. 1236361.
2. Zhao, C.M., et al., *Denervation suppresses gastric tumorigenesis.* Sci Transl Med, 2014. **6**(250): p. 250ra115.
3. Chiu, I.M., C.A. von Hehn, and C.J. Woolf, *Neurogenic inflammation and the peripheral nervous system in host defense and immunopathology.* Nat Neurosci, 2012. **15**(8): p. 1063-7.
4. Gautron, L., J.K. Elmquist, and K.W. Williams, *Neural control of energy balance: translating circuits to therapies.* Cell, 2015. **161**(1): p. 133-45.
5. Peterson, S., et al., *Basal cell carcinoma preferentially arises from stem cells within the hair follicle and mechanosensory niches.* Cell Stem Cell, 2015.
6. Ostrowski, S.M., et al., *Cutaneous denervation of psoriasiform mouse skin improves acanthosis and inflammation in a sensory neuropeptide-dependent manner.* J Invest Dermatol, 2011. **131**(7): p. 1530-8.
7. Ward, N.L., et al., *Botulinum neurotoxin A decreases infiltrating cutaneous lymphocytes and improves acanthosis in the KC-Tie2 mouse model.* J Invest Dermatol, 2012. **132**(7): p. 1927-30.
8. Roggenkamp, D., et al., *Epidermal nerve fibers modulate keratinocyte growth via neuropeptide signaling in an innervated skin model.* J Invest Dermatol, 2013. **133**(6): p. 1620-8.
9. Riol-Blanco, L., et al., *Nociceptive sensory neurons drive interleukin-23-mediated psoriasiform skin inflammation.* Nature, 2014. **510**(7503): p. 157-61.
10. Zanchi, M., et al., *Botulinum toxin type-A for the treatment of inverse psoriasis.* J Eur Acad Dermatol Venereol, 2008. **22**(4): p. 431-6.
11. Farber, E.M., S.W. Lanigan, and G. Rein, *The role of psychoneuroimmunology in the pathogenesis of psoriasis.* Cutis, 1990. **46**(4): p. 314-6.
12. Dewing, S.B., *Remission of psoriasis associated with cutaneous nerve section.* Arch Dermatol, 1971. **104**(2): p. 220-1.
13. Brownell, I., et al., *Nerve-derived sonic hedgehog defines a niche for hair follicle stem cells capable of becoming epidermal stem cells.* Cell Stem Cell, 2011. **8**(5): p. 552-65.
14. Liao, X.H. and H. Nguyen, *Epidermal expression of Lgr6 is dependent on nerve endings and Schwann cells.* Exp Dermatol, 2014. **23**(3): p. 195-8.
15. Lumpkin, E.A., K.L. Marshall, and A.M. Nelson, *The cell biology of touch.* J Cell Biol, 2010. **191**(2): p. 237-48.
16. Maricich, S.M., et al., *Merkel cells are essential for light-touch responses.* Science, 2009. **324**(5934): p. 1580-2.
17. Reinisch, C.M. and E. Tschachler, *The touch dome in human skin is supplied by different types of nerve fibers.* Ann Neurol, 2005. **58**(1): p. 88-95.
18. Doucet, Y.S., et al., *The touch dome defines an epidermal niche specialized for mechanosensory signaling.* Cell Rep, 2013. **3**(6): p. 1759-65.
19. Xiao, Y., et al., *Neural Hedgehog signaling maintains stem cell renewal in the sensory touch dome epithelium.* Proc Natl Acad Sci U S A, 2015. **112**(23): p. 7195-200.

20. English, K.B., D. Kavka-Van Norman, and K. Horch, *Effects of chronic denervation in type I cutaneous mechanoreceptors (Haarscheiben).* Anat Rec, 1983. **207**(1): p. 79-88.
21. Burgess, P.R., et al., *Patterning in the regeneration of type I cutaneous receptors.* J Physiol, 1974. **236**(1): p. 57-82.
22. Ahn, S. and A.L. Joyner, *Dynamic changes in the response of cells to positive hedgehog signaling during mouse limb patterning.* Cell, 2004. **118**(4): p. 505-16.
23. Soriano, P., *Generalized lacZ expression with the ROSA26 Cre reporter strain.* Nat Genet, 1999. **21**(1): p. 70-1.
24. Kumar, A. and J.P. Brockes, *Nerve dependence in tissue, organ, and appendage regeneration.* Trends Neurosci, 2012. **35**(11): p. 691-9.
25. Rinkevich, Y., et al., *Clonal analysis reveals nerve-dependent and independent roles on mammalian hind limb tissue maintenance and regeneration.* Proc Natl Acad Sci U S A, 2014. **111**(27): p. 9846-51.
26. Ueno, H., et al., *Dependence of corneal stem/progenitor cells on ocular surface innervation.* Invest Ophthalmol Vis Sci, 2012. **53**(2): p. 867-72.
27. Westphalen, C.B., et al., *Long-lived intestinal tuft cells serve as colon cancer-initiating cells.* J Clin Invest, 2014. **124**(3): p. 1283-95.
28. Uhmann, A., et al., *The Hedgehog receptor Patched controls lymphoid lineage commitment.* Blood, 2007. **110**(6): p. 1814-23.
29. Wright, M.C., et al., *Unipotent, Atoh1+ progenitors maintain the Merkel cell population in embryonic and adult mice.* J Cell Biol, 2015. **208**(3): p. 367-79.
30. Lau, J., et al., *Temporal control of gene deletion in sensory ganglia using a tamoxifen-inducible Advillin-Cre-ERT2 recombinase mouse.* Mol Pain, 2011. **7**: p. 100.

Chapter III – Basal cell carcinoma preferentially arises from stem cells within hair follicle and mechanosensory niches

3.1 Abstract

Basal cell carcinoma (BCC) is characterized by frequent loss of PTCH1, leading to constitutive activation of the Hedgehog (HH) pathway. Although the requirement for HH in BCC is well-established, the identity of disease-initiating cells and the compartments in which they reside remain controversial. By using several inducible Cre drivers to delete *Ptch1* in different cell compartments in mice, we show here that multiple hair follicle stem cell populations readily form BCC-like tumors. In contrast, stem cells within the interfollicular epidermis do not efficiently form tumors. Notably, we observed that innervated GLI1-expressing progenitors within mechanosensory touch dome epithelia are highly tumorigenic. Sensory nerves activate HH signaling in normal touch domes, while denervation attenuates touch dome-derived tumors. Together, our studies identify varying tumor susceptibilities among different stem cell populations in the skin, highlight touch dome epithelia as "hot spots" for tumor formation, and implicate cutaneous nerves as mediators of tumorigenesis.

3.2 Introduction

Dysregulated Hedgehog (HH) signaling is a hallmark of basal cell carcinoma (BCC), the most common cancer in North America [1, 2]. During development and homeostasis, HH is carefully regulated by a balance of upstream factors that can either promote signaling, such as Smoothened (SMO), or suppress signaling, such as Patched1 (PTCH1). In BCC, this balance is tilted decisively in

favor of pathway activation through mutations that cause either loss of PTCH1 function or constitutive activation of SMO [3, 4].

Early evidence implicating perturbed HH in BCC came from studies demonstrating that patients harboring defective PTCH1 alleles are predisposed to developing numerous BCCs (Gorlin syndrome) [3, 5, 6]. Similarly, loss of PTCH1 promotes BCC-like lesions in irradiated mice [7], as does overexpression of mutated forms of SMO, Sonic hedgehog (SHH) or downstream GLI transcription factors [4, 8-12]. Findings from these and other studies have recently culminated in the USA Food and Drug Administration's approval of GDC-0449 (vismodegib), an oral inhibitor of SMO, as a therapeutic for treating advanced BCC [13].

In the skin, multiple stem cell populations maintain tissue homeostasis and contribute to organ regeneration during hair cycling [14]. In trying to identify the stem cells which give rise to BCC, however, recent studies have yielded conflicting results [15]. For instance, work by Youssef et al., has suggested that hair follicle bulge stem cells expressing a constitutively active form of SMO (SmoM2) resist BCC formation [16]. Rather, these tumors arise primarily from the interfollicular epidermis (IFE), which we have also previously observed in intact and wounded skin [17]. In direct contrast, lineage tracing experiments by Wang et al., using irradiated *Ptch1* heterozygous animals have suggested that Keratin 15+ bulge stem cells are the primary progenitors for BCC [18]. A third possibility—that stem cells in the epidermis and bulge are both competent for developing BCC—has also been proposed for tumors induced by an activated form of GLI2 [19].

These discrepant results are likely due to the use of different animal models whereby, in some cases, oncogenic transgenes such as SmoM2 are often driven by heterologous promoters. Because up to 90% of human BCCs are thought to be caused by loss of PTCH1, mouse models that target deletion of *Ptch1* to specific skin compartments may serve as more

accurate models of human disease. Indeed, deletion of *Ptch1* in Lgr5+ stem cells in the lower bulge and secondary hair germ has been reported to yield BCC-like tumors [20]. Whether other stem cell populations residing in the hair follicle and IFE possess tumor-forming capacity currently remains unclear.

Here we demonstrate that multiple hair follicle stem cell populations are highly tumorigenic upon deletion of *Ptch1*, whereas most stem cells within the IFE do not efficiently form tumors. However, an innervated subset of IFE cells known as touch dome (TD) epithelia display activated HH signaling during homeostasis and are highly susceptible to tumorigenesis. Surgical nerve ablation blunted the formation of touch dome-derived lesions, suggesting that cutaneous sensory nerves may play a previously unrecognized role in skin cancer.

3.3 Materials and Methods

3.3.1 Animals

The following mice were used: *Gli1*$^{tm3(cre/ERT2)Alj}$ (*Gli1-Cre* ^{ERT2})[21]; *Tg(KRT14-cre/ERT)20Efu* (*K14-Cre*^{ERT})[22]; *Hes1*$^{tm1(cre/ERT2)Lcm}$ (*Hes1-Cre*^{ERT2})[23]; *Lrig1*$^{tm1.1(cre/ERT2)Rjc}$ (*Lrig1-Cre*^{ERT2})[24]; *Gt(ROSA)26Sor*^{tm1Sor} *(ROSA26A-lacZ)*[25]; *Gt(ROSA)26Sor*$^{tm1(EYFP)Cos}$ (*ROSA26A-YFP*)[26]; *Ptch1*^{tm1Hahn} [27]; and *Trp53*^{tm1Brn} [28].

3.3.2 Mouse manipulations

For tumor cell-of-origin experiments, animals were induced with tamoxifen during telogen, at 7.5 weeks of age. For nerve studies, mice were induced with tamoxifen and/or denervated according to the schedules described in the text. Mice were treated with tamoxifen as follows: one dose at 5 mg per 40 grams body weight for *Gli1;Ptch1* and *Hes1;Ptch1* mice; one dose at 1 mg per 40 grams body weight

for *Lrig1;Ptch1* mice; and three daily doses, each 1 mg per 40 grams body weight, for *K14;Ptch1* mice. Skin biopsies were harvested as previously described[17]. Denervation of dorsal back skin was adapted from previously described procedures [29]. Briefly, mice were anesthetized, and a 4.5-5 cm incision was made along the dorsal midline to expose the dorsal cutaneous nerves on the left side (T3-12). These were blunt dissected close to their anatomical entry into the skin, while nerves on the right side were left intact. Subsequently, the skin was closed with sutures, similar to the skin biopsies. All studies were performed in accordance with regulations established by the University of Michigan Unit for Laboratory Animal Medicine.

3.3.3 Tissue staining

Biopsies were fixed for 1 hour in cold 3.7% paraformaldehyde, washed and incubated overnight in 30% sucrose at 4 degrees, before embedding in OCT mounting media. Frozen sections were stained using standard protocols with the following antibodies: rabbit anti-K17 (D73C7, 1:1,500, Cell Signaling); rat anti-K8 (TROMA-I, 1:500, Developmental Studies Hybridoma Bank); rabbit anti-K14 (AF64, 1:1,000,000, Covance); guinea pig anti-K5 (03-GP-CK5, American Research Products); chicken anti-GFP/YFP (GFP-1020, 1:2,000, Aves Labs); rabbit anti-NF-L (C28E10, 1:500, Cell Signaling); rat anti-β4-integrin (346-11A, 1:500, BD Pharmingen); rabbit anti-Sox9 (H-90, 1:150, Santa Cruz Biotechnology); goat anti-Lrig1 (AF3688, 1:25, R&D Systems); rabbit anti-K10 (PRB-159P, 1:500, Covance); rabbit anti-Involucrin (PRB-140C, 1:500, Covance); and rat anti-CD200 eFluor660 (OX90, 1:2,000, eBioscience). For frozen samples stained for YFP, sections were pre-treated with cold methanol for 5 minutes prior to blocking and incubation with primary antibodies. For whole-mount β-gal staining, *Gli1 in situ* staining and qPCR, see Supplemental Information.

3.3.4 Quantitation

For quantitating TDs and TD-derived tumors, 15 non-consecutive frozen skin sections (each 10um thick, ~1 cm in length) were co-stained with antibodies against K17 and K8 to label TD epithelia and Merkel cells, respectively, for each sample. TDs were identified based on columnar morphology, proximity to guard hairs, K17 expression and association with K8-expressing Merkel cells. TD size was assessed by counting the number of K17+ cells within each cluster along ~15 cm of skin. TD-derived tumors were identified based on similar criteria as those used for normal TDs, and the total number of K17+ cells within lesions radiating down from the epidermis was scored. We were careful to exclude K17-expressing suprabasal cells normally found in the hair follicle infundibulum[30]. Importantly, K17 expression is absent in normal non-TD IFE. To quantitate hair follicle-associated tumors in *Gli1;Ptch1* mice, we measured tumor volumes from 5 non-consecutive frozen skin sections (each 10 um thick, ~1 cm in length) for each sample. We performed IHC for K17, outlined tumors in Photoshop from 20x images, and recorded tumor area in pixels. For quantitating ectopic hair buds in *K14;Ptch1* mice, we counted the number of cell clusters, defined as consisting of at least 3 continuous K17+ cells, along the entire IFE.

3.3.5 Statistics

A paired Student's *t*-Test was used to assess significance in experiments where denervated and sham-operated, matched skin samples were harvested from the same animal. For all other experiments, an unpaired Student's *t*-Test was used. Calculations were performed at http://www.physics.csbsju.edu/stats/Index.html.

3.4 Results

3.4.1 BCC-like tumors can arise from multiple hair follicle stem cell populations

A hair follicle origin for BCC has long been suggested on the basis of similarities in marker expression [31, 32]. Because the hair follicle is maintained by several independent stem cell populations, we directly tested whether these cells are able to form tumors upon loss of *Ptch1*. To target PTCH1 deletion to specific hair follicle compartments, we generated mice harboring homozygous PTCH1 floxed alleles [33] coupled with different tamoxifen-inducible Cre drivers (FIG 3.1A). We treated mice with tamoxifen at 7.5 weeks of age, then harvested skin biopsies several weeks post-induction to assess tumor formation.

During telogen, stem cells expressing the HH target gene GLI1 reside within the hair follicle upper and lower bulge and secondary hair germ [34]. In mice expressing *Gli1* promoter-driven Cre^{ERT2} and PTCH1 floxed alleles (*Gli1;Ptch1*), we observed robust tumor formation within 5 weeks after tamoxifen induction (FIG 2.1B). These tumors appeared well circumscribed and displayed BCC-like features such as peripheral basal palisading (FIG 3.1C). As expected, these lesions were typically connected to the hair follicle bulge, but not the infundibulum, consistent with the lack of contribution of normal GLI1+ stem cells to the hair canal [34]. Although GLI1+ cells can contribute to the regenerating hair follicle during anagen, we did not observe tumors associated with the lower anagen follicle, suggesting that matrix cells cannot give rise to BCCs (FIG 3.2).

We have recently reported that mice expressing *Hes1-*Cre^{ERT2} display recombinase activity in suprabasal cells of the IFE and infundibulum[30]. By coupling this recombinase with an inducible *ROSA26R* promoter-driven *YFP* reporter allele, we also observed Cre activity in inner bulge and, less frequently, in outer bulge stem cells (FIG 3.1D). We therefore assessed tumor formation in mice expressing this Cre along with PTCH1 floxed alleles (*Hes1;Ptch1*), and observed upper and lower

bulge-associated lesions similar to those in *Gli1;Ptch1* animals, within 7 weeks after tamoxifen induction (FIG 3.1E). Together, these data confirm that bulge stem cells can indeed serve as tumor progenitors.

To test whether other stem cell populations can form BCCs, we next focused on LRIG1+ cells in the isthmus. Under homeostatic conditions, these cells renew the hair follicle infundibulum independently of bulge stem cells, because bulge cells largely do not contribute to the infundibulum, while LRIG1+ stem cells do not contribute to the bulge or anagen follicle [30, 35]. In mice expressing *Lrig1* promoter-driven Cre^{ERT2} and *Ptch1* floxed alleles (*Lrig1;Ptch1*), we also observed numerous tumors associated with the isthmus and infundibulum 5 weeks after tamoxifen induction (FIG 3.1F). These findings therefore reveal that BCC-like tumors can originate from upper bulge, lower bulge and isthmus progenitor populations in the hair follicle.

3.4.2 The IFE displays reduced tumor forming capacity

To determine whether the epidermis is susceptible to tumor formation, we deleted PTCH1 in the IFE using mice expressing *Keratin 14* promoter-driven Cre^{ERT} (*K14;Ptch1*). We and others have previously shown that this recombinase displays robust activity in IFE stem cells but minimal activity in the hair follicle [17, 36], as confirmed here using the YFP reporter allele (FIG 3.3A). Surprisingly, *K14;Ptch1* mice did not develop tumors in the epidermis, 5 weeks after induction. Even after extending the interval between tamoxifen treatment and biopsy to 12 weeks, we noticed that *K14;Ptch1* animals typically possessed a hyperplastic epidermis containing small, ectopic hair follicle-like buds resembling early benign follicular hamartomas (FIG 3.3B). Larger lesions adjacent to the IFE radiated laterally from the hair follicle infundibulum and did not display a connection to the epidermis, as confirmed by examining serial sections (FIG 3.3B and 3.4).

Previous studies have found that *P53* mutations are common in human BCC and that loss of P53 can promote BCCs in the IFE of irradiated *Ptch1*-heterozygous mice [18, 37, 38]. We therefore assessed tumor formation in *K14;Ptch1* mice that additionally harbored homozygous floxed alleles of P53. In mice biopsied up to 12 weeks after tamoxifen treatment, however, we observed that loss of P53 did not enhance IFE tumorigenesis (FIG 3.3C). In stark contrast, *Gli1;Ptch1*, *Hes1;Ptch1* and *Lrig1;Ptch1* mice with wild-type P53 all developed large hair follicle-associated lesions that filled the dermis within 5-7 weeks post-induction (FIG 3.1). These findings indicate that BCC-like tumors preferentially develop from hair follicle stem cells, and that loss of P53 does not promote IFE tumor formation.

3.4.3 Hair follicle-derived tumors express similar markers irrespective of stem cell origin

Given our finding that BCC-like lesions can originate from multiple hair follicle stem cell populations, we next determined whether these tumors display differences in marker expression. Regardless of cellular origin, all hair follicle-derived tumors consistently expressed K14 as well as K17, a HH pathway target gene [39, 40] (FIG 3.5A-B). K17 was also upregulated throughout the hyperplastic epidermis of induced *K14;Ptch1* animals, indicating that IFE stem cells which had deleted PTCH1 remained in the epidermis and activated downstream HH signaling in spite of the absence of tumors.

All hair follicle-derived tumors also expressed the stem markers Sox9 and Lrig1 (FIG 3.5C-D). At the same time, these tumors frequently exhibited signs of early differentiation, as evidenced by expression of K10 (FIG 3.5E). In contrast, involucrin, a later differentiation marker, was not observed (FIG 3.5F). Because we were ultimately unable to detect differential marker expression, this suggests that all hair follicle-derived tumors display a similar phenotype irrespective of cellular origin.

3.4.4 BCC-like tumors efficiently arise from stem cells within touch dome epithelia

Although the IFE was largely devoid of tumors, we noticed that *Gli1;Ptch1* mice frequently developed highly branched lesions that radiated down from the epidermis specifically at sites adjacent to guard hairs (FIG 3.6A). Because mechanosensory TD epithelia are localized to guard hairs, we re-evaluated the activity of Gli1-Cre^{ERT2} by generating mice expressing the recombinase along with either a *ROSA26R* promoter-driven β-galactosidase (LacZ) or YFP reporter allele (*Gli1;LacZ* or *Gli1;YFP*, respectively). After tamoxifen induction, these mice indeed displayed reporter gene expression in TDs, as determined both by whole-mount staining for LacZ (FIG 3.6B) and by co-localizing YFP with K17, a marker of TDs [41, 42] (FIG 3.7). TD labeling was stably maintained in the long term (FIG 3.6B), suggesting that TDs are renewed by dedicated stem cell pools that display HH pathway activity under homeostasis.

It is interesting to note that normal TDs typically consist of keratinocytes displaying a columnar basal morphology resembling the peripheral palisades observed in hair follicle-associated BCC-like tumors (FIG 3.6C). To establish that epidermis-associated *Gli1;Ptch1* tumors are derived from TDs, we examined tumor formation at earlier time points and observed a gradual lateral as well as downward expansion of K17+ TD-derived cell clusters upon deletion of *PTCH1* (FIG 3.6D-E). Just as normal TDs are juxtaposed by innervated neuroendocrine Merkel cells [43], epidermis-associated tumors in *Gli1;Ptch1* mice were also lined by Merkel cells, as assessed by staining for the marker K8 (FIG 3.6D). In addition, neurofilament staining confirmed that tumor-associated Merkel cells were innervated by sensory afferents (FIG 3.6F). In contrast, Merkel cells were not detected near any hair follicle-associated tumors.

Infrequently, we also observed more extensive epidermis-associated lesions in *K14;Ptch1* mice (FIG 3.6G). These tumors resembled those arising from the TD in *Gli1;Ptch1* animals, and staining for

K8 confirmed the presence of Merkel cells localized to these tumors (FIG 3.6G). To assess whether K14-Cre^{ERT} can induce recombination in the TD, we analyzed mice expressing the recombinase along with the YFP reporter allele (*K14;YFP*). Indeed, TD epithelia were occasionally labeled in *K14;YFP* animals, although at a frequency that was significantly reduced compared to either IFE labeling outside of TDs, or labeling within TDs in *Gli1;YFP* mice (FIG 3.6H-I). Diminished K14-Cre^{ERT} activity in the TD is likely due to reduced expression of K14 in TDs relative to the rest of the IFE, which is apparent only upon high dilution (1:1,000,000) of an antibody against this keratin (FIG 3.6J). Altogether, our findings suggest that TD epithelia activate HH signaling during homeostasis and, unlike the rest of the IFE, are highly susceptible to forming BCC-like lesions upon loss of *Ptch1*.

3.4.5 Surgical denervation inhibits tumorigenesis

Surgical nerve ablation has been reported to cause loss of TDs and Merkel cells in rodent and feline skin [44-46]. To confirm these findings, we denervated thoracic-level cutaneous nerves to one side of the dorsal midline in 6-week-old wild-type mice, while leaving the contralateral side intact as a sham control. After collecting samples 3 or 5 weeks after surgery, we observed that denervated skin displayed a significant reduction in K17+ TD size and abundance (FIG 3.8A-B). Merkel cells were lost from denervated skin (FIG 3.8B), possibly subsequent to K17 downregulation (FIG 3.8A), while remaining Merkel cells were frequently not innervated (FIG 3.8C). To further assess HH activity after denervation, we denervated 6 week old *Gli1;LacZ* mice and treated these animals with tamoxifen 2 weeks after surgery (FIG 2.8D). Four days later, we harvested biopsies for LacZ staining and observed reduced TD labeling compared with intact contralateral control (FIG 3.8D). Given that *K17* and *GLI1* are both downstream targets of HH signaling, these findings suggest that cutaneous nerves are crucial for maintaining HH pathway activity in the TD niche.

We next extended these studies to determine whether denervation can inhibit TD-derived tumors in *Gli1;Ptch1* mice. To first confirm that denervation performed subsequent to tamoxifen induction does not affect Gli1-Cre^{ERT2} recombinase activity in the TD, we induced *Gli1;LacZ* mice with tamoxifen at 5.5 weeks of age, then subsequently denervated one side of the dorsal skin 4 days after induction (FIG 3.8B). Two weeks after nerve ablation, we harvested skin biopsies and observed similar patterns of LacZ staining in denervated and sham-operated skin (FIG 3.10A). Thus, although TD epithelia rely on nerves to activate HH (FIG 3.8B, D), nerve ablation and consequent loss of HH pathway activity do not immediately affect the abundance or distribution of already-labeled cells in the TD, which can persist for weeks without neural input [44, 46].

In *Gli1;Ptch1* mice, we utilized the same approach, inducing animals with tamoxifen at 5.5 weeks of age and subsequently denervating one side of the skin (FIG 3.10B). Two or five weeks after tamoxifen induction, we harvested biopsies and confirmed that cutaneous nerves were stably ablated (FIG 3.9). Although denervation did not affect tumor growth 2 weeks post-induction, we observed a significant inhibition of TD-derived tumors in denervated skin 5 weeks after tamoxifen treatment (FIG 3.10B-C). In nine of ten mice, fewer TD tumor cells were observed within denervated skin, compared to the contralateral sham control (mean = 81.3 versus 35.3 TD-derived tumor cells/cm for sham versus denervated skin, respectively; $p = 0.017$ by paired Student's t test). In addition, the number of Merkel cells associated with these tumors was also reduced (FIG 3.10C). This effect was specific to TD-derived tumors, as nerve ablation did not significantly affect adjacent hair follicle-associated lesions (FIG 3.10D), arguing that denervation does not induce a systemic anti-tumorigenic response.

If epidermis-associated tumors which develop infrequently in *K14;Ptch1* mice are derived exclusively from TDs, denervation should also prevent BCC-like lesions in these animals. We therefore surgically removed the nerves from dorsal back skin in 6 week old *K14;Ptch1* mice, exposed these

animals to tamoxifen 2 weeks after surgery, and harvested biopsies after an additional 5 weeks. Although nerve ablation did not affect K14-Cre^{ERT}-mediated recombination in the IFE (FIG 3.10E), the formation of rare TD-derived lesions was attenuated in denervated skin (mean = 20.7 versus 3.9 TD-derived tumor cells/cm for sham versus denervated skin, respectively; $p = 0.04$ by paired Student's t test) (FIG 3.10F). In contrast, the formation of small ectopic buds along the IFE was unaffected. Together, our findings in *K14;Ptch1* and *Gli1;Ptch1* mice indicate that epidermis-associated tumors preferentially arise from TD epithelia and that sensory nerves promote the progression of TD-derived tumors.

3.4.6 The mechanosensory niche promotes tumorigenesis

How does the perineural microenvironment foster a pro-tumorigenic niche? Because TDs display heightened *Gli1* expression, we investigated the possibility that paracrine signals released by sensory neurons can promote canonical HH signaling in the TD. In mammals, three HH ligands—SHH, DHH and IHH—activate the pathway. After dissecting dorsal root ganglia, where the cell bodies of cutaneous sensory nerves are located, we determined by qRT-PCR that these nerves express markedly higher levels of all three HH ligands compared with skin epithelia (FIG 3.11A). These findings are concordant with recent data showing that neuron-specific loss of Shh causes deterioration of TDs and Merkel cells in adult mice [47].

Although loss of *Ptch1* may seemingly bypass the requirement for HH ligands to induce pathway activity in TD-derived tumors, recent studies have shown that *PTCH1*-deficient skin upregulates a related protein, PTCH2, which can also bind HH ligands and suppress downstream signaling [48, 49]. Indeed, we confirmed by qRT-PCR that *Ptch2* expression was increased upon deletion of *Ptch1* in

K14;Ptch1 mice (FIG 3.11B), suggesting that PTCH2 may dampen HH signaling in tumor-resistant IFE (FIG 3.11B).

To further elucidate why different skin compartments vary in tumor predisposition, we searched for molecular differences that might distinguish tumor-susceptible hair follicle and TD compartments, from tumor-resistant IFE. The cell surface glycoprotein CD200 is a marker of hair follicle stem cells in humans and may promote immune privilege in various organs [50]. CD200 has also recently been found to be enriched in cells that can initiate BCC [51]. In mice, CD200 is a marker of TD epithelia [52]. and we also observed CD200 throughout the hair follicle, but not in the IFE (FIG 3.11C). Furthermore, all hair follicle- and TD-derived tumors strongly expressed CD200, whereas strikingly, CD200 was completely absent from hyperplastic IFE or weakly expressed in ectopic IFE buds in *K14;Ptch1* mice (FIG 3.11D). In keratinocytes, either loss of *Ptch1* or pharmacological activation of HH signaling elevated *CD200* (FIG 3.11E and F). Together, these findings suggest that in tumor-resistant IFE, loss of *Ptch1* only partially activates the HH signaling program, leading to upregulation of some target genes (*Gli1*, *Ptch2*, K17), but not others (CD200) (FIG 3.11B and 3.12). Within the TD niche, nerve-derived factors, possibly involving HH ligands, may potentiate full pathway activation and tumorigenesis. Notably, as normal TDs resemble BCCs in terms of basal columnar morphology as well as elevated baseline expression of GLI1, K17 and CD200, this once again argues that TDs are ‘‘hot spots’’ in the epidermis that are primed for tumor formation.

3.5 Discussion

The precise cellular origin of BCC has been controversial, as recent studies have seemingly reported diametrically opposed results. Whereas SMO-M2-induced BCC-like tumors appear to arise from stem cells in the IFE, but not from the hair follicle bulge [53, 54], tumors driven by loss of Ptch1

have been reported to originate from the bulge and secondary hair germ (SHG), but not the IFE [18, 20]. Our results are concordant with those of Wang et al., and Kasper et al., although we have identified additional stem cell populations that are also susceptible to tumorigenesis [18, 20]. Altogether, using a mouse model that recapitulates the most common genetic aberration seen in human BCCs, our findings indicate that these tumors preferentially arise from stem cells located specifically in the upper bulge, lower bulge/SHG, isthmus, and TD, but not from IFE stem cells or transit-amplifying matrix cells (FIG 3.12G).

What predisposes certain cutaneous epithelia to forming tumors upon loss of *Ptch1*? Previous studies have postulated that degradation of GLI proteins may restrict HH signaling and BCC formation in the skin [11, 55]. Supportive of this, Grachtchouk et al., showed that upon forced activation of downstream HH signaling, BCC-like tumors can arise from both hair follicles and IFE [56]. Alternatively, upregulation of PTCH2 in the absence of PTCH1 may also restrain full HH pathway activity. Indeed, Adolphe et al., recently demonstrated that mice lacking both PTCH1 and PTCH2 develop a more severe hyperplastic and BCC-like invaginating epidermal phenotype than do mice deficient for PTCH1 alone [48]. Our findings are concordant with these observations and suggest that tumor-resistant IFE cells become oncogenic only upon high activation of HH signaling requiring loss of multiple redundant inhibitors of the pathway. These data further suggest that sites in the skin which normally display high level HH signaling are likely predisposed to BCC formation and that loss of *Ptch1* alone at these sites is sufficient for tumorigenesis.

Consistent with this concept, we have found that TD epithelia display activated HH signaling during homeostasis and are highly susceptible to forming tumors. Under normal conditions, TDs function as mechanosensory organs that detect light touch and transduce signals via underlying Merkel cells to slowly adapting type 1 sensory afferents [57, 58]. We have further shown that cutaneous sensory

nerves express HH ligands and that denervation impairs HH activity in the TD and inhibits the progression of TD-derived tumors. Although these results suggest that nerve endings secrete HH ligands to promote TD-derived tumors, it is important to add, however, that TD-derived tumors did not appear to respond to a neutralizing antibody generated against Shh (FIG 3.13D). These results might be explained if multiple HH ligands simultaneously promote TD-derived tumors, and tumor inhibition can be achieved only by complete and sustained impairment of HH signaling, as might occur following long-term denervation. These findings do not rule out the possibility that nerves may also non-canonically activate downstream HH signaling via pathways such as TGF-β [59]. Alternatively, cutaneous nerves are known to secrete cytokines such as calcitonin gene-related peptide as well as substance P, which can serve functional roles during epidermal development and pathology [60]. Indeed, neural changes are often observed in patients with psoriasis and atopic eczema, and nerve removal inhibits the epidermal hyperplasia observed in experimental models of these diseases [61, 62].

Our findings complement those of previous studies showing that nerves can influence tumors in other organs. For instance, chemical denervation can inhibit tumorigenesis in the stomach and colon [63]. More recent studies in prostate cancer have found that peritumoral sympathetic nerves promote tumor growth, while intratumoral parasympathetic nerves stimulate metastasis [64]. In addition, β-blockers, which interfere with the sympathetic nervous system, can delay the progression of various cancers [65]. A tumor-modulatory role for nerves has not been described for Merkel cell carcinoma, a rare cancer thought to originate from Merkel cells, but would not be surprising given the close association between nerve endings and mechanosensory cells.

In humans, BCCs primarily develop in sun-exposed, hair-bearing skin. In addition, the majority of tumors (between 57% and 78%) typically display a nodular phenotype, while only a minority (15%–16%) present as superficial lesions [66, 67]. Interestingly, Grachtchouk et al., previously noted in mice

that tumors originating from hair follicles appear nodular, whereas IFE-associated tumors resemble superficial human BCCs, suggesting that tumor histologic phenotype can reflect cellular origin [56]. From this perspective, the high prevalence of nodular human BCCs is consistent with our finding that hair follicle stem cells likely serve as the primary progenitors for these tumors. Although our studies do not exclude the possibility that loss of *Ptch1* may give rise to tumors from the IFE after an extended latency, our findings also suggest that some human BCCs that appear to arise from the IFE might actually originate from the TD.

Because Merkel cells are invariably associated with TD-derived tumors in our studies, we also examined the distribution of these cells in a limited number of human BCC samples. In four of ten tumors, we observed clusters of Merkel cells located within small tumor foci from both superficial and deeper lesions, but not within larger tumor masses (FIG 3.11H and 3.14). These observations are consistent with a potential mechanosensory niche for BCC, or possibly even "micro-niches" within the immediately vicinity of innervated Merkel cells, which in humans are widely distributed not just in TDs, but also throughout the skin and hair follicles [68]. Moreover, these cells are particularly abundant in glabrous skin [69], where palmoplantar pits frequently develop in Gorlin patients. Merkel cells have also been observed in a minority of human BCCs, including a subtype known as fibroepithelioma of Pinkus [70, 71], but are more commonly associated with trichoblastoma [72]. It remains to be seen whether Merkel cells play an early supporting role during BCC tumor initiation, but are subsequently lost as the tumor expands. Further work will be required to determine whether both Merkel cells and nerves preferentially associate with specific BCC subtypes, or possibly early during tumorigenesis, and if so, whether targeting these niche elements might represent a viable therapeutic strategy.

3.6 Acknowledgements

This chapter was published in *Cell Stem Cell* and is included in this dissertation with the permission of the journal editors. (see citation below)

Peterson, S. C., Eberl, M., Vagnozzi, A. N., Belkadi, A., Veniaminova, N. A., Verhaegen, M. E., Bichakjian, C. K., Ward, N. L., Dlugosz, A. A., Wong, S. Y. (2015). "Basal Cell Carcinoma Preferentially Arises from Stem Cells within Hair Follicle and Mechanosensory Niches." *Cell Stem Cell* **16**(4): 400-412.

We are grateful to Dr. I. Brownell (NCI) for helpful discussions and critical reading of this manuscript, and to the Dlugosz lab at the University of Michigan for sharing reagents. S.Y.W. acknowledges the support of the National Institutes of Health/NIAMS (R00AR059796, R01AR065409); the University of Michigan Department of Dermatology; the Biological Sciences Scholars Program; the Center for Organogenesis; the UM Comprehensive Cancer Center; and the John S. and Suzanne C. Munn Cancer Fund. This work was also supported in part by NIAMS R21AR063852 to N.L.W.; by NIAMS AR045973 and NCI CA087837 to A.A.D.; and by NIGMS T32 GM007315 to S.C.P.

3.7 Author Contributions

S.C.P. and S.Y.W. conceived and performed experiments, wrote the manuscript and secured funding. M.E., A.N.V. and N.A.V. performed experiments. A.B., N.L.W. and A.A.D. provided expertise, technical support and feedback.

3.8 Figures

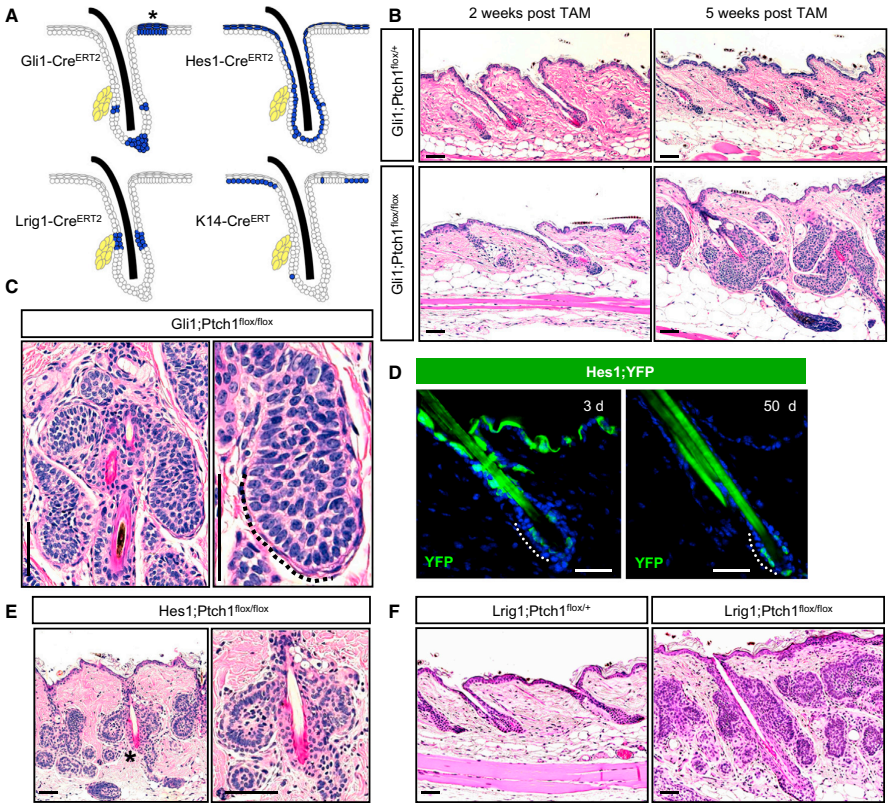

Figure 3.1 Multiple hair follicle stem cell populations readily form BCC-like tumors.
A. Schematic showing areas of activity (blue) for the different inducible Cre recombinases used in this study. Asterisk indicates TD epithelia. Yellow indicates sebaceous glands.
B. Hematoxylin and eosin (H&E) staining showing that *Gli1;Ptch1* mice, but not control animals, develop numerous hair follicle-associated tumors 5 weeks after tamoxifen (TAM).
C. Higher magnification views of hair follicle-associated tumors with peripheral palisading (dotted line).
D. Hes1-Cre^{ERT2}-mediated recombination of a floxed YFP reporter allele (green) in suprabasal cells of the epidermis, infundibulum, and, less frequently, in the bulge, 3 days (left) or 50 days (right) post-TAM. **E.** *Hes1;Ptch1* mice develop bulge-associated tumors, 7 weeks post-TAM. (Right) A higher magnification view of the region indicated by the asterisk.
F. *Lrig1;Ptch1* mice develop tumors associated with the isthmus and infundibulum, 5 weeks post-TAM.

The scale bars represent 50 μm. See also FIG 3.2.

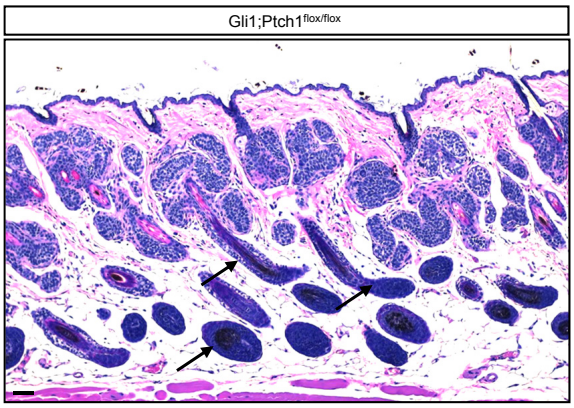

Figure 3.2 Lower anagen follicles do not form tumors in *Gli1;Ptch1* mice. H&E staining showing absence of tumors in the lower anagen hair follicle (arrows) in *Gli1;Ptch1* mice. Scale bars, 50μm.

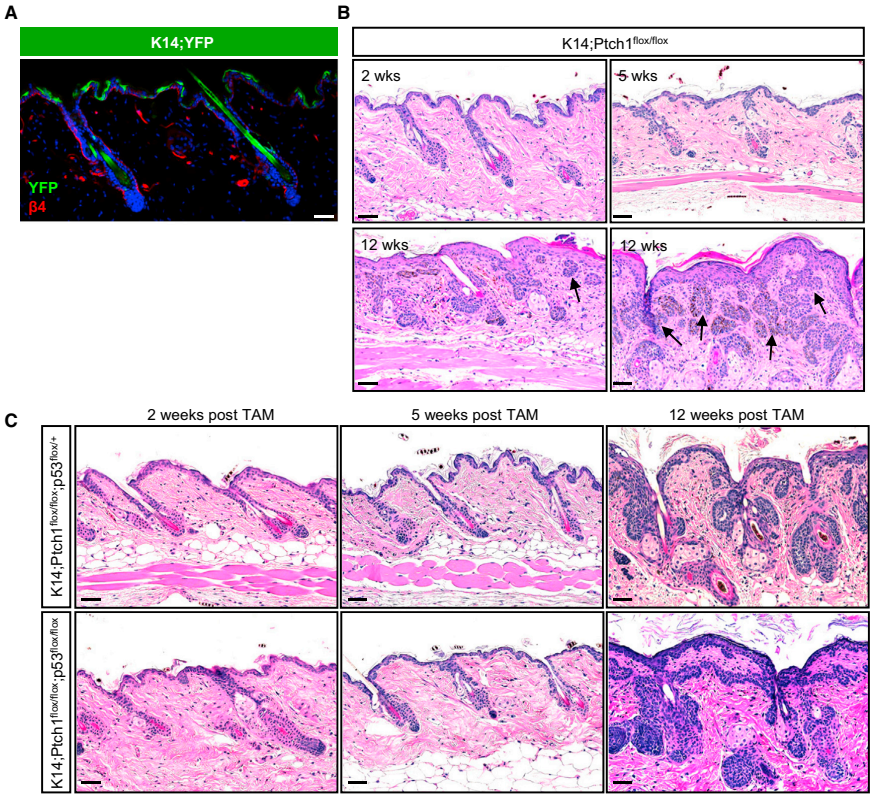

Figure 3.3 IFE stem cells do not efficiently form tumors
A. IHC showing that K14-Cre^{ERT} induces recombination of a YFP reporter allele (green) primarily in basal cells of the epidermis, as marked by integrin β4 (red).
B. *K14;Ptch1* mice develop small ectopic IFE-associated buds, 5 weeks after TAM. By 12 weeks post-TAM, the IFE is hyperplastic but largely devoid of lesions. Tumors adjacent to the IFE (arrows) are typically connected to hair follicles, as shown in serial sections (see also FIG 3.4).
C. Loss of *p53* does not promote IFE tumor formation, 12 weeks post-TAM.

Scale bars represent 50μm.

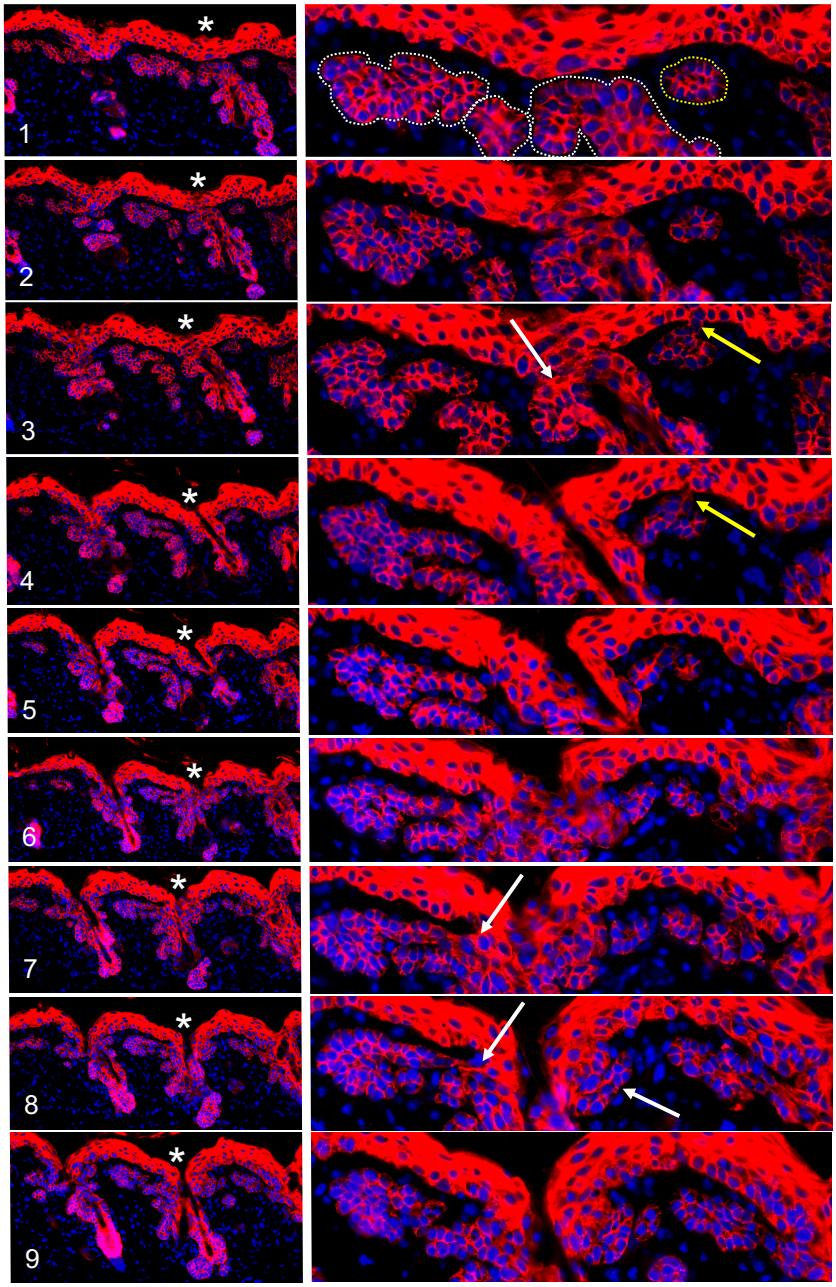

Figure 3.4 IFE lesions do not progress in *K14;Ptch1* mice.
Nine serial sections of skin from a *K14;Ptch1* mouse, 12 weeks after tamoxifen induction, immunostained for K5 (red). In the left column of panels, (*) marks a similar region of the skin overlying a hair follicle that is magnified in the right column of panels. Hair follicle-associated tumors (white dotted lines) and a smaller IFE-associated ectopic bud (yellow dotted line) are indicated in the top right panel. White arrows indicate areas where tumorigenic lesions are continuous with the hair follicle. Yellow arrows indicate areas where a smaller ectopic bud is possibly continuous with the IFE (sections #3-4), but may also be connected to the hair follicle (section #8).

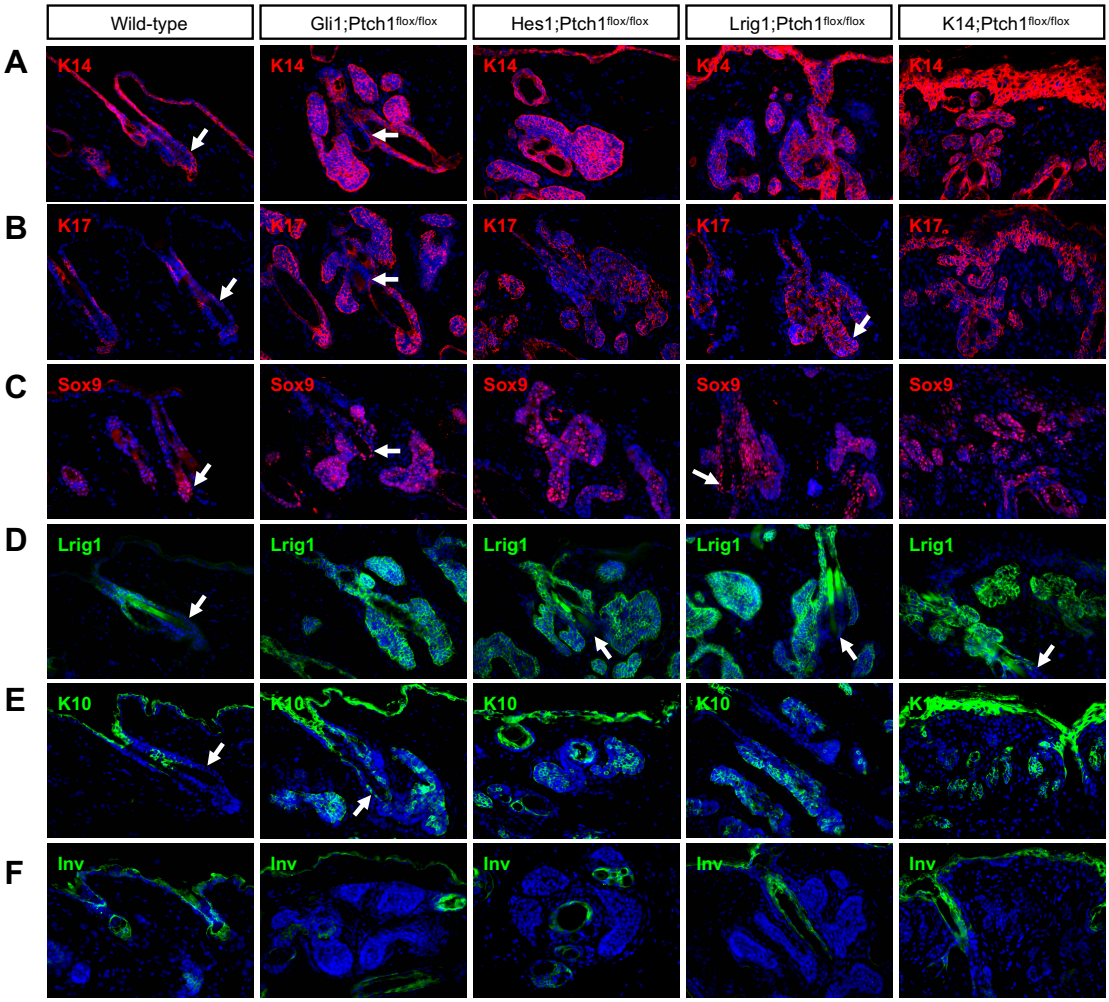

Figure 3.5 Hair follicle-derived tumors express similar markers regardless of cellular origin.
A-F. IHC for **(A)** K14, **(B)** K17, **(C)** Sox9, **(D)** Lrig1, **(E)** K10, and **(F)** Involucrin (Inv).
Wild-type telogen hair follicles were from 7.5-week-old mice. *Gli1;Ptch1* and *Lrig1;Ptch1* tumors were collected 5 weeks post-TAM, while *Hes1;Ptch1* and *K14;Ptch1* samples were harvested 7 and 12 weeks post-TAM, respectively. Arrows indicate follicles where the bulge is visible.

Scale bars represent 50μm.

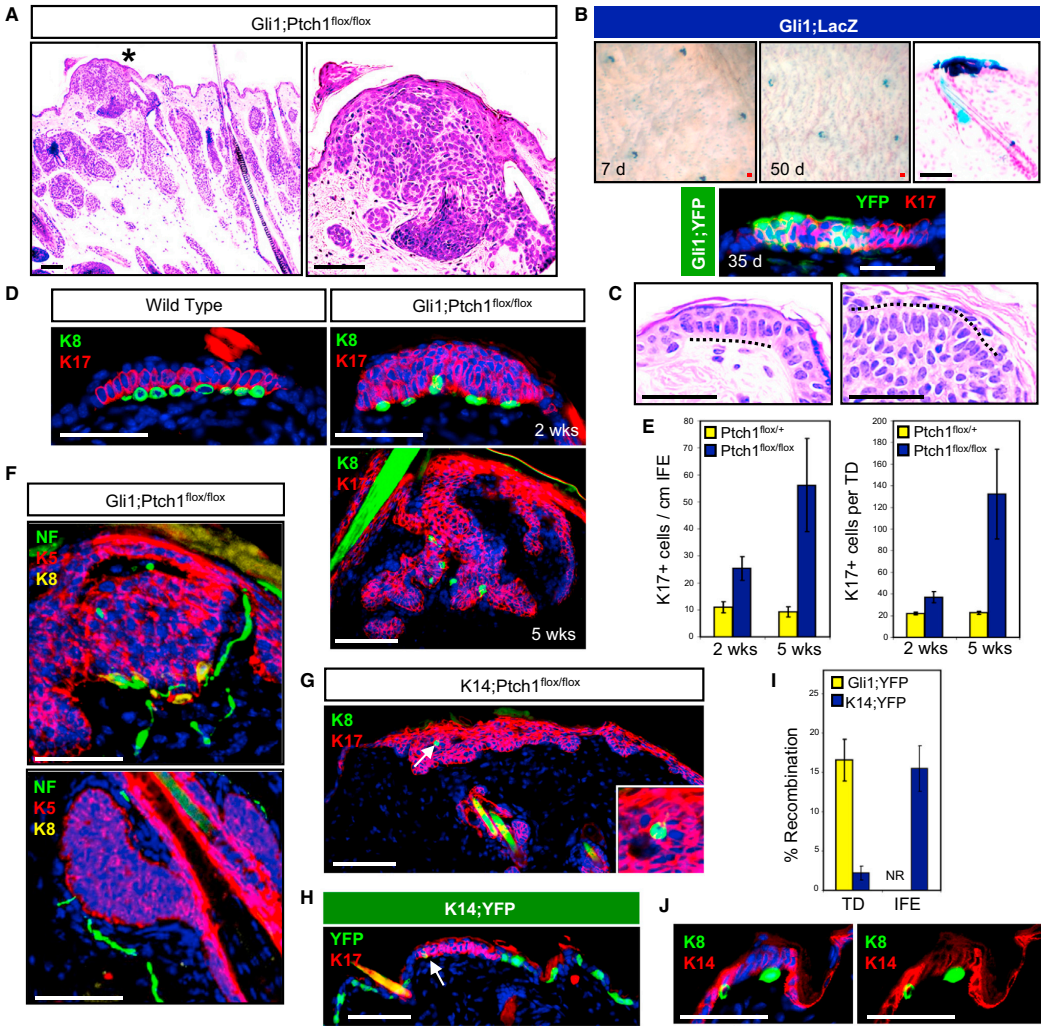

Figure 3.6 TDs are hot spots for tumor formation.

A. H&E staining of a TD-associated lesion (asterisk) in *Gli1;Ptch1* mice, 5 weeks post-TAM (left). (Right), higher magnification view of TD-associated lesion.

B. (Top) Whole mount LacZ staining of skin from *Gli1;LacZ* mice, 7 days (left) and 50 days (middle) post-TAM. (Right) LacZ staining showing TD labeling. (Bottom) IHC for YFP (green) and K17 (red) in a TD from a *Gli1;YFP* mouse, 35 days post-TAM.

C. Resemblance of TD columnar basal cells with palisading periphery of a *Gli1;Ptch1* tumor (dotted lines).

D. (Top left) IHC of a normal TD, identified by K17 expression (red) and underlying K8+ Merkel cells (green). (Right) tumorigenic TDs from *Gli1;Ptch1* mice, 2 and 5 weeks post-TAM.

E. Quantitation of K17+ cells in the IFE and TD size in *Gli1;Ptch1* mice or controls, 2 and 5 weeks post-TAM.

F. (Top) TD-derived K5+ tumor (red) retaining underlying Merkel cells (yellow) associated with nerves, as identified by neurofilament (NF, green). (Bottom) hair follicle-associated tumors (red) with nerves in the dermis (green), but no Merkel cells.
G. K8+ Merkel cells (arrow) are associated with infrequent IFE-derived tumors, suggesting a TD origin. (Inset) enlarged.
H. K14-Cre^{ERT} displays infrequent recombination in K17+ TD epithelia (red), and frequent recombination in the rest of the IFE, as assessed by YFP expression (green).
I. Quantitation of Gli1-Cre^{ERT2} and K14-Cre^{ERT} recombination rates in TD and non-TD IFE. NR, no recombination detected in non-TD IFE in *Gli1;YFP* mice.
J. Reduced expression of K14 (red) in TDs epithelia Merkel cells (green). Right panel is identical to the left, but with DAPI omitted for clarity. Data are represented as mean ± SEM. Scale bars represent 50μm.

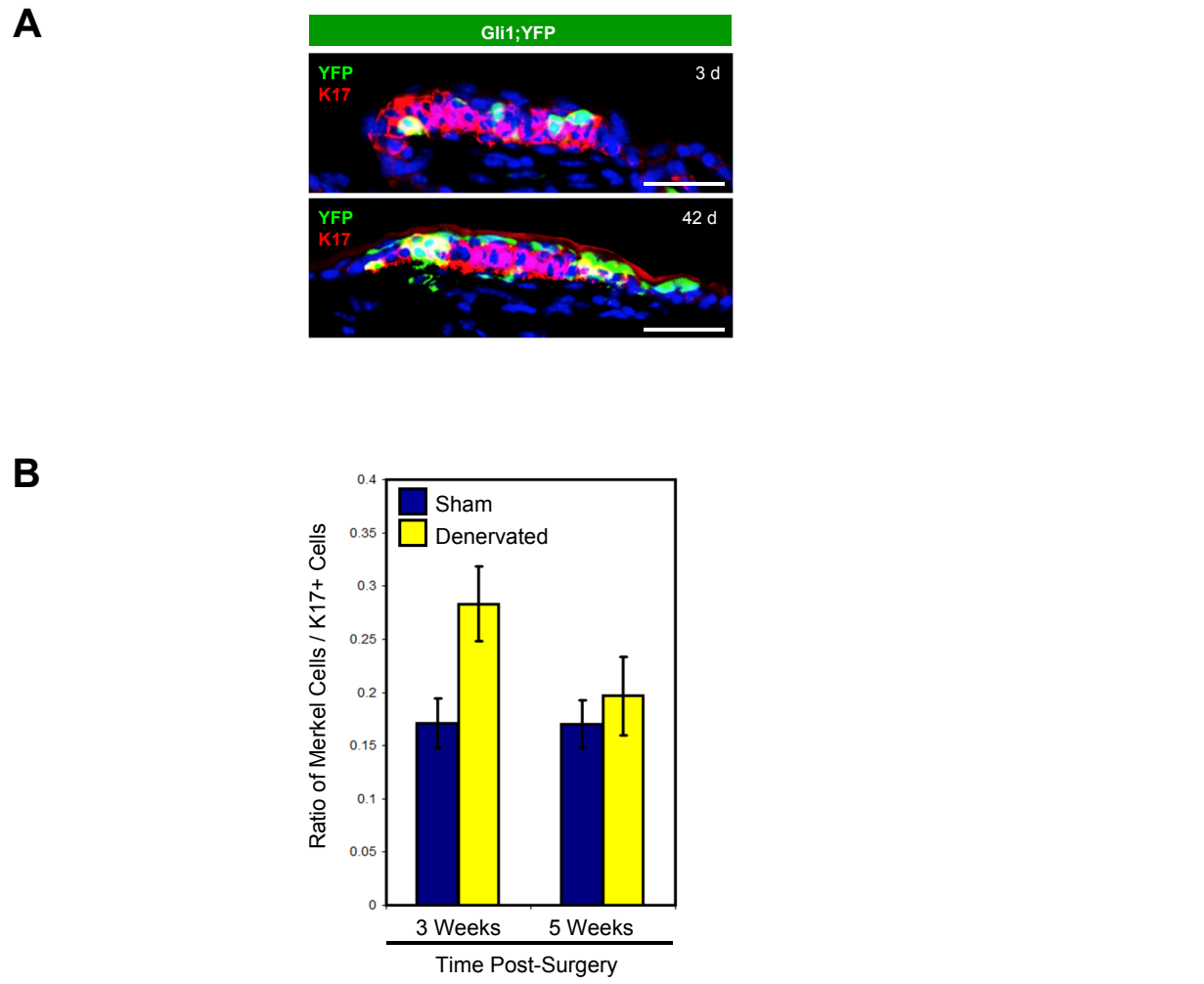

Figure 3.7 Gli1-Cre^{ERT2} labels TD epithelia.
A. IHC showing stable labeling of TD epithelia (red) by Gli1-Cre^{ERT2}-induced recombination of a floxed YFP reporter allele (green), in *Gli1;YFP* mice, 3 or 42 days post-TAM.
B. The ratio of K8+ Merkel cells to K17+ TD epithelia is increased, 3 weeks after denervation, relative to sham-operated control ($p = 0.048$). Five weeks after denervation, this ratio is unchanged between denervated and sham-operated control skin. This suggests that while denervation decreases the overall number of both K17+ TD cells and K8+ Merkel cells (FIG 3.5B), loss of K17 expression occurs more rapidly than does loss of Merkel cells. Data are represented as mean ± SEM. Scale bars, 50 μm.